CIRCULATION COPY
SUBJECT TO RECALL
IN TWO WEEKS

UCRL-53655

Initial Stages of Uranium Oxidation: A Surface Study

K. A. Winer
(Ph.D. Thesis)

July 1, 1985

Lawrence
Livermore
National
Laboratory

DISCLAIMER

This document was prepared as an account of work sponsored by an agency of the United States Government. Neither the United States Government nor the University of California nor any of their employees, makes any warranty, express or implied, or assumes any legal liability or responsibility for the accuracy, completeness, or usefulness of any information, apparatus, product, or process disclosed, or represents that its use would not infringe privately owned rights. Reference herein to any specific commercial products, process, or service by trade name, trademark, manufacturer, or otherwise, does not necessarily constitute or imply its endorsement, recommendation, or favoring by the United States Government or the University of California. The views and opinions of authors expressed herein do not necessarily state or reflect those of the United States Government or the University of California, and shall not be used for advertising or product endorsement purposes.

Work performed under the auspices of the U.S. Department of Energy by Lawrence Livermore National Laboratory under Contract W-7405-Eng-48.

UCRL-53655
Distribution Category UC-4

Initial Stages of Uranium Oxidation: A Surface Study

K. A. Winer
(Ph.D. Thesis)

Manuscript date: July 1, 1985

LAWRENCE LIVERMORE NATIONAL LABORATORY
University of California • Livermore, California • 94550

Available from: National Technical Information Service • U.S. Department of Commerce
5285 Port Royal Road • Springfield, VA 22161 • $14.50 per copy • (Microfiche $4.50)

Initial Stages of Uranium Oxidation: A Surface Study

By

KRIS ALAN WINER
B.A. (California State University, Fullerton) 1980
M.S. (University of California, Davis) 1982

DISSERTATION

Submitted in partial satisfaction
of the requirements for the degree of

DOCTOR OF PHILOSOPHY

in

Engineering/Applied Science

in the

GRADUATE DIVISION

of the

UNIVERSITY OF CALIFORNIA

DAVIS

Approved: ______________________________
____
____
Committee in Charge

Deposited in the University Library ______________________________
Date Librarian

CONTENTS

Page

Acknowledgements iv

Abstract v

1. Introduction 1

2. Uranium and Its Oxides 4

    2.1 Uranium Metal 5

    2.2 Oxidation of Uranium 6

3. Surface Analytical Techniques 16

    3.1 Auger Electron Spectroscopy 19

    3.2 X-Ray Photoelectron Spectroscopy 24

    3.3 Thermal Desorption Spectroscopy 29

    3.4 Electron-Induced Luminescence 32

4. Experimental Apparatus and Procedures 36

    4.1 Experimental Apparatus 37

    4.2 Sample Preparation 43

    4.3 Experimental Procedures 48

        4.3.1 AES 48

        4.3.2 XPS 49

        4.3.3 TDS 51

        4.3.4 EIL 53

5. Experimental Results and Discussion 56

5.1 Auger Electron Spectroscopy 57

5.2 X-Ray Photoelectron Spectroscopy 69

5.3 Thermal Desorption Spectroscopy 99

5.4 Electron-Induced Luminescence 103

5.5 Surface Morphology 115

6. Initial Reaction Mechanisms 121

7. Summary and Suggestions for Future Work 130

8. Literature Cited 135

ACKNOWLEDGEMENTS

I wish to express my deepest appreciation to the faculty and staff of the Department of Applied Science for their encouragement and thoughtful advice during my academic career at U.C.D. I particularly thank Fred Wooten for giving me the chance to succeed.

I thank Bunny Beck and her staff at Employee Development for their support and attention while I was in their charge.

The successful completion of this work would have been impossible without the generous technical support of the Chemistry and Materials Science Department at LLNL and the patient cooperation of members of the Surface Science section. I am particularly indebted to Bob Smith, for his generous gift of practical knowledge, and to Carlos Colmenares, for promoting my interest in and actively supporting this project for these many years. Their personal warmth and friendship have made my stay at Livermore a pleasurable experience.

Finally, and most importantly, I am grateful for the patience and consideration of Becky Springmeyer during the preparation of this thesis. I only hope I can be as thoughtful when she is writing hers.

ABSTRACT

The initial oxidation reactions of clean, high-purity polycrystalline uranium metal surfaces with dry oxygen, pure water vapor, and dry carbon monoxide for temperatures between 85 and 298 K were studied with Auger electron spectroscopy (AES), X-ray photoelectron spectroscopy (XPS), thermal desorption spectroscopy (TDS), and electron-induced luminescence (EIL).

The formation of an oxide layer was found to occur rapidly upon exposure to each reactant gas, even at 85 K. The resultant oxide in each case was near-stoichiometric UO_2. The previously reported formation of a stable UO phase was not substantiated. Oxide formation during carbon monoxide exposure was impeded by the competition between carbon and oxygen atoms for surface adsorption sites and the formation of uranium carbide.

The presence of strongly chemisorbed oxygen and hydroxyl species on the oxide surface after oxygen gas and water vapor saturation, respectively, was inferred. The active oxide surface promoted the formation of hyperstoichiometric UO_{2+x} in the initial stages of the oxidation reaction. Point defect clustering was speculatively inferred from the luminescence results, as was the presence of molecularly adsorbed oxygen or large OH-O surface complexes. Surface pitting during exposure to water vapor at 85 K, followed by warming to 298 K, indicated the electrochemical interaction of liquid water with the uranium surface and the possible formation of uranium hydride.

Initial oxidation reaction mechanisms were discussed on the basis of the results obtained. It was determined that insufficient information is available to distinguish between the various mechanisms proposed for the inhibition of the water vapor-uranium reaction by oxygen.

He went into a small bar there, announced that any one who could produce a volunteer fireman's badge could drink with him free. He built to a crying jag, during which he claimed to be deeply touched by the idea of an inhabited planet with an atmosphere that was eager to combine violently with almost everything the inhabitants held dear. He was speaking of Earth and the element oxygen.

"When you think about it boys", he said brokenly, "that's what holds us together more than anything else, except maybe gravity. We few, we happy few, we band of brothers---joined in the serious business of keeping our food, shelter, clothing, and loved ones from combining with oxygen."

Eliot Rosewater-

President of the
Rosewater Foundation

1. INTRODUCTION

Uranium is an interesting metal. It undergoes spontaneous fission, becomes superconducting at low temperatures and is highly chemically reactive. The complex chemical and physical behavior of uranium has been the subject of scientific study and the basis of important technologies for more than fifty years. Nuclear energy technologies make extensive use of uranium metal, often in atmospheric environments. The corrosion of uranium by atmospheric gases is therefore an important engineering problem and has received considerable attention in recent years. Although significant progress has been made in understanding uranium oxidation, the present state of knowledge is incomplete.

In simple terms, the oxidation of uranium involves the adsorption of reactant gas molecules onto the metal surface, their dissociation into atomic species, and the chemical binding of the gas atoms with surface uranium atoms. As this process continues, an oxide layer begins to form which eventually covers the entire surface. Subsequent oxidation requires the diffusion of adsorbed gas atoms through the oxide layer. This diffusion process is profoundly influenced by the defect structure and electronic properties of the oxide layer. The characterization of the surface oxides formed during the initial stages of oxidation is essential to the understanding of the oxidation mechanisms of uranium and is the purpose of this study.

Recent advances in the methods of surface analysis allow a detailed investigation of surface reactions with what has now become a myriad of techniques. Several of these techniques serve as the "workhorses" of surface analysis and were employed in this study. Auger electron spectroscopy (AES) allows the elemental composition of surfaces to be analyzed. This was useful for monitoring the cleanliness of the metal surface prior to reactant gas exposure, the surface species coverage before saturation, and the surface oxide composition. X-ray photoelectron spectroscopy (XPS) can provide information about the chemical environment of surface atoms. This technique allowed the determination of surface stoichiometry and the chemical composition of the near-surface region, both of which were necessary for the characterization of the surface oxides. Thermal desorption spectroscopy (TDS) provides information about the surface adsorption and molecular dissociation processes that take place during oxidation. Together, these complementary techniques provided detailed quantitative information about the initial stages of the oxidation process.

In addition to using these three standard techniques of surface analysis, uranium oxide surfaces were studied with a promising new technique that is still under development. Preliminary studies of surfaces with electron-induced luminescence (EIL), also known as cathodoluminescence, have shown this technique to be a sensitive quantitative monitor of adsorbed gases and able to detect qualitative changes in the defect structure of surface oxides. This study provides a preliminary evaluation of the sensitivity and the utility of EIL as a surface analytical tool by correlating its results with those of the standard techniques.

The physical properties of uranium and its oxides are summarized in section 2. Proposed mechanisms for uranium oxidation in different gaseous environments are reviewed and results of previous studies of bulk uranium oxides are examined. The analytical techniques used in this study, the physical basis for each technique, and the information obtainable from its application are described in section 3. The results of previous investigations employing these techniques to the study of uranium oxidation, if any, are reviewed and experiments based on their application are proposed. The experimental aspects of the study is the topic of section 4. Sample preparation, the experimental apparatus and procedures for each of the measurements are described. Detailed experimental data obtained with the surface analytical techniques are presented and discussed in section 5. Reaction mechanisms for the initial oxidation of uranium by atmospheric gases are proposed on the basis of the experimental results in section 6. Suggestions for future work are made in section 7.

2. URANIUM AND ITS OXIDES

Much has been learned about the uranium-oxygen system since it was first studied more than fifty years ago [1]. A large part of this knowledge results from work performed in just the last decade. Several recent investigations of the defect structure of uranium oxides and the kinetics of uranium oxidation are pertinent to the present study and are discussed below. A comprehensive review of the current state of knowledge of the oxidation mechanisms and catalytic properties of the actinide elements has been written by Colmenares [2]. The continuing interest in the properties of uranium and other actinides is demonstrated by regularly held international conferences devoted to this topic. The last conference was held in Pacific Grove, Ca. in 1981 and the proceedings provide a useful perspective of current actinide research [3].

This section begins with a brief summary of the physical properties of uranium metal. The process of oxidation is then examined and the structure and stoichiometric behaviour of uranium oxides discussed. Previous studies of uranium oxides in the bulk are reviewed here, and those involving surface-sensitive techniques are covered in the next section. The identification of areas requiring further investigation is made.

2.1 Uranium Metal

Pure uranium has a high density and a silvery appearance. It is shiny when freshly scraped or polished but tarnishes readily in air due to the high chemical reactivity of the clean metal surface. The crystallography of uranium has been established with high precision; it exists in three allotropic phases and structures: the α-phase with an orthorhombic unit cell, the β-phase with a tetragonal unit cell and the γ-phase with a body-centered cubic unit cell, as given in Table 2.1.

Phase	Temperature (°C)	Density (g/cm^3)
	20	19.04
α (Orthorhombic)	200	18.88
	400	18.67
	650	18.33
	670	18.16
β (Tetragonal)	700	18.13
	770	18.07
	775	17.93
γ (Body-centered cubic)	900	17.79
	1110	17.55

Table 2.1. Physical properties of uranium.

Additional information on the thermal and mechanical properties of uranium metal can be found in reference [4].

2.2 Oxidation of Uranium

The initial stages of the oxidation of uranium involve three poorly understood processes: the surface adsorption of gases and vapors, their dissociation on the surface, and the diffusion of the oxidizing species through an oxide layer to the bulk metal.

Consider a clean polycrystalline uranium surface in the presence of an oxidizing environment, say, oxygen gas. Oxygen molecules strike the surface at random as a result of their kinetic motion. Some of the molecules will stick to the surface, where they may remain physically adsorbed, wander about the surface, or become chemically bound (chemisorbed) to the surface. Adsorbed oxygen molecules will dissociate into atomic oxygen and combine chemically with surface uranium atoms, for example, by acquiring two electrons to form the chemisorbed species O^{-2}. As chemisorption proceeds, UO_2 nuclei begin to form on the surface. The nuclei continue to grow and merge until the entire surface is covered with an oxide layer. At room temperature, a monolayer of chemisorbed oxygen forms in about 40 seconds in 1.33 x 10^{-4} Pa of oxygen (~40 Langmuirs, 1 Langmuir = 1.33 x 10^{-4} Pa-s).

Epitaxial oxide layers form in metal single-crystals, with the oxide taking on the same crystal orientation as the underlying metal; however, epitaxial oxide growth has not been observed on uranium single crystals [5]. Polycrystalline uranium metal is highly disordered and consists of very fine crystallites of random orientation. Oxidation of polycrystalline uranium results in a polycrystalline oxide layer, also with a large concentration of randomly oriented crystallites. The grain boundaries between the crystallites provide paths of least resistance for oxygen diffusion into the bulk. Surface defects such as steps and other irregularities can have an important effect on the surface adsorption process. Little work has been done on the adsorption of gases on uranium single crystals and the effects of surface structure on the adsorption processes on uranium are unknown.

Once an oxide layer is formed, the adsorption, dissociation and diffusion processes continue, but now the oxide layer itself plays an important role in the further oxidation of the metal. The oxide layer forms a barrier that separates the metal uranium atoms from the adsorbed/chemisorbed oxygen species on the surface of the oxide. In very thin oxide films (<3 nm), quantum mechanical tunneling can be important in the continued growth of the oxide layer. As the oxide thickens, electronic and ionic transport begin to control the continued growth of the oxide.

Nearly-stoichiometric oxides are semiconductors with the conduction thought to occur by the hopping of electrons or holes from one cation to another [5]. Because electronic conduction (electrons and holes) predominates in uranium oxides, the rate limiting factor to further oxidation is the transport of ionic species across the oxide layer. Anionic diffusion is most important because the diffusion coefficient for oxygen is orders of magnitude larger than that for uranium [6].

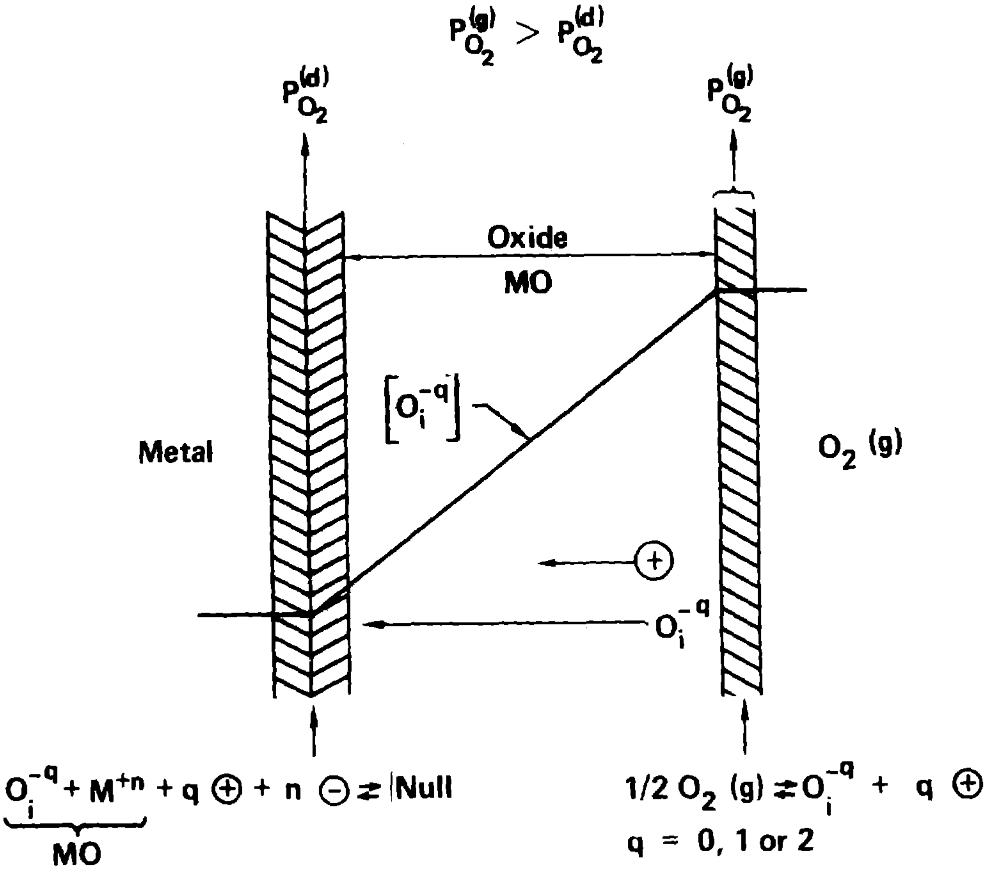
$P_{O_2}^{(g)} > P_{O_2}^{(d)}$
$P_{O_2}^{(d)}$
$P_{O_2}^{(g)}$
Oxide
MO
$[O_i^{-q}]$
Metal
O_2 (g)
⊕
O_i^{-q}
$\underbrace{O_i^{-q} + M^{+n}}_{MO} + q \oplus + n \ominus \rightleftharpoons \text{Null}$
$1/2\, O_2\,(g) \rightleftharpoons O_i^{-q} + q \oplus$
$q = 0, 1 \text{ or } 2$

Fig 2.2.1 Diagram of the oxidation of uranium by an oxygen interstitial transport process.

The intrinsic defect structure of uranium oxides is of the anion Frenkel type (oxygen interstitials and vacancies). In hyperstoichiometric oxides (UO_{2+x}), oxygen interstitials predominate which gives rise to oxidation by an oxygen interstitial transport process in this phase (Fig 2.2.1).

UO_{2+x} is a p-type semiconductor. The majority carriers arise from the transfer of electrons from the O 2p valence band to the vacant U 5f levels (see Fig. 2.2.6). The oxygen molecules chemisorbed on the UO_{2+x} surface oxide layer dissociate and acquire electrons from these levels to produce interstitial oxygen ions that diffuse toward the bulk metal. The dominant mode of oxygen ion transport is thought to be by diffusion through the oxide layer via an interstitialcy mechanism (Fig. 2.2.2) [7]. This involves the displacement of a lattice anion into an interstitial site by an oxygen interstitial which then takes the lattice site. A similar mechanism for OH^- transport has also been proposed [2].

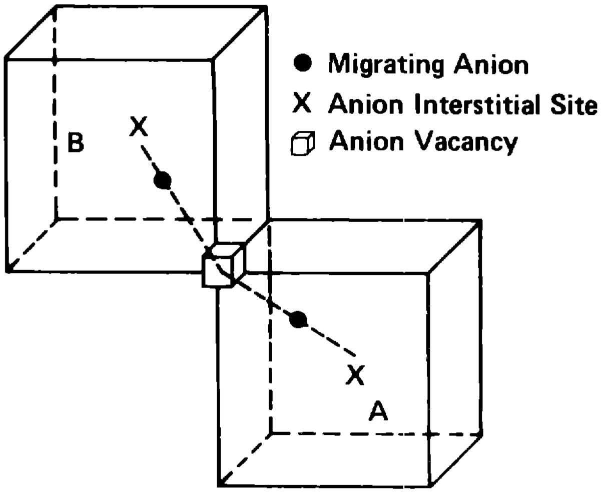

Fig. 2.2.2 Interstitialcy mechanism of oxygen diffusion in UO_{2+x}. A lattice anion moves to an interstitial site in A, and the interstitial anion in B fills the vacant lattice site.

Stoichiometric uranium dioxide crystallizes in the fluorite structure that has cubic symmetry and a coordination number of four. Each uranium atom is at the center of a cube with an oxygen atom at each corner, and each oxygen atom is at the center of a tetrahedron of uranium atoms. In a purely electrostatic approach, uranium ([Rn]$5f^3 6d^1 7s^2$) would give up four electrons to its oxygen ($1s^2 2s^2 2p^4$) neighbors to give $U^{+4}(O^{-2})_2$. However, bonding in uranium oxides is not strictly ionic. There is substantial evidence for at least some covalent character in the bonding [9-11].

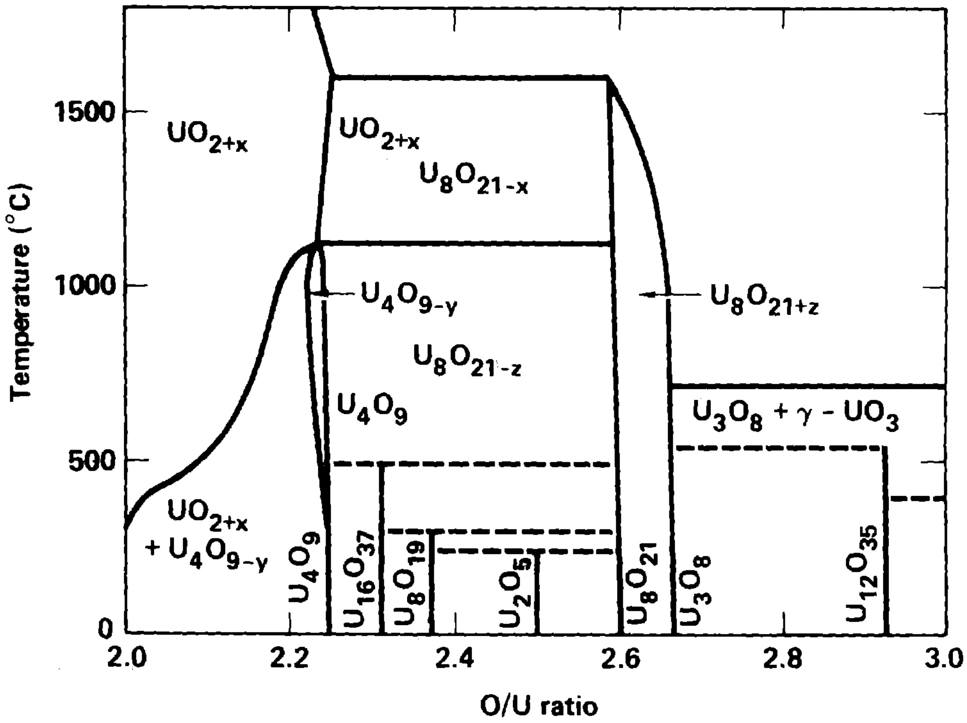

Fig. 2.2.3 Phase diagram of the uranium-oxygen system.

The oxidation of uranium metal by either water vapor, oxygen, carbon monoxide or carbon dioxide results in the formation of a hyperstoichiometric oxide UO_{2+x} for high exposures [12]. The value of x is determined by the gas pressure and the temperature. The phase diagram for the uranium-oxygen system is shown in Fig. 2.2.3 [13].

The uranium sublattice is virtually undisturbed upon further oxidation of UO_2. As oxygen diffuses into the lattice, the fluorite structure is progressively modified and stoichiometric point defects are thought to form into defect complexes. Neutron diffraction studies of $UO_{2.12}$ have shown the most likely model for these complexes to be the 2:2:2 cluster which contains two oxygen interstitials along the (110) direction, two along the (111) direction, and two vacancies in the oxygen sublattice as shown in Fig. 2.2.4 [14].

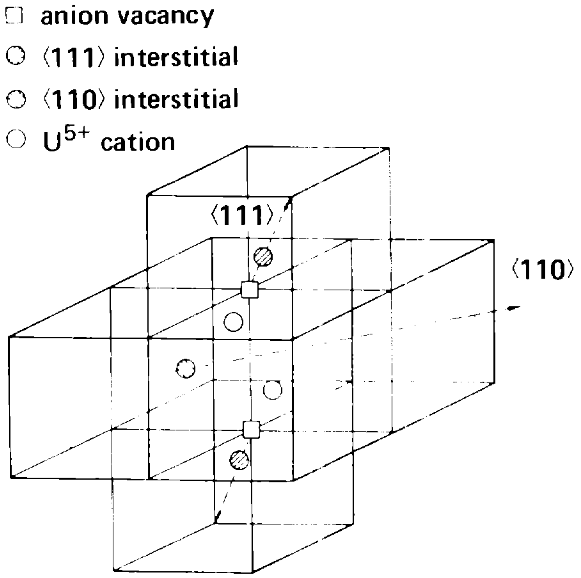

Fig. 2.2.4 The 2:2:2 cluster model.

It has been proposed that at low values of x in UO_{2+x} the 2:2:2 clusters are distributed at random. As x increases, chains of clusters form. As oxidation proceeds toward $UO_{2.25}$, ordering occurs to give the U_4O_9 structure shown in Fig. 2.2.5 [15].

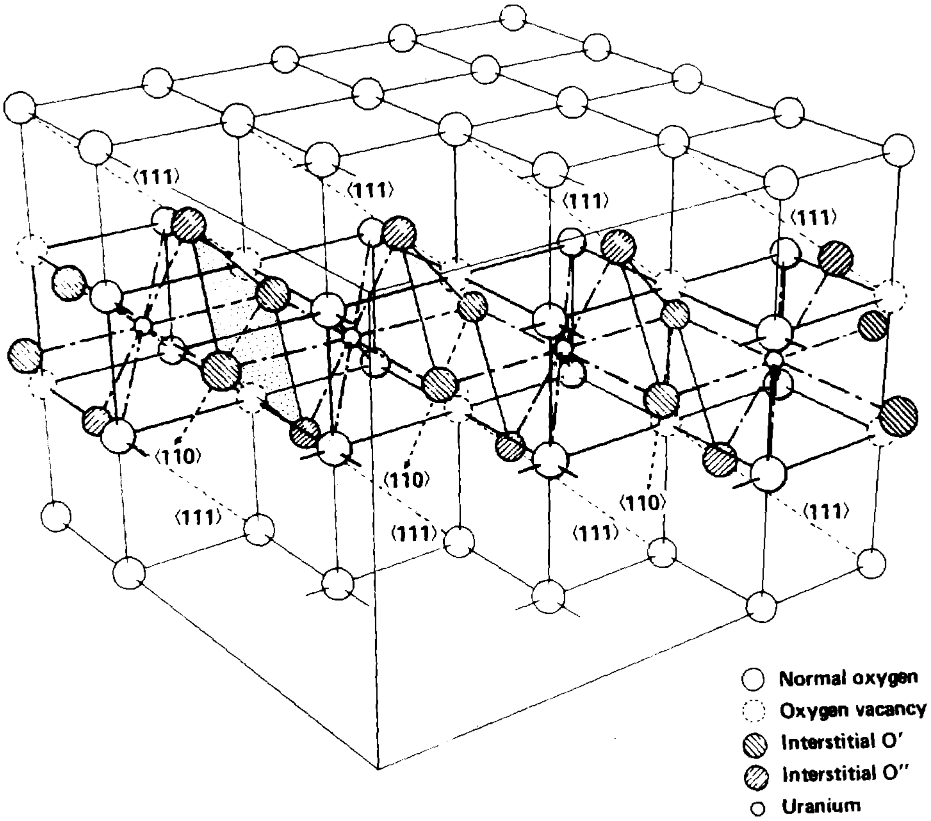
⟨111⟩
⟨111⟩
⟨111⟩
⟨111⟩
⟨110⟩
⟨110⟩
⟨110⟩
⟨111⟩
⟨111⟩
⟨111⟩
⟨111⟩
○ Normal oxygen
◌ Oxygen vacancy
▨ Interstitial O′
▨ Interstitial O″
○ Uranium

Fig. 2.2.5 Structure of U_4O_9.

An approximate band structure of uranium dioxide has been proposed on the basis of reflectance measurements [9] and computer calculations [16], and is shown in Fig. 2.2.6. There is a broad valence band composed of oxygen 2p levels. The conduction band is composed of uranium 6d and 7s levels. There is a narrow set of states between the valence and conduction bands composed of partially localized uranium 5f levels. The degree of localization of these levels is not certain. There is evidence for some mixing of the 5f levels in the character of bonds in uranium oxides. This mixing provides the small amount of covalency that has been implied by some experiments [11]. It has been suggested that the bottom of the conduction band should exhibit some 5f character as well. This is necessary in order to account for the large degree of electron-hole disorder in stoichiometric UO_2. The reaction $2U^{+4}(U\ 5f^2) \longleftrightarrow U^{+5}(U\ 5f^1) + U^{+3}(U\ 5f^3)$ is energetically more favorable than Frenkel pair formation. This leads to the predominance of electronic disorder over atomic disorder in this phase [16].

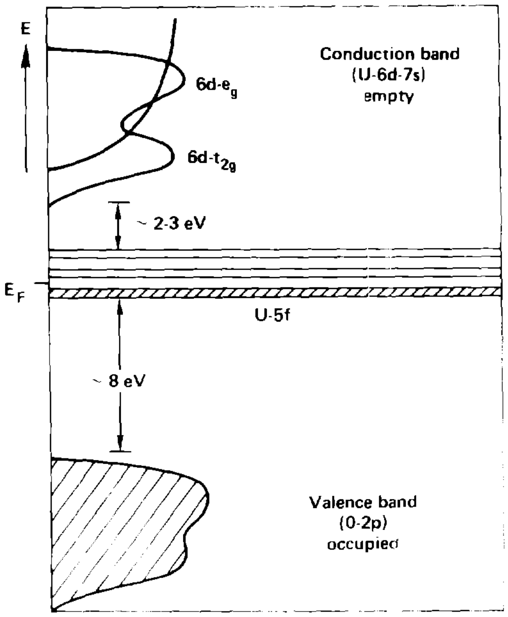

Fig. 2.2.6 Proposed band structure of UO_2. Energies refer to thermal processes as described in ref. [16]

Recently, the oxidation of uranium in atmospheric gases has been studied with thermogravimetric techniques [12]. Interstitial defect clusters were proposed to control the oxidation of uranium in dry oxygen, pure water vapor and low pressure (<1.33 x 10^4 Pa) water vapor-air mixtures. Vacancy-rich defect clusters were proposed to control the oxidation of uranium in high pressure (>1.33 x 10^4 Pa) water vapor-air mixtures. Defect complexes are widely believed to exist in uranium oxides although their presence has not been rigorously proven. Positron annihilation [12,17] and electron paramagnetic resonance experiments [18] have provided further support to the proposed defect cluster-controlled uranium oxidation mechanisms. One particularly interesting result of this study is the quantification of the inhibition of uranium oxidation in water vapor when oxygen is present. This effect is illustrated in Fig. 2.2.7.

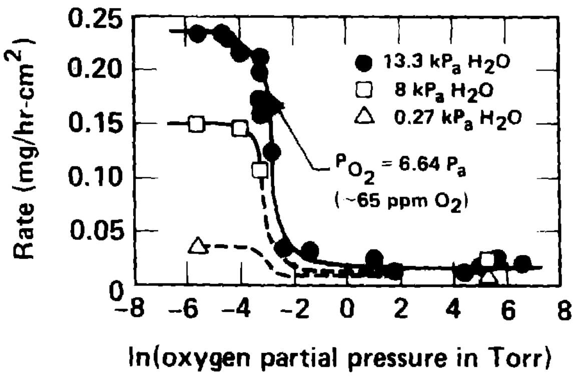

Fig. 2.2.7 Effect of oxygen on uranium-water vapor reaction [12].

Extremely small concentrations of oxygen (~65 ppm) are sufficient to decrease the oxidation rate by an order of magnitude. The sharpness of the cutoff is striking. Colmenares [2] has suggested that chemisorbed oxygen inhibits the hydrolysis of water at the surface which slows the water vapor-uranium reaction. Allen et al. [19] have suggested that oxygen controls the transport of OH^- by forming defect-cluster complexes that impede the diffusion of OH^- interstitials through the oxide layer. It is clear that further investigation of the inhibiting effect of oxygen on the water vapor-uranium reaction is needed.

Most of the work on uranium oxidation has concentrated on the properties of the bulk oxides and the kinetics of oxidation. Few studies of the adsorption of reactive gases such as O_2 or CO on clean uranium surfaces have been done. The study of the oxidation of uranium in water vapor and water vapor-oxygen mixtures with surface-sensitive techniques has been totally neglected until very recently [19]. Studies of this kind are essential for the complete characterization of the oxidation process.

3. SURFACE ANALYTICAL TECHNIQUES

Uranium oxides and uranium oxidation have been studied with a variety of techniques, yet the number of studies employing surface-sensitive techniques are relatively few. In some cases, these studies are less than definitive. Results of early XPS and AES studies of uranium oxides suffer from an imprecise knowledge of the stoichiometry of the samples. This is due to the readiness with which uranium dioxide (UO_2) reacts with oxygen to produce hyperstoichiometric UO_{2+x}. Some of the studies reported to be of $UO_{2.0}$ were in fact of hyperstoichiometric oxides. This has only recently become apparent with the availability of high-resolution XPS data for well characterized samples.

What is meant by a surface-specific analytical technique? Both AES and XPS measure the kinetic energy of electrons that leave the sample during some excitation process. If the measured energy is to be characteristic of the binding energy of the electron in an atom of the solid, it must be able to diffuse to and escape from the solid surface without losing energy through inelastic scattering. The inelastic mean free path of an electron in a solid is the average distance an electron travels in a solid without undergoing inelastic scattering. The dependence of the inelastic mean free path on kinetic energy for many materials is shown in Fig. 3.1.

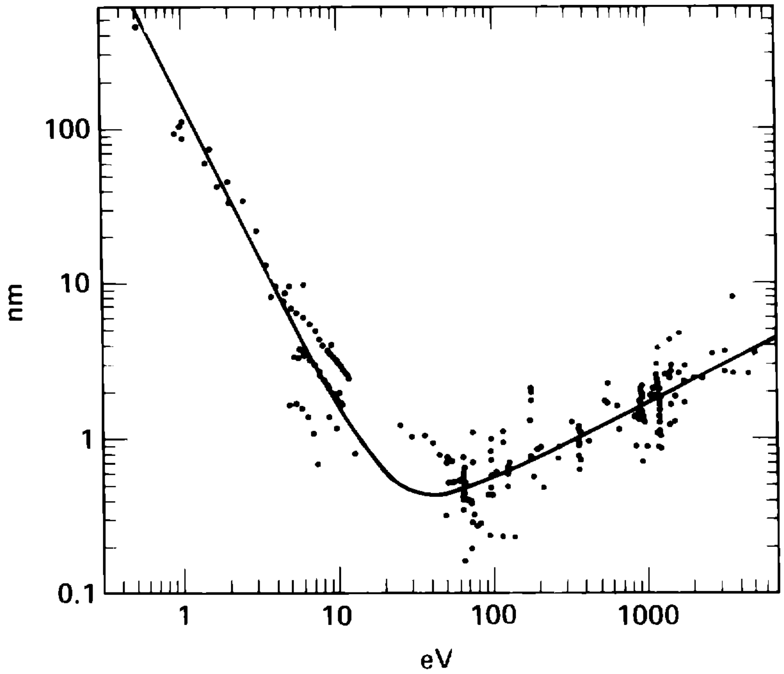

Fig. 3.1 Universal curve for the inelastic mean free path of electrons in a solid [20].

XPS electron kinetic energies of interest typically range from 250 to 1250 eV and those for AES range from 10 to 1000 eV. Information gained from these techniques will then pertain to the first 1-2 nm of the sample surface. These techniques are therefore surface-specific.

TDS is clearly a surface specific technique because it directly measures the amount of surface adsorbate that leaves a sample surface during heating. The situation is not so clear for EIL. The optical mean free path of photons can be determined from optical absorption data. For photons in the range 300-900 nm, which is the range considered in this study, the optical mean free path in uranium dioxide thin films varies from about 75 nm for the near ultraviolet to more than 3000 nm for the near infrared [21]. This data would seem to indicate that EIL is not surface specific because the material 75 nm away from the surface, which is clearly representative of the bulk, can contribute to the luminescence. However clean uranium metal does not exhibit significant luminescence. The luminescence of a uranium surface that has been exposed to small amounts of gas should be indicative of the state of the metal-gas interface, that is, the near-surface region. Thus, luminescence measurements should be sensitive to changes in the the near-surface oxide layer and to the presence of adsorbates on the surface.

Because AES, XPS, TDS and EIL are well established experimental techniques that have been widely used and described, only a brief description of the physical basis underlying each technique is given. The information, both qualitative and quantitative, that can be gained from the application of each technique is specified. The results, if any, of previous investigations of uranium oxide surfaces with the particular techniques are also discussed. In the case of no previous application of a particular technique to the study of uranium, results for other metal surfaces are discussed to give some idea of the type of results one might expect for uranium.

3.1 Auger Electron Spectroscopy

Several excellent reviews of Auger electron spectroscopy have recently appeared in the literature. The review of Auger techniques in analytical chemistry by Riviere [22] contains a fairly comprehensive and up-to-date treatment of the state of the art of Auger electron spectroscopy as applied to corrosion and catalysis studies. The review by Seah [20] emphasizes the application of AES to surface studies of high temperature materials. A somewhat older article by Gallon [23] discusses some of the current (1978) problems in AES. It is useful as a perspective on the development of methods of obtaining quantitative information from Auger spectra as well as providing a wealth of source material for their application.

Consider an electron beam of several keV impinging on a solid surface. The primary beam will penetrate a few microns into the solid and produce a cascade of secondary electrons through the excitation of electrons from the valence band and lower lying atomic core levels. Most of the secondary electrons will diffuse through the solid and lose energy through inelastic scattering. Some will leave the surface of the solid which allows their energy to be measured. A typical plot of the energy distribution of the secondary electrons that leave the surface is shown in Fig. 3.1.1. Most of the secondaries have very low energies, with the distribution slowly tailing off as the energy increases. Superimposed on the tail of the distribution are several small bumps that are due to Auger electron transitions.

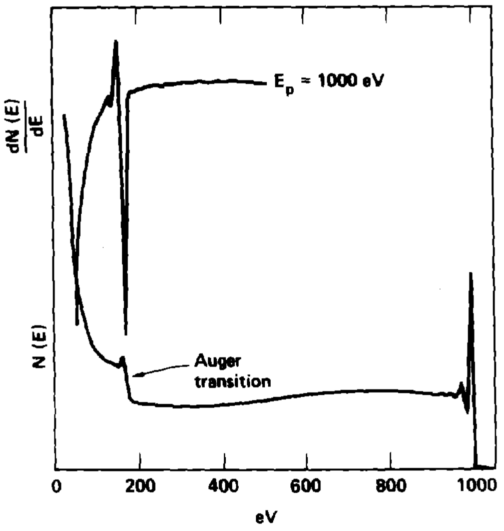

Fig 3.1.1 Secondary electron energy distribution a) N(E) and b) dN(E)/dE.

When a core level of a surface atom is ionized by an impinging electron beam, relaxation of the atom back to its ground state occurs by the filling of the core level with an electron from an outer level as depicted in Fig. 3.1.2. The excess energy corresponding to the difference in binding energies of the two atomic states can appear either as a photon of characteristic energy or as an Auger electron. The two processes compete, but for core level binding energies of less than about 2000 eV, the probability of Auger emission is close to unity. The Auger electron need not come from the same level as the electron that fills the empty core level, but its binding energy is always characteristic of the atom of origin

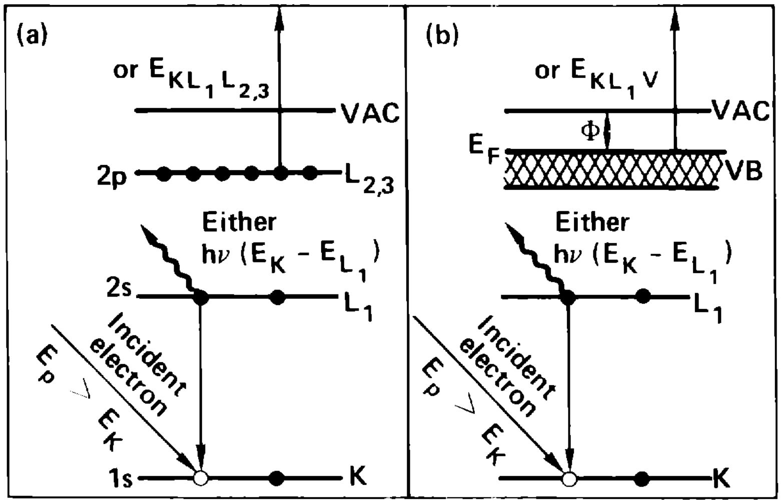
(a)
or $E_{KL_1L_{2,3}}$
VAC
2p
$L_{2,3}$
Either
$h\nu$ $(E_K - E_{L_1})$
2s
L_1
Incident electron
$E_p > E_K$
1s
K
(b)
or E_{KL_1V}
VAC
Φ
E_F
VB
Either
$h\nu$ $(E_K - E_{L_1})$
L_1
Incident electron
$E_p > E_K$
K

Fig. 3.1.2 Diagram of the Auger process a) in an isolated atom and b) in a solid. Φ is the work function of the sample.

Auger electron spectroscopy is a surface sensitive technique. Only Auger electrons that originate within 1 to 2 nm of the surface can escape without loss of energy and give rise to peaks in the secondary electron energy distribution. Because Auger electrons produce small peaks on a broad continuous background, they are more easily detected by differentiating the energy distribution function. Virtually all Auger data then is presented as a plot of dN(E)/dE v.s. E.

AES is most often used as a chemical "fingerprinting" technique. The energy and shape of Auger peaks can be used to unambiguously identify the elemental composition of the solid surface. The peak-to-peak magnitude of the Auger peaks in the differentiated spectrum is directly related to the surface concentration of the element that produced the Auger electron. This is particularly useful in preparing clean metal surfaces because as little as ~0.1 atomic percent of surface impurities such as oxygen or carbon can be detected. AES can be used to determine the approximate stoichiometry of an unknown oxide by comparing the oxygen peak height with that of a well characterized sample.

Shifts in energy or peak shapes often occur in Auger transitions from valence levels (those with low binding energies) when two or more atoms are present on a surface. The chemical interaction of the atoms produces a redistribution of electronic charge which appears as a "chemical shift" in the Auger energy spectrum. Quantitative analysis of these shifts is complicated by the extra ionization that occurs during the Auger transition. However, large changes in the intensity or shape of Auger valence peaks is a clear indication of strong chemical interaction between a substrate and an adsorbed species.

The reaction of clean, high-purity uranium surfaces with dry oxygen has been studied by Ellis [24] with AES. Ellis found that saturation of the near surface with ~150 Langmuirs of O_2, after repeated heating and oxygen exposure, produced UO_2, which upon heating to 973 K gave an O/U ratio of 1.0 in the Auger spectrum. Ellis claimed that this phase was stable UO because the sample could be cycled from 298 K up to 973 K for ~5 min. several times without a change in the O/U ratio. Carbon was not detected so it was concluded that the phase did not require carbon to be stabilized.

McLean et al. [26] performed similar experiments using both XPS and AES. They found that a saturation coverage of ~40 Langmuirs produced $UO_{1.85}$. The low O/U ratio was found to be due to incomplete oxidation of the near surface region because about 10% of the XPS core peak intensities were from unoxidized uranium metal. Similar results were obtained by Nornes and Miesenheimer [27] in their oxidation study of uranium at 120 K. One interpretation is that small domains or islands of oxide dispersed on an underlying uranium matrix were forming. This calls into question the finding by Ellis of a stable UO phase, which may in fact be due to incomplete oxidation of the uranium surface resulting from transport of surface oxygen into the bulk. XPS data for samples prepared under the same conditions as reported by Ellis are needed to prove the formation of a stable UO phase.

In this study, AES is used to monitor the cleanliness of uranium surfaces prior to gas exposures. The peak-to-peak height of the oxygen (KLL) Auger transition is measured as a function of exposure to various gases to determine the saturation curves for clean uranium surfaces.

3.2 X-Ray Photoelectron Spectroscopy

X-ray photoelectron spectroscopy is a well established surface analytical technique that has recently been reviewed by Riviere [28]. Experimentally, the sample surface to be analyzed is irradiated with monoenergetic X-rays from the Kα transitions of either aluminum (1486.6 eV) or magnesium (1253.6 eV). The X-rays travel several microns into the sample and transfer all of their energy to electrons in the atoms of the solid. If the photon energy is greater than the binding energy of an electron in an atom, the electron can leave the atom, diffuse to the surface and be ejected as a photoelectron. This process is shown schematically in Fig. 3.2.1.

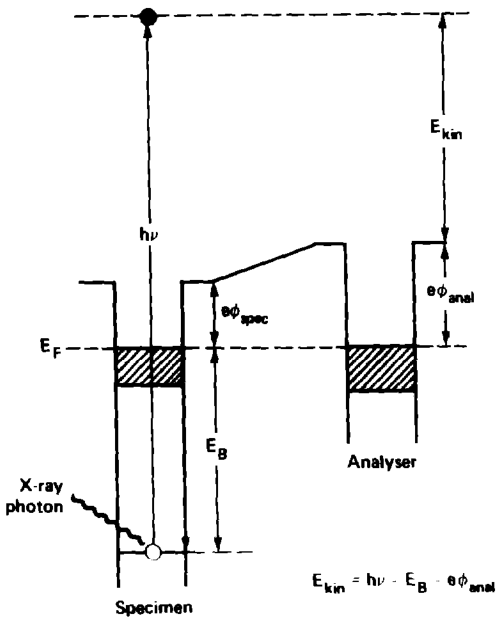
E_{kin}
hν
$e\phi_{anal}$
$e\phi_{spec}$
E_F
E_B
Analyser
X-ray photon
$E_{kin} = h\nu - E_B - e\phi_{anal}$
Specimen

Fig. 3.2.1 The photoelectric effect.

The kinetic energy of the electrons as measured by the analyzer is directly related to their binding energy. Because no two elements have the same set of atomic binding energies, XPS is able to provide elemental compositional analysis of the surface just as is AES. However AES is an order of magnitude more sensitive to surface contaminants such as oxygen and carbon [29] so that elemental analysis is not the prime application of XPS data. Chemical interaction of an atom with other atoms involves electronic charge transfer or charge sharing which may result in shifts in the binding energy of core and valence electron peaks, just as in AES. These "chemical shifts" are easily measured in XPS and usually easier to interpret than those in AES measurements. The ability to provide both compositional and chemical information about a surface is the main strength of XPS.

The narrowest and usually most intense features of an XPS spectrum are the photoelectron peaks arising from the direct excitation of electrons in core levels with high binding energy. Valence levels have low binding energies and therefore electrons from valence levels have high kinetic energy. The larger escape depth of these electrons makes the valence peaks broader, less intense, and less characteristic of conditions at the surface than other features in the spectrum.

Quantitative analysis of XPS spectra peak heights and peak areas can provide an estimate of the relative concentrations of surface species. Shifts in core level peaks and the appearance of satellite peaks in the spectra indicate a changing chemical environment and can be quantitatively correlated to the stoichiometry of the surface oxide layer. Non-destructive depth profiling of the surface may be accomplished by varying the angle of the sample surface with respect to the analyzer. Electrons emitted at a small angle relative to the surface tangent are more characteristic of the state of the surface than electrons emitted at larger angles. In this work, the angle is varied with the use of an acceptance slit in the electron analyzer itself so that the flux of incident photons impinging on the sample surface remains constant. Chemical information concerning the chemical distribution of the oxide layer can be obtained in this manner.

Allen et al. have studied the oxidation of clean uranium in dry oxygen with XPS [30]. With successive exposures to oxygen they produced oxides from $UO_{2.0}$ to $UO_{2.07}$ respectively. They also studied well characterized samples of U_3O_8 and U_4O_9 with XPS. A comparison of their results with those for a well-defined $UO_{2.001}$ sample showed that the binding energy of several satellite peaks was shifted in direct proportion to the increase in oxygen content of the samples. This correlation of stoichiometry and shifts in XPS spectral peaks has been confirmed in studies by McLean et al. [26], Nornes and Meisenheimer [27], and Teterin et al. [31] and is illustrated in Fig. 2.3.1.

Only two studies of the uranium-water vapor reaction with surface-sensitive techniques have been performed. Nornes and Meisenheimer [27] exposed clean, high-purity uranium surfaces to water vapor at 120 K and followed the reaction with XPS measurements. They reported three oxygen peaks in the XPS spectrum ascribed to condensed water, oxide formation and an OH-complex with the uranium surface.

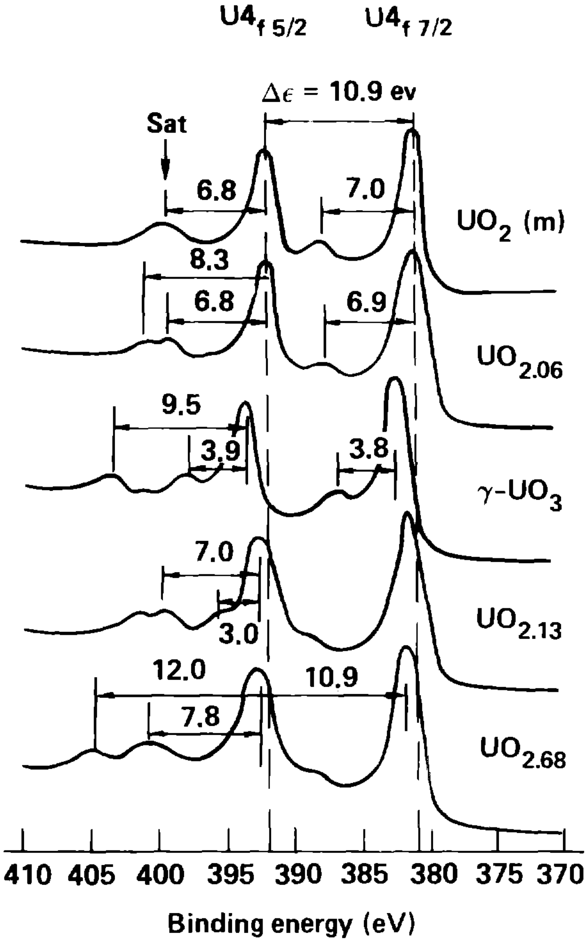

Fig. 2.3.1 XPS spectra for various uranium oxides (Ref. 2,30).

The base pressure in their analysis chamber was in the low 10^{-9} torr range and practical experience suggests that this is too high a pressure to maintain clean uranium surfaces for more than a matter of seconds. Given that small partial pressures of oxygen can have a large effect on the reaction of uranium with water vapor, the results of their study are probably characteristic of the reaction of water vapor with an oxygen-covered uranium surface. Their observation that the reaction rate for water vapor with uranium was slower than the corresponding reaction rate for oxygen supports this view.

Allen et al. [19] studied the reaction rate of clean uranium exposed to water vapor and water vapor-oxygen mixtures with XPS. They found that water vapor reacted more rapidly with clean uranium than dry oxygen contrary to the findings of Nornes and Meisenheimer. They also found that the presence of oxygen retarded the water vapor-uranium reaction. They suggested that oxygen controls the transport of OH^- through the oxide layer by forming defect-cluster chains that would migrate more slowly and thereby impede the diffusion of OH^- interstitials. They observed none of the structure in the core level satellite peaks after water vapor exposure that is characteristic of defect cluster formation. They postulated that this was due to the involvement of OH^- in the surface oxide growth and the presence of hydrogen in the surface film.

It is clear that further investigation of the early stages of uranium oxidation in water vapor and oxygen-water vapor mixtures is needed. This is the focus of the present study, where detailed XPS measurements of clean and oxygen-predosed uranium surfaces exposed to water vapor are performed. Luminescence and thermal desorption measurements are made along with the XPS measurements to characterize more completely the surface oxides.

3.3 Thermal Desorption Spectroscopy

Thermal desorption spectroscopy (TDS), first described by Apker [32] and later developed by Redhead [33] for the study of gas desorption from filaments, has been increasingly used for the characterization of adsorption on metal surfaces The technique has been reviewed by King [34], and more recently by Menzel [35]. Experimentally, the sample is exposed to a measured amount of gas at low temperatures, heated at a constant rate, and the pressure in the continuously pumped system recorded as a function of temperature generating a desorption trace. The rate of desorption per unit sample surface area, A, is given by

$$dN/dt=(V/AkT)[dP/dt+(S/V)P]$$

where N is the surface coverage in molecules/cm^2; P is the partial pressure of the desorbed species; V is the volume of the desorption chamber; S is the effective pumping speed k is Boltzmann's constant and T is the gas phase temperature. If the pumping speed is high and the heating rate is low, the desorption rate is proportional to the partial pressure of the desorbing gas.

In addition to the identification of different adsorption states, TDS measurements can provide useful information about the adsorption process. Changes in the desorption peaks as a function of initial adsorbent coverage can yield an estimate of the desorption reaction order, which may indicate whether the adsorption is dissociative. Qualitative changes in the desorption spectra after co-adsorption of different molecular species may indicate the presence of adsorbate-adsorbate interactions.

Quantitative analyses of desorption peaks usually rely on the Polanyi-Wigner model which assumes that the rate of desorption from a surface species in some state i can be written in the form

$$-dN_i/dt=\nu_i N_i^{x_i}\ e^{(-E_i/RT)}$$

where x_i is the reaction order for desorption from state i; ν_i is a frequency factor and E_i is the desorption activation energy. This expression is identical to that used in the analysis of thermoluminescence glow curves [34,35]. Because adsorption on metal surfaces is generally a non-activated process, the desorption activation energy E_i is approximately equal to the differential heat of adsorption, which is a measure of the chemisorption bond energy.

TDS has not been applied to the study of adsorption on uranium surfaces, but several recent studies of H_2O adsorption on clean and oxygen-predosed single-crystal, transition metal surfaces with TDS serve to illustrate its application.

Jupille et al. [38] studied H_2O adsorption on clean and oxygen-predosed Re(0001) surfaces with TDS. They found that oxygen preadsorption prevented the dissociation of water but did not affect the H_2O sticking probability, indicating that the influence of oxygen was limited to the first layer of adsorbed water. Stuve et al. [39] studied the adsorption of water on clean and oxygen-predosed Pd(100) by TDS, EELS and LEED. They found that H_2O adsorbed molecularly on the clean surface and exhibited two desorption states, one due to multilayer ice and the other due to H_2O directly bonded to the surface. H_2O adsorbed on an oxygen-precovered surface reacted to produce stable OH groups for oxygen coverages of less than 0.22 monolayers, but for higher coverages, the oxygen was found to block the initial adsorption of water molecules.

These two studies illustrate the kind of information that is possible to obtain from TDS and provide some insight into possible mechanisms for the inhibition of the water vapor-uranium reaction by oxygen. In this study, TDS measurements are performed after exposing clean and oxygen-covered uranium to water vapor at 100 K.

3.4 Electron-Induced Luminescence

An idealized model of an electronic semiconductor contains a filled valence band, an empty conduction band, and a small energy gap of several electron volts between them. Based on the approximate band diagram in section 2, this model provides an adequate description of uranium oxides for a discussion of the processes that occur during luminescence.

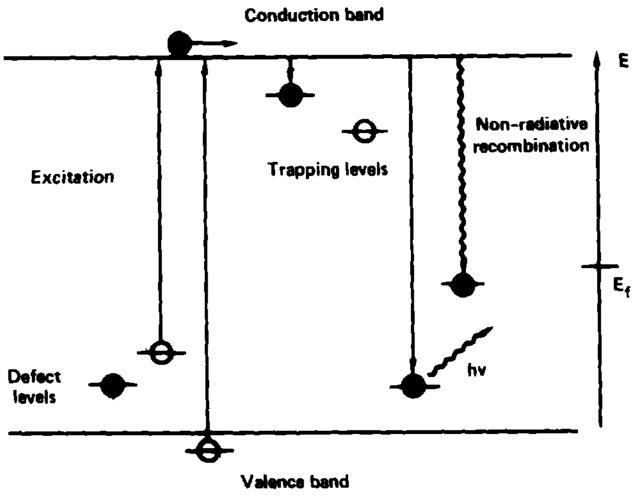
Conduction band
E
Non-radiative recombination
Excitation
Trapping levels
E_f
Defect levels
hv
Valence band

Fig. 3.4.1 Luminescence model; filled and empty circles represent occupied and unoccupied electronic levels respectively.

A typical luminescence transition for such an idealized model is illustrated in Fig. 3.4.1. Energy is absorbed by the crystal from the excitation source, in this case, medium-energy (5 keV) electrons. Some of this energy is transferred to an electron in or near the valence band. The electron is promoted to the conduction band where it is free to travel throughout the crystal. The electron may fall directly into a recombination center with the emission of a photon, decay non-radiatively to a recombination center releasing its energy as heat to the crystal or become trapped in a metastable state near the conduction band. If the electron is trapped, it can be released by the energy of thermal vibrations in the crystal to return to the conduction band and wander again through the crystal

Electron excitation is accompanied bv strong perturbations of the entire crystal lattice. Primary electrons lose energy through the production of secondary electrons by the ionization of lattice ions. The secondaries continue to diffuse through the crystal creating more secondaries until the electrons become thermallized. The intensity of the luminescence increases as the beam voltage and current density increases [40].

As previously stated, point defects composed of oxygen vacancies and interstitials are the dominant stoichiometric defects in uranium oxides. Free electrons and holes produced by external excitation that wander near the defects can be attracted to them and bound coulombically. The trapped charges occupy localized energy levels in the normally forbidden band gap. A study of optical transitions involving these levels can provide detailed information about the nature of the trapping sites and the defects responsible for their formation. Monitoring the changes in the luminescence spectra as a function of oxidation conditions can aid in the determination of likely oxidation mechanisms.

Several studies of the optical properties of uranium ions existing as dopants in other materials have been made [39-42], but no known investigations of the luminescence of uranium oxides have been performed. However, studies of the luminescence properties of thorium oxides have been done [45-47] and provide some guide to the applicability of luminescence techniques to the study of surface reactions on uranium.

Rodine [45] studied the thermoluminescence of thoria doped with rare earths and correlated his results with electron paramagnetic resonance (EPR) data obtained on the same samples. He concluded that oxygen vacancies were the key defects giving rise to the thermoluminescence. Bastasz et al. [46] followed the reaction of oxygen on a clean thorium surface with AES and EIL (cathodoluminescence). They found that the intensity of the luminescence induced by electron bombardment was affected by both the oxygen pressure at the surface and by the total amount of adsorbed oxygen. On the basis of AES data they concluded that the two types of luminescence they observed were due to a weakly adsorbed molecular species in the case of the strong, pressure-dependent luminescence, and to a chemisorbed species in the case of the less-intense, pressure-independent luminescence. Their study demonstrated that luminescence intensity measurements can provide important information about adsorbates on surfaces that may not be obtainable by other means. Vook et al. [47] examined the cathodoluminescence of thorium metal surfaces exposed to various gas mixtures. The luminescence was interpreted as arising from the formation of ThO_2 and the excitation of F-centers in the form of oxygen vacancies Exposure to CO was found to leave as much oxygen on the surface as exposure to O_2, but did not produce appreciable luminescence.

Luminescence measurements can provide qualitative information regarding the relative concentration of defects and can be sensitive to the concentration of adsorbed gases. Qualitative differences should appear in the spectra of samples prepared in different oxidizing environments. These differences can be related to differences in the defect structure of the various oxides.

Luminescence measurements are performed on samples prepared from clean uranium surfaces exposed to increasing amounts of dry oxygen, carbon monoxide and pure water vapor. All exposures are performed at room temperature. Emission spectra are measured at various temperatures between 80 K and 298 K.

4. EXPERIMENTAL APPARATUS AND PROCEDURES

The experimental measurements were performed in two separate ultra-high vacuum systems. The majority of luminescence and thermal desorption measurements were performed in one system, hereafter referred to as system A, while the XPS measurements were performed in system B. Many of the Auger and thermal desorption experiments were carried out in both systems to test the reproducibility of the data. The use of two separate systems was necessitated by the lack of XPS capability in the system originally chosen for this study and the subsequent need for XPS measurements.

This section is organized into three parts. The first describes the analysis chambers, the procedures and apparatus for gas handling and the method for controlling the sample temperature. The second part contains the details of sample preparation where procedures for sample cleaning and exposure to reactant gases are given. The experimental aspects of making the measurements are discussed in the last part. A description of the measurement equipment and detailed experimental procedures are given, as well as methods of recording and storing the data.

4.1 Experimental Apparatus

Both systems A and B consisted of standard stainless-steel ultra-high vacuum chambers with base pressures below 1 x 10^{-8} Pa. The vacuum was maintained for each system by a liquid nitrogen (LN)-trapped diffusion pump and an ion pump equipped with a water-cooled titanium sublimator. Pressure in the sample chambers was monitored with a single Bayard-Alpert ionization gauge operated at 10 μA current.

Sample chamber A was equipped with a single-pass cylindrical mirror analyzer (CMA) for Auger electron analysis; a 0-5 keV sputter-ion gun for sample cleaning; a quadrupole mass spectrometer for residual gas analysis and a 0-5 keV grazing incident electron gun for luminescence excitation.

System B was equipped with a scanning Auger microprobe (SAM) (single-pass CMA) for Auger electron analysis; an AES/XPS double-pass CMA for XPS measurements; a differentially-pumped sputter-ion gun for sample cleaning; a dual-anode X-ray source for XPS excitation; a quadrupole mass spectrometer and a grazing incident electron gun.

Thermal desorption experiments required temperatures below 100 K and the ability to increase the temperature in a linear fashion. Sample cooling was also desirable for luminescence and XPS measurements. For this purpose, a liquid nitrogen-cooled cold finger was designed and constructed as shown in Fig. 4.3.

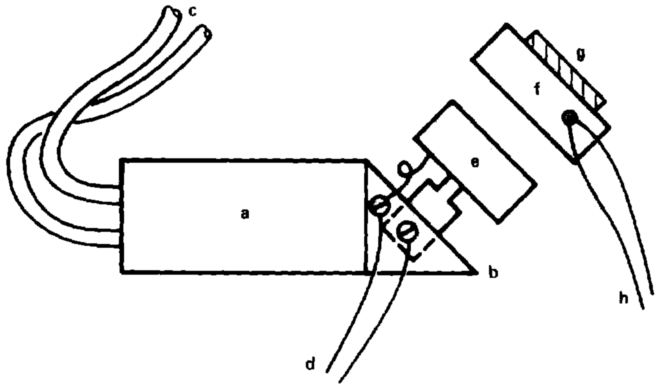

Fig. 4.3 LN-cooled cold finger and sample mount; a) Reservoir, b) Copper plug, c) Supply lines, d) To DC power supply, e) Sample heater, f) Sample cap, g) Sample, h) Thermocouple junction.

The cold finger consisted of a thin stainless-steel cylinder with a copper plug vacuum-brazed onto one end. The copper plug, whose face was oriented 60 degrees with respect to the horizontal, was designed to hold a Varian 50 W molybdenum sample heater, on which the sample was mounted. A detailed discussion of sample mounting procedures is given in section 4.2. To cool the sample, liquid nitrogen at ~20 psi was circulated through the sixteenth-inch diameter stainless-steel lines that supplied and vented the cold finger reservoir. Cooling from room temperature to 80 K took about five minutes. The sample temperature could be varied from 80 K to 1100 K.

A simple temperature programmer was constructed to produce the required linear heating. The initial temperature and desired heat rate were set on the programmer which monitored the temperature via the thermocouple *emf*. Using standard feedback techniques, the heater was supplied with whatever power was required to make the thermocouple voltage increase at a linear rate. By maintaining a flow of liquid nitrogen during heating, the sample could be cycled from 80 K to 373 K continuously while maintaining linearity in the heating rate to within 2%.

Each of the experimental systems included an inlet system for the introduction of gases into the sample chambers. Bottles of research-grade oxygen (99.997%), carbon monoxide (99.999%) and carbon dioxide (99.999%) were mounted on precision leak valves attached to the inlet system, shown in Fig. 4.4. Prior to opening the gas bottle valves, the inlet lines to the bottles were evacuated to below 0.133 Pa with a LN-trapped mechanical pump. The inlet lines were flushed several times by cracking open the gas bottle valve with the leak valve closed to fill the inlet line, then closing the gas bottle valve and evacuating the line by opening the leak valve. This procedure removed water vapor and air adsorbed on the teflon packing of the gas bottle valve. After flushing, the inlet lines were heated to ~373 K and pumped on for several hours with the diffusion pump to minimize water vapor contamination. After the inlet lines cooled to room temperature and the pressure in the main chamber fell below 6.7×10^{-7} Pa, the leak valves were closed and the gas bottle valves fully opened. During exposures, the gases were bled into the vacuum chamber through the leak valves without further preparation.

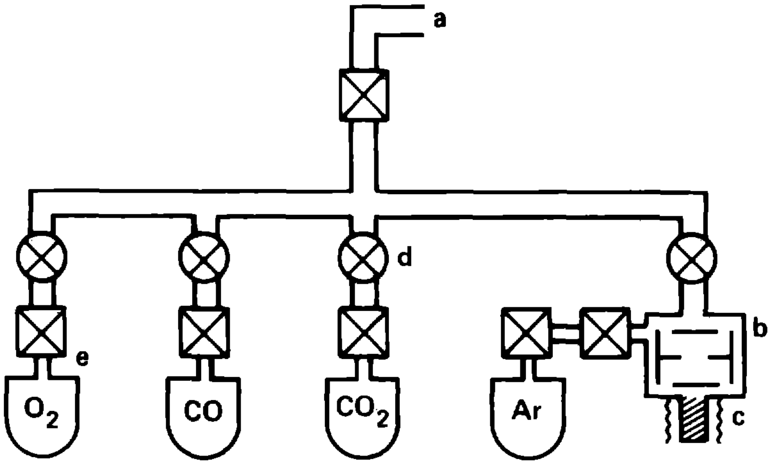

Fig. 4.4 Gas Inlet System; a) To sample chamber, b) Baffled chamber, c) Calcium with heater, d) Leak valves, e) Gas bottles.

Argon used for sputter-cleaning was stored in a three liter chamber containing a calcium getter for the removal of water vapor and oxygen. Before introducing the research grade argon (99.9998%) into the chamber, it was evacuated to less than 0.133 Pa with a LN-trapped mechanical pump. The chamber walls were then heated to ~425 K and the calcium heated to 955 K to coat the baffles of the chamber with calcium by evaporation. When the pressure fell to below 0.133 Pa during this heating, the mechanical pump was valved off and the chamber opened to the diffusion pump. The chamber was evacuated to less than 4×10^{-4} Pa before it was isolated from the pumps and then filled to 20 psi with argon. After several minutes the heat was reduced, but only to 373 K to prevent a protective oxide layer from forming on the calcium. A single charge of argon prepared in this manner would last for several months of sputtering. This procedure was followed every time the system was brought up to atmospheric pressure because the system was backfilled with argon through the calcium getter chamber. Contamination of the argon prepared as above was estimated to be less than 1 ppm for both oxygen and water vapor based on a residual gas analysis of the argon with the quadrupole mass spectrometer.

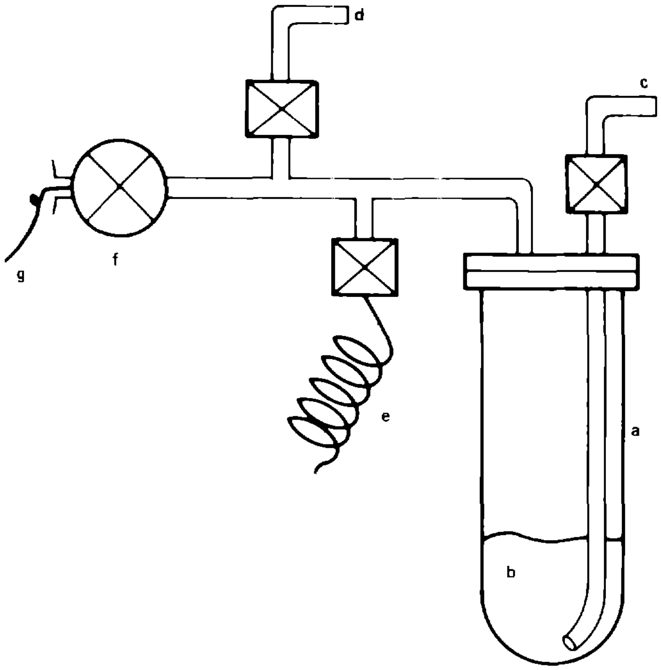

Fig. 4.5 Water vapor handling apparatus; a) Quartz envelope, b) Water, c) Argon purge inlet, d) To mechanical pump, e) Copper coil for purge exhaust, f) Leak valve, g) Dosing needle.

The apparatus for delivering water vapor to the sample is shown in Fig. 4.5. Doubly-distilled, de-ionized H_2O or spectroscopically pure

D_2O obtained from Aldrich Chemical Company was used for the water vapor exposures. The water was contained in a quartz envelope that was fused to a kovar sleeve attached to a stainless-steel conflat flange. A stainless-steel tube dropped down from the mating flange to the bottom of the envelope and was used to pass research grade argon through the water to remove all traces of air, especially oxygen. The argon was passed through the water and out through an opening in the mating flange to a long coil of 1/8 in. id copper-tube that was used to prevent the back diffusion of air during purging. After a thorough argon purge of ~10 minutes, the envelope was evacuated to the vapor pressure of water (~2.26 kPa at 298 K) by a LN-trapped mechanical pump.

During exposure, the water vapor in the envelope passed through a precision leak valve to a sixteenth-inch diameter stainless-steel capillary whose opening could be positioned directly in front of the sample. The calibration of exposures through the capillary is discussed in section 5. Contamination of the water vapor by oxygen was estimated to be less than 1 ppm based on a residual gas analysis with the quadrupole mass spectrometer.

4.2 Sample Preparation

Substitutional impurities with valences different than that of uranium (U^{+4}) can alter the electronic defect density and therefore affect the oxidation processes of uranium Similarly, luminescence measurements can be sensitive to small amounts of rare earth impurities that can interfere with the luminescence of the oxides themselves. The use of high-purity uranium metal ensured that the effects of substitutional impurities were minimized. The high affinity that uranium has for surface contaminants such as carbon and oxygen required unusual care in the production and maintenance of clean metal surfaces prior to exposure to reactant gases. Ultra-high vacuum (UHV) conditions ($<1 \times 10^{-8}$ Pa) had to be maintained in order to limit the contamination of the clean surface by residual gases in the vacuum system before exposures.

High-purity (<100 ppm total metallic impurities) polycrystalline depleted uranium metal coupons (6 mm x 6 mm x 1 mm) were prepared for mounting in the UHV system by first etching in a 50%-50% solution of distilled water and nitric acid (Analytical Reagent 70% HNO_3) for ~5 minutes to remove surface oxide layers, and then rinsing in ethyl alcohol. The samples were then mechanically polished with silicon carbide paper (280 grade) until all gross macroscopic defects (deep scratches, cut marks, inclusions etc.) were removed. They were further polished with fine silicon carbide paper (600 grade) until their surfaces appeared smooth and uniform. At this stage, the samples were shiny and had a silvery color. The impurity analysis of the uranium samples is given in Table 4.2.1.

Element	Oxidation States	Impurity Level(ppm)
C		19
N		17
O		18
Ca	+2	0.2
Mo	+6	0.03
Ti	+2,+3,+4	0.2
Al	+3	10
As	+3,+5	0.06
Nb	+3,+5	0.01
Cr	+2,+3,+6	3.1
Ni	+2,+3	5
Si	+2,+4	10
P	+3,+5	1.2
W	+6	0.05
Cu	+1,+2	2
Pb	+2,+4	3.6
Sr	+2	0.01
Zn	+2	10
Fe	+2,+3	12
Mg	+2	11
Mn	+2	7.7
Total Metallic Impurities (including unlisted elements)		97

Table 4.2.1. Impurity Analysis of Uranium Samples.

The samples could not be mounted directly on the Varian 50 W molybdenum heater because either molybdenum diffusing through the sample upon heating or molybdenum sputtered from the heater could contaminate the sample. A 0.5 mm thick uranium-foil cap was machined for use as a buffer between the heater and the sample. The cap was etched and polished as described above. The sample was spot-welded to the cap to provide good thermal contact. The mounted sample was next polished with 6 μm diamond paste. After a final polish with 1 μm diamond paste, the sample was ultrasonically cleaned in distilled water and mounted on the molybdenum heater.

The cap was fashioned to fit snugly over the heater to maintain good thermal contact between the heater and the sample. The heater was coated with a MgO/methanol slurry to minimize the potential for alloying between the molybdenum heater and the uranium cap. A type K thermocouple junction was wrapped with tantalum foil and spot-welded to the side of the cap to monitor the sample temperature. The tantalum foil prevented the alloying of the thermocouple metals with uranium in the cap. The heater with the sample was then placed on the liquid nitrogen-cooled cold finger.

The thermocouple measured the temperature of the side of the cap and not of the sample surface. However, the temperature gradient between the sample surface and the cap was estimated to be small because of the good mechanical contact between the sample and the cap. Also, the small mass of the sample compared to that of the cap ensured temperature uniformity. Measured temperatures are estimated to be accurate to within 5%.

As soon as the heater was mounted, the manipulator was placed in the UHV system and the chamber was evacuated. A system bake-out at 425

K for 48 hours produced the desired pressure (~1 x 10^{-8} Pa) in the sample analysis chamber.

The sample surface was sputtered at 298 K with 2-3 keV Ar^+ ions (5.2 x 10^{-3} Pa Ar) at ~20 $\mu A/cm^2$ until the oxygen (KLL) Auger signal was no longer detectable. This took about eight hours. The sample was then slowly heated to 1073 K while sputtering, its temperature maintained at 1073 K until no oxygen could be detected, and then allowed to cool to room temperature while still sputtering. The sample was then annealed in vacuum at 1073 K for several minutes and allowed to cool. This sputter-anneal process was continued until the surface remained free of oxygen and other contaminants from the residual gas for at least several minutes at room temperature. The uranium surface remained clean (<0.1% of a monolayer of oxygen) for typically three minutes in flowing argon. This was enough time to pump out the excess argon from the chamber and introduce the reactant gas into the system before contamination of the sample by residual CO occured.

All gas or vapor exposures were performed in a dynamic mode, with the gas flowing from the leak valve to the sample chamber and out through a throttled gate valve to the diffusion pump. Before exposing the uranium surface to reactant gas, it was sputter-cleaned while monitored with AES to ensure that a clean surface had been obtained. The standard of cleanliness is discussed in section 5. Sputtering took place in a dynamic flow of argon through the chamber. During sputtering, the ion pump was turned off and the ion pump valve left open to allow the active titanium surfaces to remove any remaining impurities in the argon. Just before the introduction of a reactant gas to the system, the argon was valved off and rapidly pumped out. When the pressure reached below 2.6 x 10^{-7} Pa (~1 minute), the ion pump was turned on and isolated from the sample chamber. The pressure dropped below 1.33 x 10^{-7} Pa after 2 minutes whereupon the reactant gas was introduced at the appropriate pressure (usually 6.6 x 10^{-6} Pa). All exposures were measured in Langmuirs (1 L = 1.33 x 10^{-4} Pa-s) and calibrated to provide an estimate of the surface coverage as described in section 5. The sample was thoroughly cleaned between exposures either by sputter cleaning at room temperature or by sputter-anneal cycling in the case that oxygen could not be removed easily from the sample surface.

4.3 Experimental Procedures

4.3.1 AES

AES measurements were performed with a standard Physical Electronics (PHI) single-pass cylindrical mirror analyzer (CMA) in system A, and with a PHI AES/XPS double-pass CMA or a single-pass scanning Auger microprobe (SAM) in system B. The samples were excited by an electron beam from the analyzer at either 3 or 5 keV at typical beam currents of 20 μA. Before acquiring Auger spectra, the sample was always aligned with the spectrometer such that the maximum elastic peak signal from a 2 keV electron beam appeared at the 2000 eV analyzer ramp voltage. This was done to maximize the Auger signal and to provide a reproducible starting point for the Auger measurements.

Auger measurements of clean and exposed samples were performed for electron kinetic energies between 50 and 1000 eV because all elements have strong Auger peaks in this range. During Auger measurements, the electron energy analyzer was ramped from 50 to 1000 eV with a peak-to-peak modulation voltage between 1 and 6 eV. Electrons collected by the analyzer were measured with an electron multiplier operating between 1000 and 1200 V. The signal was passed to a lock-in amplifier where it was electronically differentiated. In system A the Auger spectra were displayed on an oscilloscope and recorded on a chart recorder. In system B, a Nicolet multichannel analyzer was used to record the spectra which were transferred directly to a PDP-11/23 computer system for storage and analysis.

The Auger spectrum from a sample was continuously monitored on an oscilloscope during sputter-cleaning. When the Auger O (KLL) transition signal could no longer be detected, the sample was considered clean (more about the standard of cleanliness in the next section). Before a reactant gas exposure, the argon in the chamber was pumped out, all filaments except the ionization gauge and electron beam were turned off and the reactant gas was let into the chamber at 6.6 x 10^{-6} Pa. The oxygen (KLL) transition signal was then recorded at one minute (3 L) intervals for up to 20 minutes (60 L). A plot of the O (KLL) peak-to-peak intensity v.s. exposure allowed a direct determination of the exposure required for saturation. The Auger spectrum from 10 to 700 eV was also recorded at regular intervals to monitor changes in the surface composition as a function of exposure.

4.3.2 XPS

The samples were aligned for the XPS measurements by adjusting the position of the sample in front of the electron analyzer to maximize the Auger elastic peak signal at 2000 eV. The dual-anode (Mg or Al) X-ray source was positioned close to the sample surface at grazing incidence and adjusted to maximize the photoelectron signal. Thus both

AES and XPS measurements could be performed without having to reposition the sample.

The X-ray source was operated at 300 watts and illuminated a spot approximately 4 mm x 10 mm. All measurements were made using the Mg anode which produced Mg Kα radiation at 1253.6 eV that was partially filtered to reduce bremstrallung.

The analyzer had an aperture that was adjusted to accept only photoelectrons from a 4 mm diameter circular area of the sample. The analyzer was calibrated by adjusting the ramp energy to the Au $4f_{7/2}$ photoelectron peak at 84.0 eV and the Cu $2p_{3/2}$ photoelectron peak at 932.6 eV. The analyzer was operated in the pulse-counting mode with a pass energy of 50 eV; at this energy, the Au $4f_{7/2}$ photoelectron peak full width at half maximum (FWHM) was 2.2 eV. Multiple scans were accumulated at a 10 eV/s scan rate to obtain a good signal-to-noise ratio. XPS spectra were recorded by a Nicolet multichannel analyzer and were transferred directly to a PDP 11/23 computer system for storage and analysis.

XPS spectra of clean uranium, and clean uranium exposed to dry oxygen and pure water vapor were taken at room temperature to compare the oxides produced by the two reactants.

Clean and oxygen-covered uranium surfaces were cooled to 85 K and exposed to various amounts of water vapor through the capillary doser. Several minutes after the exposure, the chamber pressure returned to the low 10^{-8} Pa range and the X-ray source was turned on. The sample was then heated to drive off the condensed water vapor. Because the pressure in the chamber could rise several orders of magnitude near a desorption peak, the X-ray source was turned off during this heating. When a particular temperature of interest was reached, the sample would be rapidly recooled to lower the pressure and the XPS spectra were recorded. In this way, the water vapor reaction with the surface could be slowed and studied in various stages of completion.

4.3.3 TDS

Before exposing a clean uranium sample to water vapor for thermal desorption experiments, it was cooled to below 100 K while sputter-cleaning. When the temperature had stabilized and the sample was determined to be clean, all filaments except those in the mass spectrometer and ionization gauge were turned off. The argon in the chamber was pumped out and the sample moved in front of the dosing needle. When the chamber pressure fell below 2.6×10^{-7} Pa (~1 minute after sputtering stopped), the ion pump was turned on and isolated from the sample chamber, and water vapor was let in through the dosing needle to a pressure of 1.33×10^{-6} Pa.

With the sample in front of the dosing needle, the exposure was enhanced by a factor of twenty which was experimentally determined (see next section). Water vapor saturation coverages could be adsorbed on the sample surface without contaminating the sample chamber with large amounts of water vapor. However, successive exposures to water vapor did eventually increase the base pressure of the analysis chamber. When the base pressure would not fall below 1.33 x 10^{-8} Pa, the system was baked overnight at 425 K.

After a water vapor exposure, the chamber was evacuated with the diffusion pump. The mass spectrometer was set at 18 amu (20 in the case of D_2O) and the sample positioned near the opening to this instrument. Positioning the sample in approximately the same place before each desorption experiment eliminated any position dependence in the desorption traces. With the pressure at ~1.33 x 10^{-7} Pa, the temperature ramp was started. The 18(20) amu mass spectrometer signal and the thermocouple *emf* were simultaneously recorded on a strip chart recorder.

There are some experimental problems that can complicate the quantitative interpretation of thermal desorption spectra. The problem of non-linearity in the heating rate was not serious here because the temperature programmer maintained linearity to within 2%. Readsorption of desorbed gas can always occur but is not significant in these experiments because the pressure in the sample chamber during a desorption peak never rose above 2.6 x 10^{-5} Pa, and after each peak, fell back to the low 10^{-7} Pa range in just a few seconds. The high pumping speed of the diffusion pump (~150 liters/s) and the low heating rates used ensured that readsorption was minimal. Desorption from sample supports was examined by repeating some desorption measurements with the sample surface positioned away from the dosing needle during water vapor exposure. In each case, no desorption peaks could be detected with the quadrupole mass spectrometer using the same sensitivity as in the measurements with the sample in front of the dosing needle during exposure.

4.3.4 EIL

Luminescence was excited with 5 keV electrons at a typical current density of 50 mA/cm^2. Light emitted from the sample surface passed through a glass viewport and was collected by a quartz telescope. The telescope contained a precision aperture that was adjusted to allow only light emitted from the excited area of the sample to pass through the telescope. The aperture was adjustable from 6 minutes to 3 degrees of arc. The telescope was focused on the sample surface and light from the luminescence was focused on the slit of a monochromator. The slit width was varied from 2000 μm for faint signals to 25 μm for bright ones. The grating of the monochromator was blazed at 450 nm and ruled with 150 grooves per mm allowing a spectral region 600 nm wide to be viewed. The wavelength range for all luminescence spectra was 300 to 900 nm. The light passing through the monochromator was collected by a diode array backed by a channel plate which was cooled to 268 K to reduce noise. The spectra, usually composed of several hundred scans of one second each, were stored in a multichannel analyzer for subsequent analysis. Spectral lines from a mercury arc lamp were used to calibrate the spectrometer. All spectra were corrected for the response of the telescope-monochromator-detector system using a standard lamp with a known output. This response is shown in Fig. 4.3.1. Spectra were also corrected for the optical characteristics of the glass viewport through which the luminescence emission was measured.

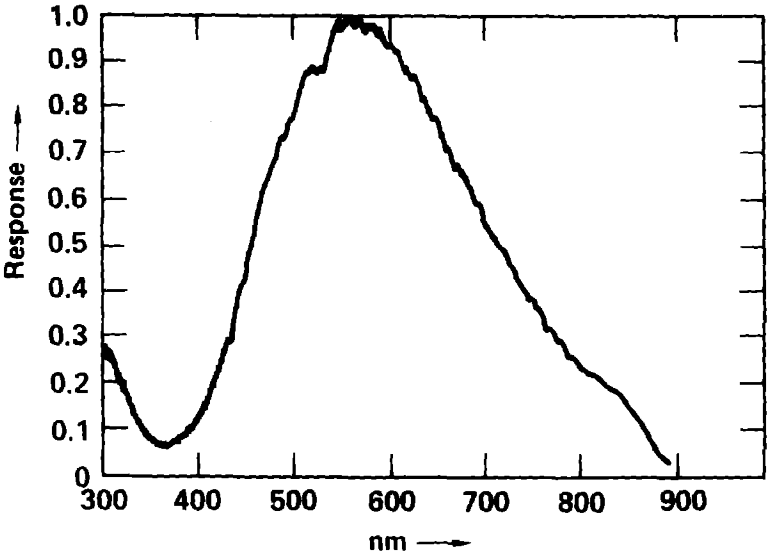

Fig. 4.3.1 Spectral response of luminescence detection system.

Clean uranium samples were exposed to a reactant gas with all filaments turned off, except the ionization gauge. After exposure the chamber was evacuated, all light sources in the chamber and the room were turned off and the luminescence scan begun. The light from the filament of the electron gun used for exciting the luminescence as well as that from several small light sources in the room that could not be conveniently turned off may have been detected by the spectrometer during the luminescence measurements. Background removal was therefore performed by repeating each set of scans with the electron accelerating voltage turned off and subtracting the result from the initial spectrum. The use of the telescope aperture and background subtraction ensured that each spectrum represented only the luminescence emitted by the excited region of the sample.

5. EXPERIMENTAL RESULTS AND DISCUSSION

The purpose of this study was to characterize the reaction of clean uranium metal surfaces with small amounts of various atmospheric gases and the resulting oxides. It was hoped that any new information obtained would provide a better understanding of the initial stages of uranium oxidation. The reaction of clean uranium with CO, CO_2, O_2 and H_2O has been studied at low exposures with surface techniques and at high exposures with thermogravimetric techniques. Although the previous studies do not afford a complete understanding of these reactions, they do provide a firm foundation for further investigation. Because the state of knowledge of the initial stages of the water vapor–uranium reaction is particularly poor, this reaction was made the focus of the present study.

The results presented in this section show that uranium oxidation is quite complex for low exposures of reactant gases and vapors. The data provide important clues to four aspects of the initial surface oxidation reaction: the surface adsorption processes, the nature of ions transported through the oxide layer, the electronic defect structure of the oxide layer, and the surface oxide growth morphology.

5.1 Auger Electron Spectroscopy

One of the main advantages of using surface-sensitive techniques to probe oxidation reactions is the ability to obtain well characterized substrates at each stage of the oxidation process. The starting point for any surface oxidation study must be a clean surface. The production and maintenance of clean surfaces is most easily determined by AES, which allows the detection of carbon and oxygen contamination to about 0.1 at%.

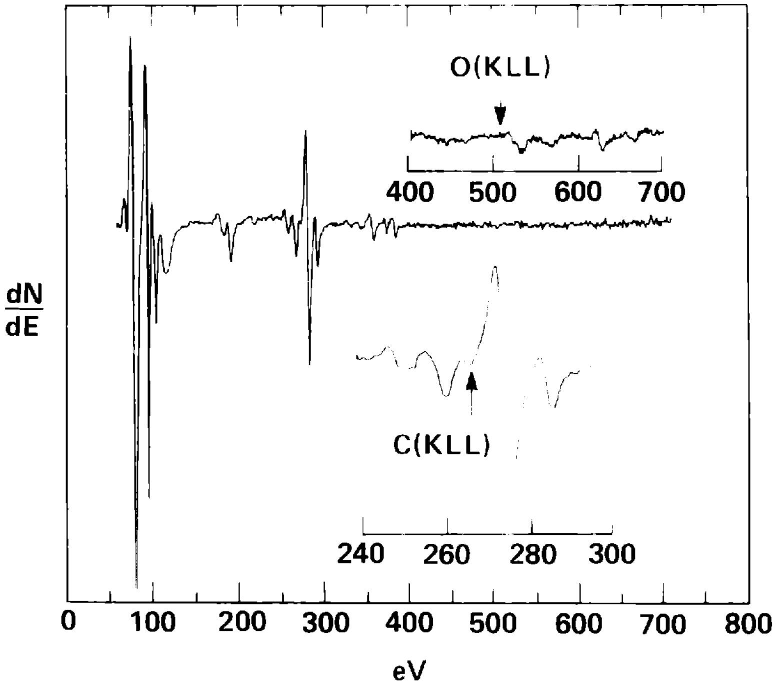

Fig. 5.1.1 Auger spectrum of clean uranium which defines the standard of cleanliness in this study. The position of oxygen and carbon is marked, all other lines have been assigned to uranium [48,49].

The Auger electron spectrum of clean uranium is shown in Fig. 5.1.1. The spectrum was taken with an excitation beam energy of 3 keV, beam current of 25 μA, modulation voltage of 1 eV peak-to-peak, using a time constant of 30 ms. The spectrum is in good agreement with published spectra of clean uranium [50,51]. The two major contaminants of a clean uranium surface are carbon and oxygen. The oxygen (KLL) transition appeared in the Auger spectrum at ~505 eV and was easily removed after several hours of sputter-anneal cycling. The carbon (KLL) transition appeared as a small peak at ~268 eV just to the left of the uranium (NOP) peak at 275 eV. This was more difficult to remove from the Auger spectrum than the oxygen peak. All efforts to completely remove this peak in the Auger spectrum were unsuccessful. Even after several days of repeated sputter-anneal cycling, the peak would not completely disappear. The secondary-ion mass spectrum (SIMS) for clean uranium showed that the C^- peak was only about 5% as large as the O^- peak under identical sputtering conditions (see Fig. 5.2.3). Because the relative sputter yield of carbon is about twice that of oxygen [52] and oxygen was not detected by AES, it must be concluded that the carbon content of the near surface was negligible.

AES is about an order of magnitude more sensitive to surface contamination by oxygen and carbon than XPS. The standard of cleanliness used in this study was therefore the disappearance of the oxygen peak in the AES spectrum, as in Fig. 5.1.1 above. Before each exposure to a reactant gas, the Auger spectrum of the surface was recorded to make sure that there was nc detectable oxygen.

Studies with atmospheric gases were made to determine what exposure of each was required to produce a surface saturation coverage. The sample chamber was backfilled with continuously flowing reactant gas, through a precision leak valve, to a pressure of 6.6 x 10^{-6} Pa and the O (KLL) peak-to-peak intensity was recorded at one minute intervals. The O (KLL) signal is plotted as a function of exposure in Fig. 5.1.2.

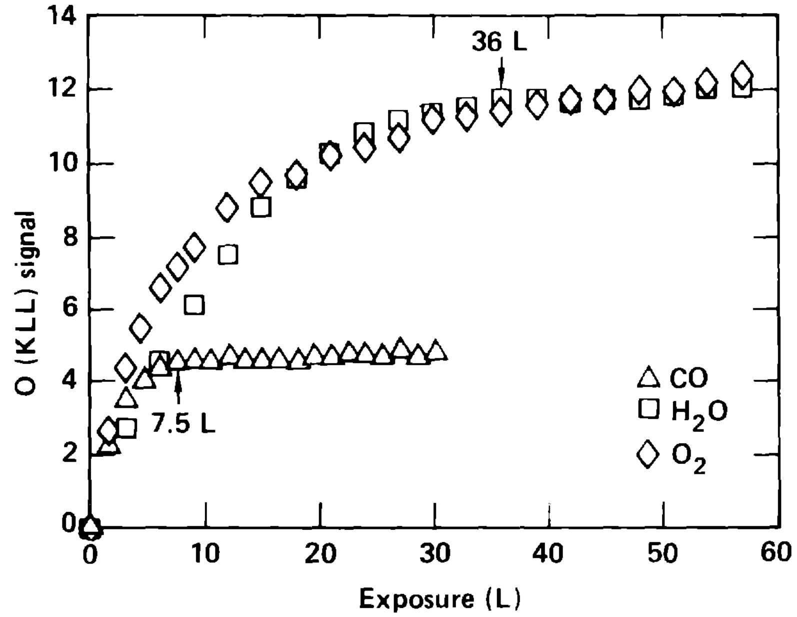

Fig. 5.1.2 Saturation curves for clean uranium exposed to atmospheric gases.

Carbon monoxide saturated the surface after 7.5 L with a final oxygen peak intensity less than half that for either O_2 or H_2O. The initial slopes for oxygen and carbon monoxide are about the same while that for H_2O is slightly less, possibly indicating a slower initial reaction rate. Saturation for O_2 and H_2O was reached after about 40 L and 36 L coverage, respectively, although both curves were still gradually increasing after 40 L. The electron beam necessary for the Auger measurements has a definite but unknown effect on the reaction of uranium with each gas, so that only qualitative comparisons can be made. However, these curves are useful in calibrating gas exposures as a percentage of surface saturation.

Roughly speaking, the O_2 and H_2O saturation curves can be divided into three regions. The initial ~linear rise (slope~0.5 L^{-1}) in the O (KLL) signal is indicative of rapid, coverage-independent (constant sticking coefficient) adsorption and oxide formation. A change of slope occurs between 10 and 25 L exposure which correlates with the splitting of the U (OVV) valence peak (see below). At this point, oxygen adsorption slows as more of the reactive metal is covered by the less reactive oxide. The gradual ~linear rise (slope~0.04 L^{-1}) beyond 25 L exposure indicates that the metal surface is completely covered by the oxide. Oxidation reaches a steady state as oxygen has to diffuse through the oxide layer before reacting with the bulk metal. The continuing increase in the O (KLL) signal beyond 40 L exposure may be due in part to the accumulation of chemisorbed or interstitial oxygen on the oxide surface.

The dosing needle was calibrated by measuring the oxygen Auger peak-to-peak intensity as a function of water vapor exposure for the sample surface placed in front of the doser opening during exposures. The shape of the saturation curve was the same as in Fig. 5.1.2, but saturation was reached after only 1.8 L, giving an enhancement factor for exposures through the dosing needle of 20. This agrees well with a theoretical calculation for the enhancement factor (~18) based on a formula applicable to single-capillary needle dosers [54].

The reaction of clean uranium with dry O_2, pure H_2O, and CO at room temperature was followed with AES as shown in Figs. 5.1.3-5, respectively. Progressive oxidation produced distinct changes in the AES spectra that are readily apparent in the three figures. In particular, the uranium (OVV) peak just to the right of the uranium (OPV) peak at 72 eV split at about 10 L coverage with the new component moving to progressively higher energies as the oxidation continued. The peaks near 275 eV also underwent drastic changes as oxidation proceeded, indicating a strong interaction between the reactants and the metal surface.

The uranium (NOP) peak at 275 eV decreased in intensity as exposure to O_2 and H_2O progressed, and was reduced to about 20% of its initial peak-to-peak height at saturation The oxygen (KLL) peak at 505 eV increased in intensity during these exposures to become the dominant peak, while the peak at 268 eV increased in intensity up to 10 L

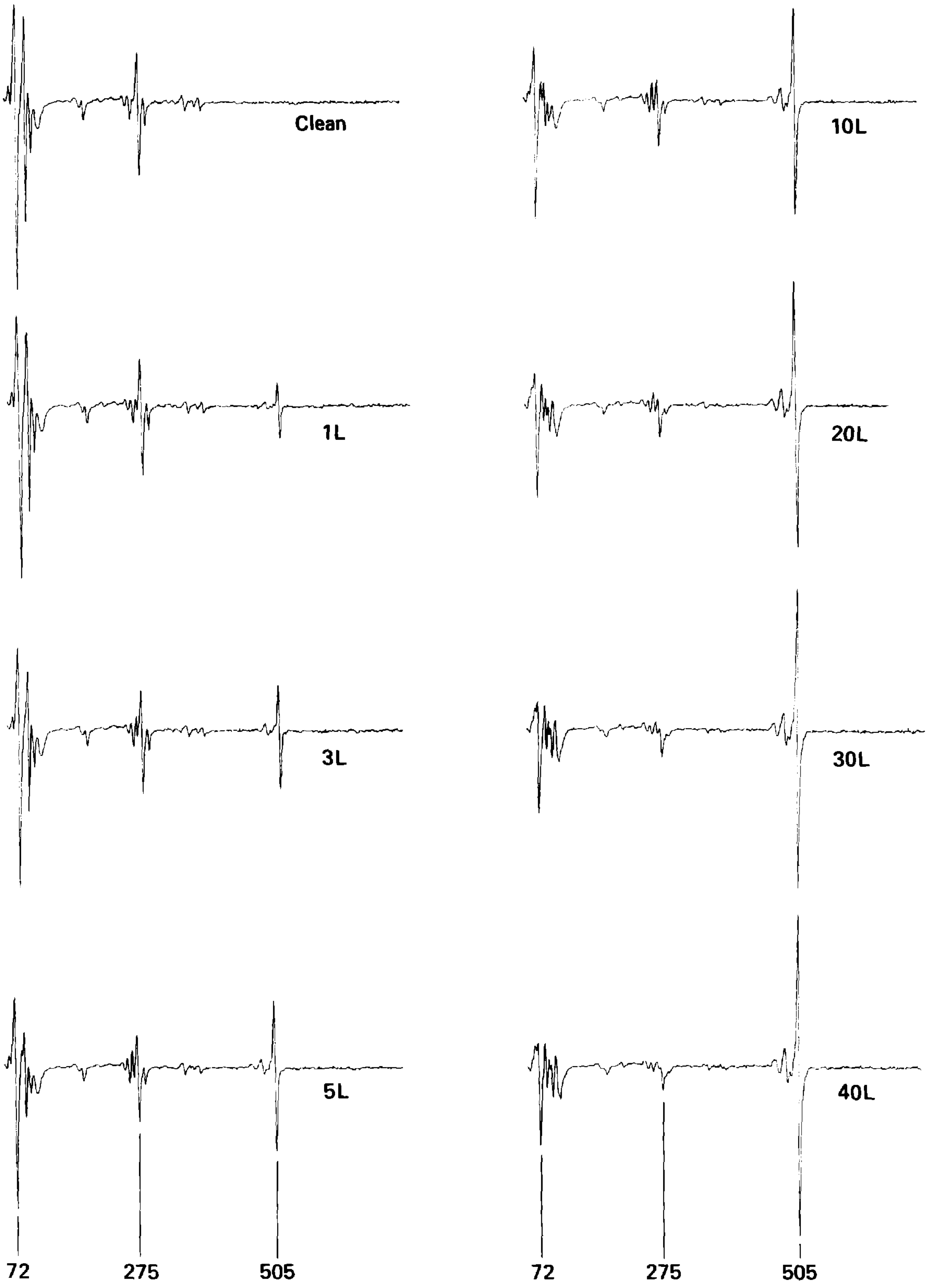

Fig. 5.1.3 Clean uranium exposure to dry O_2 gas.

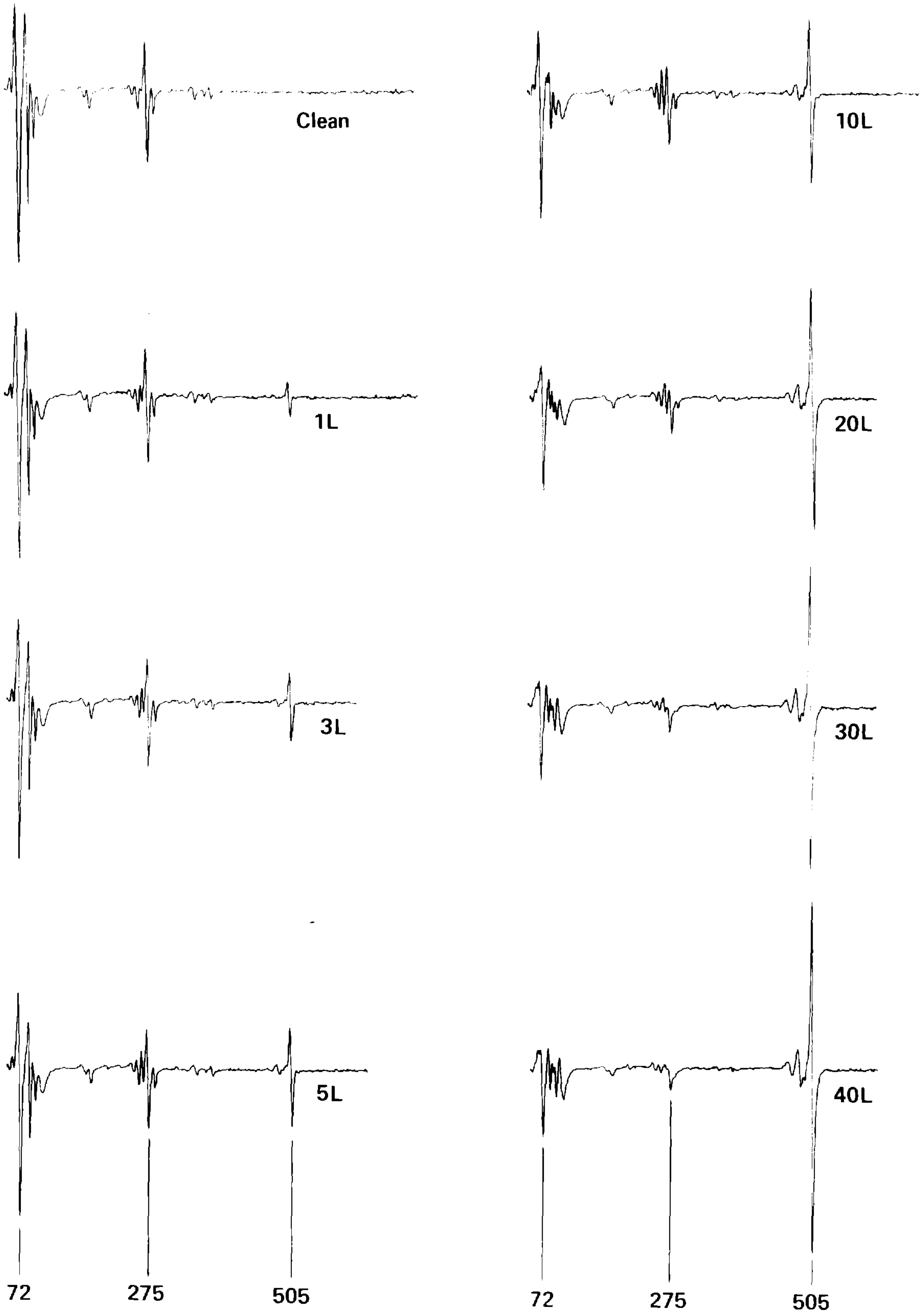

Fig. 5.1.4 Clean uranium exposure to pure water vapor.

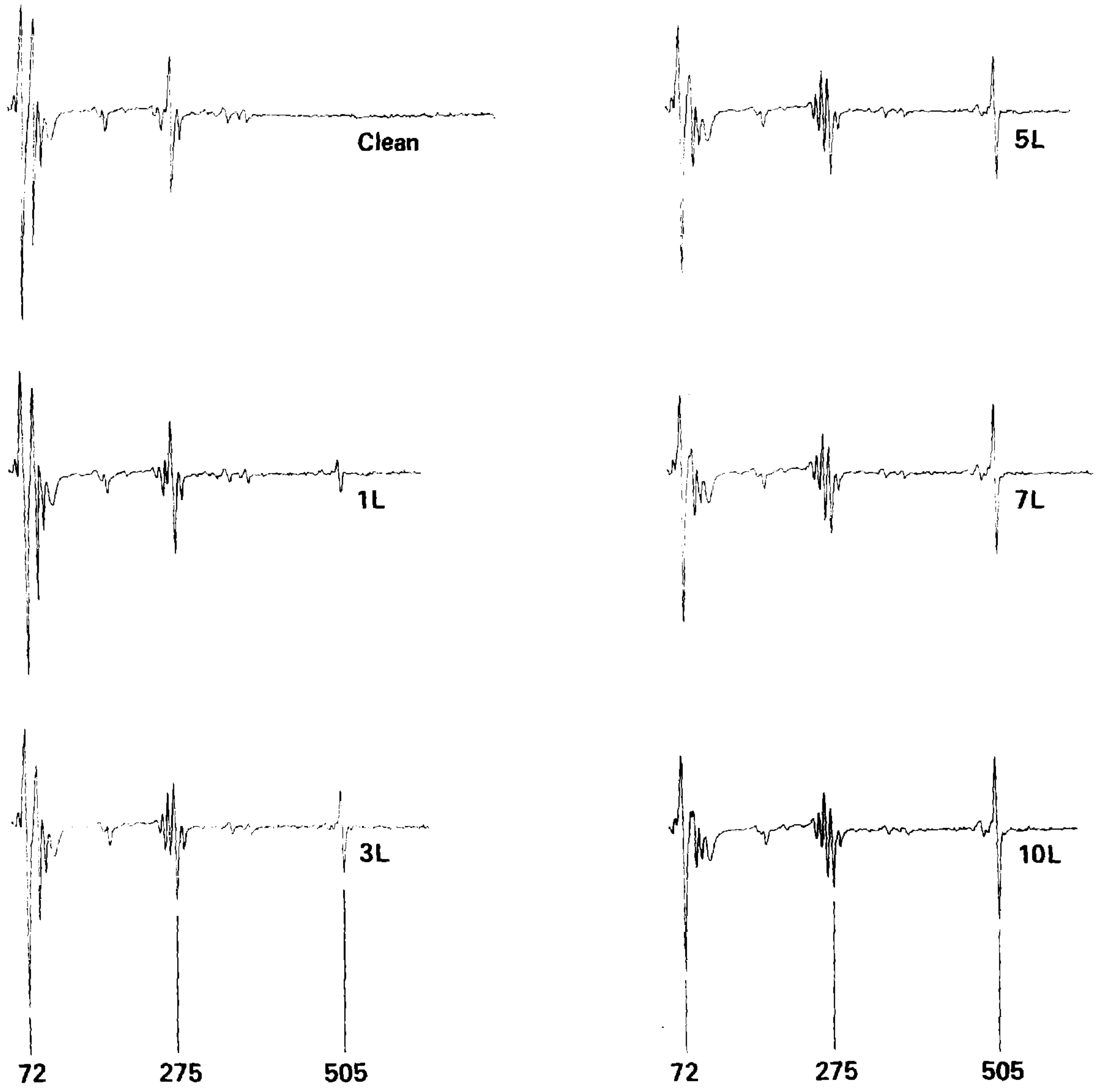

Fig. 5.1.5 Clean uranium exposure to dry CO gas.

exposure and then almost completely disappeared at saturation (see Figs. 5.1.3–4). There is a moderately strong uranium (NOP) transition at 270 eV that could account for this peak [48], as could carbon contamination from CO in the residual gas during exposure.

The behavior of these peaks was modified somewhat for exposure of clean uranium to CO. The intensity of the uranium (NOP) peak at 275 eV after exposure to 10 L CO was about the same as the corresponding peak after exposure to 10 L H_2O or O_2, while the oxygen (KLL) peak intensity was significantly reduced. The peak intensity at 268 eV was 63% greater after 10 L CO than after 10 L H_2O or O_2, which indicates that adsorbed carbon (C (KLL)) is responsible for the peak at 268 eV.

McLean et al. [26] have studied the reaction of clean thorium and uranium exposed to saturation coverages of CO and O_2. They observed similar AES spectra after saturation with CO and O_2, and showed that after exposure to 10 L CO, a subsurface carbide layer was formed underneath the oxide. Assuming that the peak at 268 eV is mostly due to the carbon (KLL) transition, the disappearence of this peak as exposure to O_2 and H_2O was increased can be understood as a result of the elimination of CO adsorption sites on the metal through chemisorption of oxygen, and the covering up of the initially adsorbed CO [26]. The carbon (KLL) peak intensity reached its maximum and began to decrease just as the uranium (OVV) peak at 90 eV split, indicating the formation of an oxide layer. The C/O ratio (~1) at the uranium surface after exposure to 10 L CO is the same as that found by McLean et al. [26], so that subsurface carbide formation must have taken place.

The lower exposure (10 L) required to saturate the clean uranium surface with CO compared to that required for O_2 or H_2O saturation (40 L) results from the reactivity of the carbon with the metal substrate. Carbon atoms compete with oxygen atoms for adsorption sites on the surface, even though the carbon eventually travels below the surface to form uranium carbide [26]. This competition reduces the amount of surface oxygen available for oxide formation and results in the lower AES oxygen signal at saturation.

Ellis [24] has reported the formation of a stable UO phase after sequential oxygen saturation and heating of clean, high-purity uranium. UO has been proposed to exist in the presence of uranium carbide [25] and might exist as a transient phase during uranium oxidation, but its formation as a stable surface phase has not been substantiated. Here, Ellis' prescription [24] was followed and the surface monitored with AES in an attempt to verify whether stable UO could be produced.

Beginning with clean, annealed, high-purity uranium (see Fig. 5.1.1), the surface was exposed to 10 L dry oxygen. A large oxygen signal (~60% of the U (OPV) peak at 72 eV) from the O (KLL) transition was observed immediately after the exposure. This was not a surprising result, but was contrary to the findings of Ellis, who observed no oxygen signal for this exposure. He concluded that the oxygen was rapidly transported into the bulk, thereby leaving no detectable oxygen on the surface. In this study, a detectable oxygen signal normally appeared on clean uranium in ~3 minutes at pressures of ~1 x 10^{-8} Pa. That Ellis could not detect the oxygen signal after 10 L O_2 exposure shows that the sensitivity of his system (a 4-grid LEED/Auger analyzer) was much lower than typical AES sensitivities available today.

Continuing with Ellis' exposure schedule, after each oxygen exposure, the O (KLL) signal grew, while during heating, the signal diminished. This pattern was observed for each of the steps in the exposure schedule and is clearly due to the diffusion of surface oxygen into the bulk during heating as noted by Ellis [24]. At the last step, saturation of the surface with 150 L O_2, an O/U ratio of ~2.4 was observed, indicating the presence of chemisorbed oxygen on the saturated surface. Heating to 973 K reduced this ratio to ~0.5, not ~1 as claimed by Ellis [24], as oxygen was removed from the surface and transported into the bulk. After cooling to 298 K, this ratio decreased even further to ~0.25. XPS measurements of the surface at this stage were similar to those for clean uranium saturated with oxygen at 298 K (see Fig. 5.2.4b,c), except for even smaller oxide contributions to the core and valence level spectra. No unusual features were observed that might have indicated the formation of a new phase. This is consistent with the interpretation that surface oxygen is continuously diffusing into the bulk and that this diffusion is accelerated by heating.

The repetition of Ellis′ experiment took several hours, and in that time, significant carbon contamination from CO in the residual gas took place. A strong C (KLL) peak was observed in the AES spectra after each heating, which disappeared after subsequent oxygen exposure. It is likely that formation of oxycarbide (UO_xC_y, $x \sim y \sim 1$) layers took place on the surface, which has been previously observed [53].

5.2 X-Ray Photoelectron Spectroscopy

A broad scan of the X-ray photoelectron spectrum of clean uranium indicating the origin of major peaks is shown in Fig. 5.2.1. Three regions of the spectrum are of interest in this study: the U 4f core levels at ~380 eV, the O 1s core level at ~530 eV, and the valence band region (~0–35 eV) just above the Fermi energy.

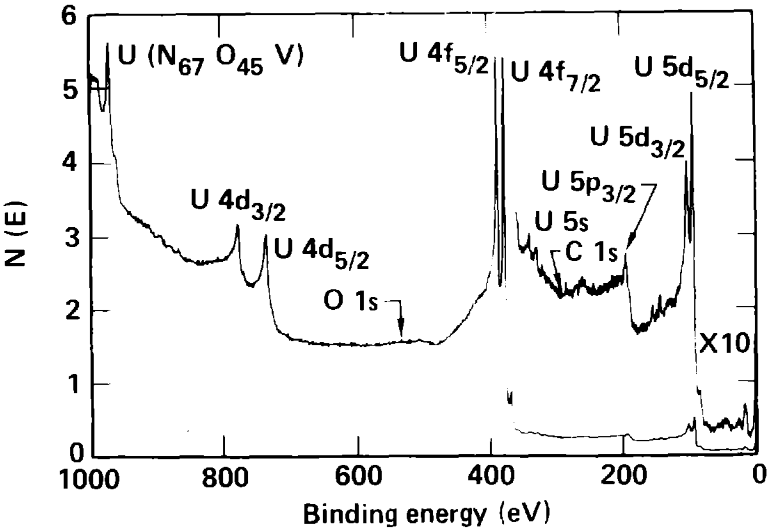

Fig. 5.2.1 Survey scan of the X-ray photoelectron spectrum of clean uranium.

The behavior of these regions for exposure of clean uranium to saturation coverages of water vapor and dry oxygen at 298 K is shown in Figs. 5.2.2–4. The first spectrum in each figure reflects the true signal-to-noise ratio of the experimental data, all other spectra have been numerically smoothed.

The peak energies, widths and relative intensities are compiled in Table 5.1. Some binding energies and all peak widths were determined by fitting the spectra using a combination of Gaussian and Lorentzian peak shapes [55]. An example of the fit is shown in the inset of Fig. 5.2.2. Unfortunately, the fits were usually not unique so that care must be excercised when comparing peak intensities. However, the trends exhibited in the O 1s peak intensities are believed to be correct.

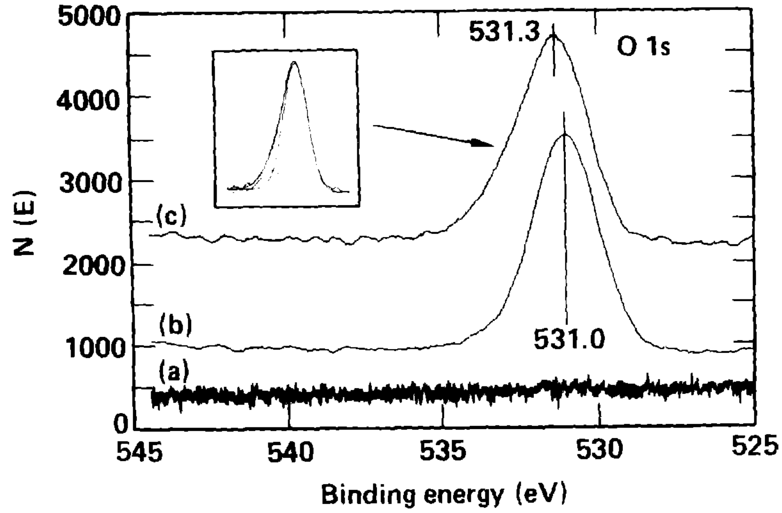

Fig. 5.2.2 The O 1s spectra for a) clean uranium, b) U + 40 L O_2, and c) U + 40 L D_2O at 298 K.

Clean uranium exposed to 40 L O_2 produced a nearly symmetric O 1s peak at 531.0 eV in agreement with previous results [26] as shown in Fig. 5.2.2. This binding energy is 1.0 eV higher than that reported for $UO_{2.0}$ [13,31]. The significance of this shift is discussed shortly. A small component (~7% of the total integrated peak intensity) was also observed at 533.0 eV. Clean uranium exposed to 40 L D_2O resulted in a broader, more asymmetric peak that was shifted higher in binding energy to 531.3 eV. The asymmetry in this peak also resulted from a small component (~14% of the total integrated peak intensity) at 533.4 eV (see inset Fig. 5.3.2).

Yates and Erickson [56] have reported a small residual peak in the O 1s spectrum after adsorption of O_2 on the W(111) surface at 120 K. Because the area of the residual peak remained constant for increasing oxygen exposures, it was attributed to multiple surface binding states of oxygen and not to energy loss processes. Moroney et al. [57] have studied the thermal decomposition of βNiO(OH) with XPS. Upon heating the surface to 773 K, they observed an asymmetric O 1s spectrum. The main peak at 529.7 eV was attributed to O^{2-} in the surface oxide. The smaller companion peak at 531.7 eV was attributed to chemisorbed or interstitial O_2^{2-} or O^- species because the hydroxide, which produced a peak at 531.4 eV at lower temperatures, had been completely driven off upon heating. Similarly, Au et al. [58] studied the reaction of water vapor on an oxygen-predosed Ag(110) surface. They also observed two components in the O 1s spectrum after oxygen exposure at 473 K. They assigned the main peak at 530.3 eV to O^{2-} from the oxide and the companion peak at 532.5 eV to strongly chemisorbed O_2^-.

Strongly chemisorbed oxygen has been shown to exist on thoria surfaces at room temperature and to persist even at elevated temperatures [59]. Similarly, strongly chemisorbed oxygen has been observed on Ag(110) at 473 K [58]. The ability to achieve O/U ratios in excess of 2 for low coverages (see section 5.1) suggests that chemisorbed oxygen forms readily on uranium surfaces as well. The strong chemisorption of oxygen on uranium oxides has been previously proposed [60]. Therefore, the small companion peak in the O 1s spectrum for exposure of clean uranium to oxygen may be due to chemisorbed O_2^- or O^-.

The difference in the relative intensity of the O 1s companion peak for oxygen saturation (7%) compared to water vapor saturation (14%) suggests a different origin for this peak in the case of water vapor adsorption. Koel et al. [61] studied the adsorption of D_2O on clean polycrystalline Ce surfaces. They observed two peaks in the O 1s photoelectron spectrum after saturation of the surface with D_2O at 300 K. The main peak observed at 530.3 eV was attributed to the formation of an oxide, and the companion peak at 532.7 eV, which was ~30% of the total integrated peak intensity, was attributed to adsorbed OD. Roberts and Wood [62] observed similar behavior after adsorption of water vapor on clean Fe surface at 290 K. Two peaks in the O 1s photoelectron spectrum were observed at 530 eV and 532 eV, attributed to chemisorbed oxygen or surface oxide, and adsorbed hydroxyl groups, respectively. On the basis of these studies, the small companion peak observed in the

O 1s spectrum after water vapor exposure is tentatively assigned to the presence of an OD-complex on the surface or to incorporation of OD into the oxide lattice. However, strongly chemisorbed O_2^- or O^- cannot be ruled out. MacCrone et al. [18] studied the oxidation of uranium metal and UO_2 in pure water vapor and water vapor–oxygen mixtures with EPR. They found that the UO_2 surface was highly reactive with water vapor and proposed that the EPR results were consistent with the hydrolysis of water on the surface to produce surface chemisorbed O^- or O_2^-.

Similarly, contamination by water vapor in the residual gas after oxygen exposure is possible after many minutes in ultra-high vacuum and is usually difficult to rule out on the basis of XPS measurements alone due to the proximity of the O_2^- and hydroxyl ion O 1s peak positions. Hopster and Brundle [64] studied the adsorption of dry O_2 on Ni(100) at saturation exposures with XPS and SIMS. They observed a small companion peak at 531.4 eV above the main O 1s photopeak at 530.0 eV under certain conditions that was correlated with a large OH^- contribution ($OH^-/O^- \sim 1$) to the static SIMS spectra. They concluded that OH^- species were responsible for the companion peak, that it occurred only for low O_2 pressure exposures, and that it was necessary to have both oxygen gas and residual water vapor present for the OH^- formation.

The peak assignments are facilitated by the results of static SIMS measurements as shown in Fig. 5.2.3. The amount of surface OH^- present on the surface from the residual gas was negligible ($OH^-/O^- < 0.01$) after oxygen exposure while there was a significant amount of OD^- on the surface ($O^-/OD^- \sim 0.1$) after D_2O adsorption.

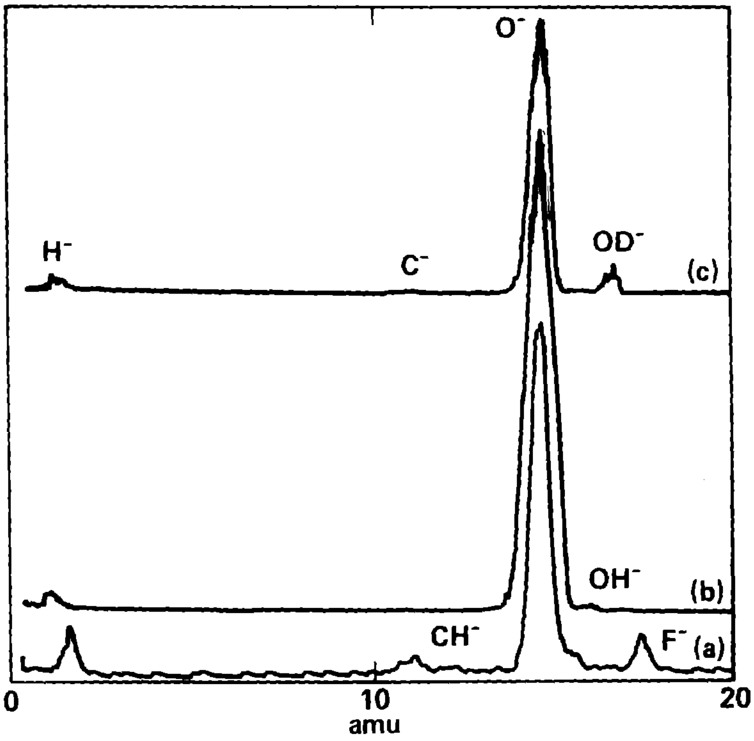

Fig. 5.2.3 a) SIMS spectra of clean uranium during sputtering at 3x3 mm^2 with a 3 keV, 25 μA Ar^+ beam. Static SIMS (accelerating voltage and raster off) for b) U + 40 L O_2, and c) U + 40 L D_2O at 298 K.

The hydroxide contribution to the SIMS spectrum after water vapor adsorption is smaller than that observed on Ni(100) [64], but is definitely present. This in itself is surprising because one might have thought that the highly-reactive uranium metal would combine with all available oxygen to form oxide at such low exposures. The persistence of OD^- after water vapor exposure is due to the rapid formation of an oxide layer and suggests that OD^- might also strongly chemisorb on the oxide surface or even form a surface hydrate [44]. It also suggests that the water vapor-oxide reaction is slower than the water vapor-metal reaction.

The small contribution from OH^- on the oxygen-saturated surface makes residual water vapor contamination an unlikely cause for the O 1s companion peak at 533.0 eV (see Fig. 5.2.2b). Rather, strongly chemisorbed O_2^- or O^- are more probable candidates. However, a negligible amount of O_2^- was observed in both static SIMS spectra. If the chemisorbed species was in fact O_2^-, then its absence in the SIMS spectra could be explained by its strong interaction with the surface which might cause the oxygen atoms to be sputtered separately [64]. This could account for the larger intensity of the O^- SIMS peak for the oxygen-saturated surface compared to the water vapor-saturated surface. A more likely explanation for this two-fold increase in intensity is that the strongly chemisorbed species is O^-. O^- has been proposed to form very strong covalent bonds and has been proposed to exist in abundance in MgO and other oxides that contain trace amounts of water or carbon dioxide [65].

Whether O^-, OH^-, or O_2^-, strongly chemisorbed species would seem to be present on uranium oxides at very low exposures and probably greatly influence the further oxidation of the uranium. This is discussed further in section 6.

The behavior of the U 4f core levels after oxygen and water vapor exposure is shown in Fig. 5.2.4. The clean metal exhibited peaks at

377.6 eV and 388.4 eV for the U $4f_{7/2}$ and U $4f_{5/2}$ core levels, respectively. These values are in good agreement with previously reported values [2,19,47]. The peaks are shifted to 380.7 eV and 391.5 eV upon saturation with dry oxygen, also in good agreement with previously reported values for O_2-saturated uranium [26]. The residual contribution from the metal accounts for about 40% of the U $4f_{7/2}$ peak, a result consistent with the findings of McLean et al. [26] and Fuggle et al. [66] who observed similar behavior for identical exposures.

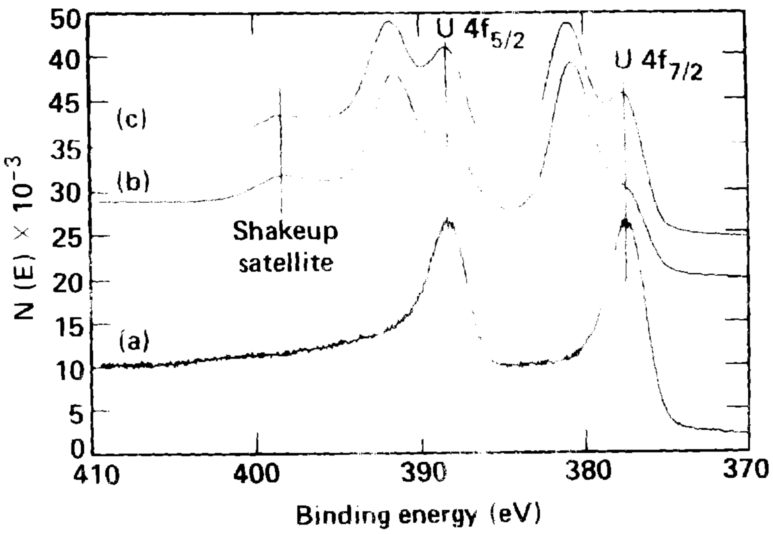

Fig. 5.2.4 U 4f core levels for a) clean uranium, b) U + 40 L O_2, and c) U + 40 L D_2O at 298 K.

Satellites were observed to the high binding energy side of the U $4f_{5/2}$ (398.5 eV) and U $4f_{7/2}$ core level peaks, although the latter was obscured by the residual metal component. These satellites are usually attributed to the shakeup of an electron from the O 2p valence band into the unoccupied U 5f levels accompanying photoionization [67,68].

Objections to this interpretation have been raised by Schneider and Laubschat [69] who attributed both the U $4f_{7/2}$ satellite and the "O 2p bonding band" peaks to poorly-screened two-hole final states in the photoemission process resulting from decreasing fd hybridization and consequent increasing 5f localization in uranium compounds. This issue has been recently addressed by Naegele et al. [70] who concluded that the presence of core satellites was not simply an indication of decreasing fd hybridization. This issue is beyond the scope of the present study and will not be discussed further.

Compared to oxygen saturation, exposure of clean uranium to 40 L D_2O shifted the U 4f oxide peaks by ~0.2 eV to higher binding energies of 380.9 eV and 391.8 eV for the U $4f_{7/2}$ and U $4f_{5/2}$ peaks, respectively. The metal contribution to the U 4f peaks for water vapor saturation (~43%) is greater than that for oxygen saturation (~30%), indicating that oxidation is greater for the oxygen-uranium reaction than for the water vapor-uranium reaction for the same exposure.

Although the surface seems to be oxidized less by water vapor than by oxygen for identical exposures, the U $4f_{7/2}$ core level still exhibited a strong oxide peak after adsorption of 40 L D_2O. This was not observed by Nornes and Miesenheimer [27], whose results showed that after adsorption of 54 L of water vapor, the metal line still completely dominated the U $4f_{7/2}$ spectrum. They concluded that the water vapor-uranium reaction was very much slower than the oxygen-uranium reaction and suggested that this may have been due to long-term Ar^+ bombardment

The valence band region is presented in Fig. 5.2.5. The clean metal exhibited peaks at 28.8 eV and 16.3 eV due to the U $6p_{1/2}$ and U $6p_{3/2}$ levels respectively, and at 1.0 eV due to the partially localized U 5f states in agreement with previously reported values [26]. Upon reaction with dry oxygen, two new peaks developed. The O 2s peak occured between the two U 6p peaks at 2[illegible].5 eV, and a small shoulder at ~6.6 eV on the high binding energy side of the U 5f peak appeared due to contributions from the O 2p, U 6d and U 5f bonding levels [11,67]. This is the O 2p valence band (see Fig. 5.2.6). It can be seen that

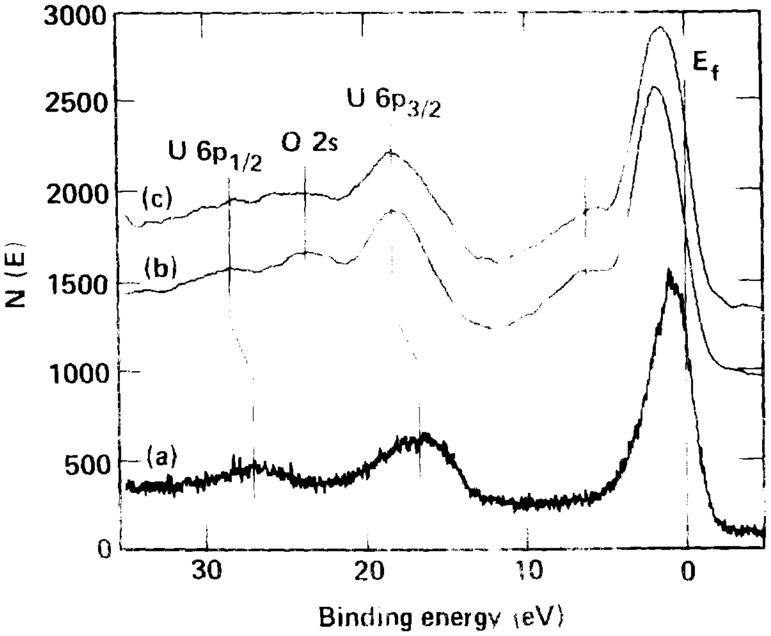

Fig. 5.2.5 Valence band spectra for a) clean uranium, b) U + 40 L O_2, c) U + 40 L D_2O at 298 K.

the water vapor reaction produced a ~20% broader U $6p_{3/2}$ peak (see Table 5.1) while the O 2s contribution to the spectrum was suppressed. Similarly, the O 2p valence band broadened upon exposure to water vapor and the peak shifted to lower binding energy, possibly indicating increased participation of the U 5f levels in the bonding [11].

Peak positions and widths are compiled in Table 5.1 for various exposures at room temperature and during controlled heating. Exposure to water vapor resulted in a significant broadening of the O 1s and U $6p_{3/2}$ peaks compared to oxygen exposure. The energy shifts in the photoelectron peak positions displayed for the various exposures in Table 5.1 are indicative of the complex nature of the surface oxidation reactions encountered in this study However, special care must be taken to separate charging effects, which can occur on insulating surfaces, from true chemical shifts. If all peak energies of the spectra of a surface are shifted by the same amount compared to some reference, then charging effects are likely responsible for the shifts.

A comparison of the peak positions for saturation with dry oxygen and water vapor shows that the U $6p_{3/2}$ core and U $4f_{5/2}$ satellite peak energies do not change, but the U 4f core level peak energies shift by ~0.2 eV to higher binding energies for the water vapor-saturated surface. Because there is no uniform shift of peak energies, the core level shifts must result from the changed chemical environment on the surface. Examination of the U 4f metal lines in Fig. 5.2.4 shows that they too maintain their position for each surface, confirming the chemical nature of the U 4f oxide peak shifts from the oxygen-saturated surface to the water vapor-saturated surface.

Binding Energy (eV)/FWHM (eV)

Surface	U 5f	U $6p_{3/2}$	U $4f_{7/2}$	U $4f_{5/2}$	U $4f_{5/2}$ sat.	O 2s	O 1s
				T = 298 K			
Clean U	1.0/2.6	16.9/5.0	377.6/2.6	388.[illegible]			
U+40L O_2	1.9/3.3	18.2/4.3	380.7/2.8(o) 377.5/2.7(m)	391.5/3.[illegible](o) 388.4/2.8(m)	398.5/4.2	23.5/4.4	(93)531.0/2.4 (7)533.0/2.4
U+40L D_2O	1.6/3.3	18.2/5.2	380.9/2.9(o) 377.7/2.7(m)	391.8/3.[illegible](o) 388.4/2.[illegible](m)	398.5/4.5		(86)531.3/2.4 (14)533.4/2.3
U+1800L O_2	1.5/2.5	17.6/4.0	379.9/2.9	390.[illegible]/3.[illegible]	397.5/4.6	22.8/4.0	(92)530.0/2.4 (8)532.0/2.4
U+1800L O_2 +40L D_2O	1.6/2.5	17.7/4.0	380.1/2.9	390.[illegible]/3.[illegible]	397.7/4.2	22.8/4.2	(89)530.3/2.4 (11)532.3/2.4
				Controlled Heating			
U+40L D_2O 85 K			377.5	388.		28.9/4.0	536.8/2.8
197 K	1.0	17.8	380.6(o) 377.3(m)	391.4(o) 388.[illegible](m)	397.5	29.6/5.0	(24)531.5/2.8 (41)534.5/2.8 (35)537.2/2.6
220 K	1.1	17.9					(45)531.4/2.6 (17)533.0/2.0 (38)534.5/2.6
298 K	1.5	18.3	380.8(o) 377.7(m)	391.5(o) 388.3(m)	397.[illegible]		(81)531.2/2.5 (19)533.3/2.1
U+40L O_2+70L D_2O 197 K	1.3	17.7	380.[illegible]	390.9	397.8	22.3 23.5	(22)530.3/2.6 (26)533.5/2.8 (52)537.1/2.8
220 K	1.5	17.9	380.5	391.[illegible]	398.5	23.7	(51)530.8/2.3 (4)532.5/2.3 (45)534.0/2.9
298 K	2.5	18.8				24.2 25.7	(87)531.5/2.3 (13)533.6/2.2

Table 5.1 Summary of XPS peak positions and widths. Relative integrated peak intensities are given in parentheses.

The U 4f region for clean uranium exposed to 1800 L O_2 at 298 K is shown in Fig. 5.2.6. The positions of the U 4f peaks, which are given in Table 5.1, are ~0.8 eV lower than the values measured for saturation coverage of O_2, but agree with previously reported values for $UO_{2.001}$ [30]. The shakeup satellite peak positions, 6.9 eV (U $4f_{5/2}$) and 6.8 eV (U $4f_{7/2}$) above the respective photopeaks, agree well for reported values for $UO_{2.0}$ [13,31,51]. Also, the measured O 2p/U 5f integrated peak intensity ratio, 0.64, is in good agreement with that reported for UO_2 (0.7) [51]. It must be concluded that exposure of clean uranium to 1800 L O_2 at room temperature produced a stoichiometric oxide layer.

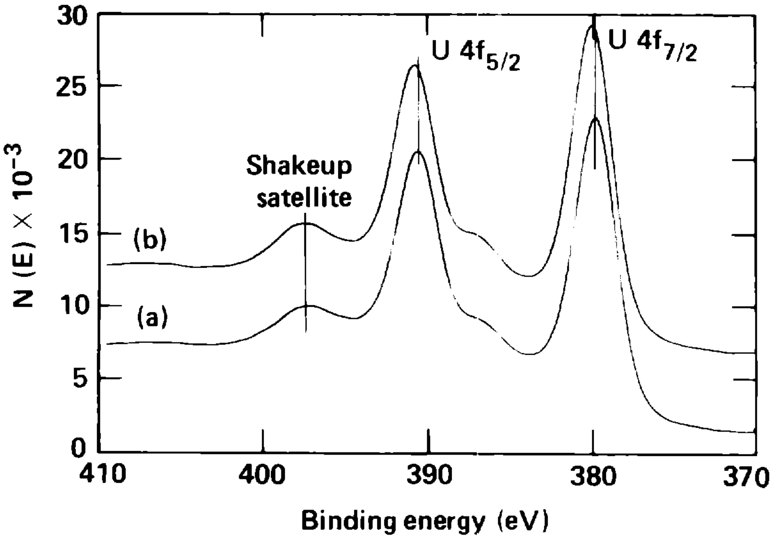

Fig. 5.2.6 U 4f spectrum of clean uranium exposed to a) 1800 L O_2, and b) 1800 L O_2 + 40 L D_2O at 298 K.

The higher binding energies of the photoelectron peaks for surfaces exposed to saturation coverages of O_2 and D_2O, as well as the presence of a residual metal contribution to the U 4f core level peaks, suggests that oxidation of the uranium surface is incomplete for low exposures. Such oxidation may result in islands of $UO_{2.0}$ interspersed on the clean metal substrate, or in a substoichiometric oxide layer as some of the oxygen moves into the bulk. Binding energies higher than those for the stoichiometric oxide might then result from differential charging effects [19].

Because of the very low exposures required for saturation, residual metal contributions to the photoelectron spectra might alternatively arise from the underlying bulk metal. Assuming that a thin (d~1 nm) uniform monolayer of oxide forms on the surface at saturation and that the photoelectron escape probability varies exponentially with the thickness of the oxide layer, the relative contribution to the U $4f_{7/2}$ core level (for KE = 1253.6-377.6 = 876 eV, λ = electron mean free path~1.2 nm) is approximately

$$I_m(\text{oxide})/I_m(\text{clean}) = e^{-d/\lambda\cos\theta} \sim 0.32,$$

where I_m(oxide) and I_m(clean) are the integrated peak intensities of the U $4f_{7/2}$ core level for the saturated and clean uranium surface, respectively, and cos θ is taken to be 0.74 [illegible]. This is close to the values observed for this ratio after oxygen saturation (0.21) and after water vapor saturation (0.34)

The surface concentration of oxygen at saturation can be estimated with the following expression [71]

$$c = I_a/I_s \times \rho N \lambda \cos\gamma / M$$

where c is the surface adsorbate concentration; I_a/I_s is the adsorbate to substrate XPS intensity ratio, corrected for photoionization cross section; ρ is the substrate density, 19.05 gm/cm^3 for uranium; N is 6.0225 x 10^{23} mol^{-1}; M is the molecular weight of the substrate, 238.07 gm/mol for uranium; and $\lambda\cos\gamma$ is as above The oxygen surface concentration is calculated to be 1.2 x 10^{15} atoms/cm^2 for both oxygen and water vapor saturation. If it is assumed that one oxygen atom per surface uranium atom provides one monolayer coverage (θ=1), and that there are approximately 1.3 x 10^{15} atoms/cm^2 on the clean uranium surface, then the coverage is calculated to be θ=0.92. On the other hand, if oxide formation is rapid, two oxygen atoms could be expected to react with each surface uranium atom to give θ=0.46. This surface oxide coverage is consistent with the 0.30 and 0.43 oxide to metal U $4f_{7/2}$ core level peak intensity ratios observed for oxygen and water vapor saturation, respectively.

It is certain that part of the metal contribution to the photoelectron spectra arises from the underlying bulk metal, but the large difference in the amount of metal detected after oxygen saturation compared to water vapor saturation at the same exposure (40

L) indicates that surface attack might not be uniform in both cases. Because of surface roughness (see section 5.[illegible]), the adsorbed molecules could be expected to migrate to the lowest energy adsorption sites before strongly binding with the surface (precursor model of adsorption). The higher metal contribution in the case of water vapor saturation may just be due to the clustering of water molecules at adsorption sites [72].

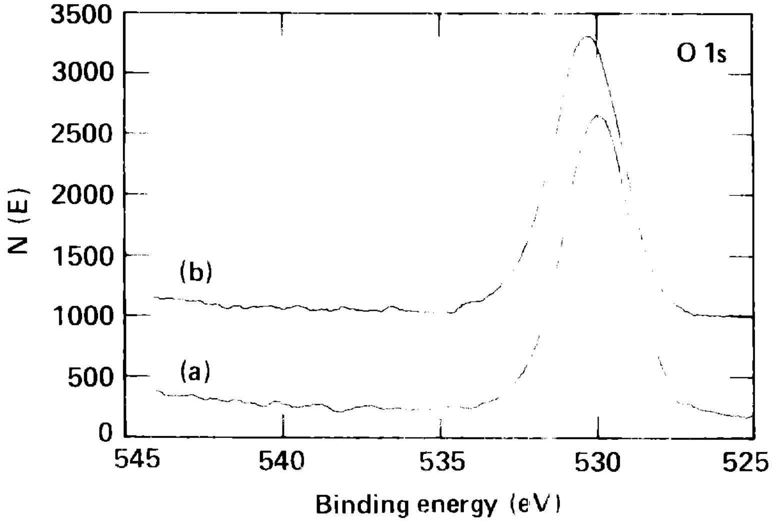

Fig. 5.2.7 O 1s spectrum of clean uranium exposed to a) 1800 L O_2, and b) 1800 L O_2 + 40 L D_2O at 298 K

The O 1s peak (Fig. 5.2.7) again exhibited a small component (~8% of the total integrated peak intensity) 2.0 eV higher in binding energy than the main peak at 530.0 eV. Upon exposure to 40 L water vapor, these peaks shifted 0.3 eV to higher binding energies and the small peak at 532.3 eV increased to ~11% of the total integrated peak intensity. This is still 20% less than the companion peak contribution to the O 1s spectrum for the clean metal exposed to 40 L D_2O, indicating that the relatively thick oxide layer either inhibited the formation of the contributing oxide species or accelerated their depletion.

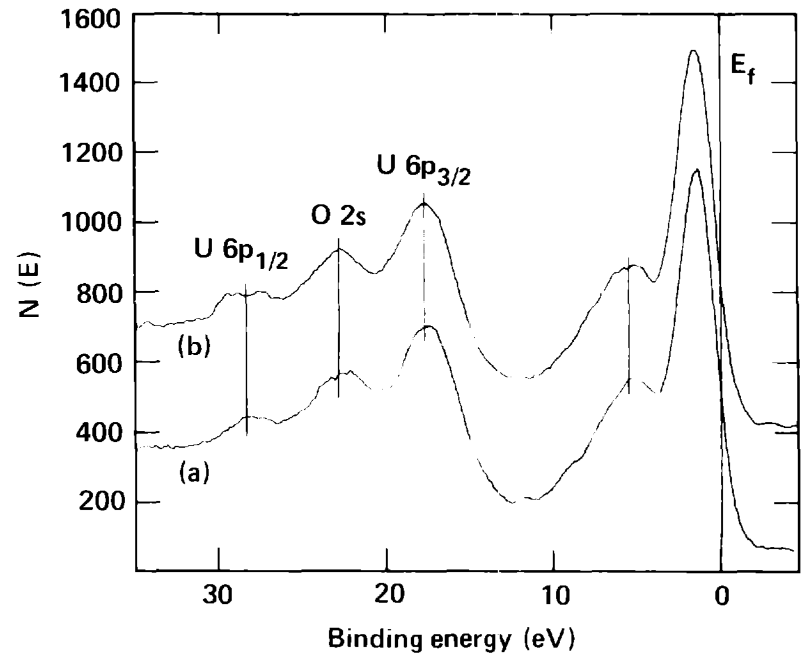

Fig. 5.2.8 Valence band region for clean uranium exposed to a) 1800 L O_2 and b) 1800 L O_2 + 40 L D_2O at 298 K.

The valence band region exhibited several interesting changes upon water vapor exposure as shown in Fig. 5.2.8. The O 2p valence band broadened and intensified, and the O 2s peak became sharper with adsorption of water vapor on the oxide surface. Similarly, the U $6p_{1/2}$ peak split into at least two components and the U $6p_{3/2}$ peak intensified. Because the valence band region is less sensitive to conditions at the surface than the O 1s or U 4f core levels, the distinct changes in the valence spectra show that a large region of the oxide layer is affected by the adsorption of water vapor onto the stoichiometric oxide. This could mean that OH^- ions can easily diffuse through the oxide layer.

The photopeak binding energies shifted uniformly higher by 0.1–0.3 eV (see Table 5.1) after exposing the stoichiometric oxide layer to water vapor. Enikeev et al. [73] studied the adsorption of water vapor on air-oxidized aluminum and iron surfaces and concluded that the physisorbed water molecules were hydrogen-bonded to oxygen atoms of the oxide lattice which led to the observed increase in the work of electron escape of between 0.07 and 0.3 eV. Such an increase would lead to a decrease in measured XPS binding energies by the same amount. Benndorf et al. [74] have studied the reaction of water vapor on clean and oxygen-predosed Ni(110) surfaces. The 0.9 eV shift to lower binding energy they observed for the O 1s photopeak in going from water vapor adsorption on the clean metal to adsorption with an oxygen precoverage was also attributed to hydrogen-bonded water molecules on the surface.

Shifts to higher binding energy would be expected if water molecules were bound to the the surface through their oxygen atoms. This would produce a positive surface charge as a result of the orientation of the hydrogens away from the surface and increase the O 1s binding energy through a lowering of the local work function. This effect may be responsible for the +0.3 eV shift to higher O 1s binding energy observed here in going from oxygen to water vapor saturation of the clean metal. After formation of the first adsorbed layer, water molecules or hydroxyl ions could be strongly chemisorbed on the oxide overlayer by the same mechanism that O_2^- or O^- is chemisorbed after dry oxygen exposure. The similarity in chemisorption of OD^- after water vapor exposure and the chemisorption of O_2^- or O^- after oxygen exposure could account for the near identical 2.0 eV shift between the main and companion peaks observed for all exposures (see Table 5.1).

Enikeev et al. [73] observed that the amount of water vapor adsorbed increased and the work function decreased after exposure of the metal surfaces to chlorine. Blyholder and Sheets [75] have observed similar results during the adsorption of water vapor on Ni surfaces in the presence of BF_3. Both Cl and BF_3, like oxygen, are strongly electronegative. It has been argued that the presence of these molecules on the surface changes the electron population of the metal valence levels and enhances the H_2O–metal bond [74], which would lead to a decrease in the local work function, as was observed by Enikeev et al. [73]. This effect would also result in a shift toward higher binding energies. The presence of chemisorbed oxygen (O_2^- or O^-) or hydroxyl ions on the surface, inferred from the companion peak in the O 1s spectra, provides the electronegative species required for this effect, which may play a part in the shift of the photopeaks to higher binding energies after water vapor adsorption on either the clean or oxygen-covered metal.

However, nominally stoichiometric UO_2 is a semiconductor, with different electrical properties than the adsorbate-covered metal. Changes in the work function of the surface depend upon whether the oxide is p-type (UO_{2+x}) or n-type (UO_{2-x}) [5], and whether the adsorbate is an electron acceptor or an electron donor. The nearly uniform shift (~0.8 eV, see Table 5.) toward lower binding energies observed for the stoichiometric oxide in comparison with the saturated metal is probably due in part to the presence of negatively-charged adsorbed species on the semiconductor surface. The bonding of oxygen atoms in hydroxyl ions to the oxide surface would also increase the O 1s binding energy after water vapor adsorption on the stoichiometric oxide, as it would on the saturated metal. Formation of a dipole layer after adsorption of water vapor is the most likely cause of the small (0.1-0.3 eV) shifts toward higher binding energies observed here, although the orientation of the dipoles must be opposite to that required to account for changes in the photoelectron binding energies on Ni(110) [74], or changes in the work function on aluminum and iron oxides [73], after water vapor adsorption.

The distinct changes exhibited in the photoelectron spectra of the oxide surface upon saturation with water vapor shows that the water vapor-uranium reaction depends very much on the composition of the reacting surface. However, it is difficult to be more specific about the influence of the surface layer without some detailed knowledge of the intermediate steps between initial adsorption and final oxide formation. This information is difficult to obtain at room temperature because the reactions proceed to quickly to observe anything but the final reaction products. This is the reason that Allen et al. [19] cite to explain why they could not observe the presence of an OH^- contribution to the O 1s peak for low water vapor exposures at 298 K, although such a contribution was observed in this study. By cooling the sample surface to cryogenic temperatures and heating the sample in a controlled manner, the reactions can be slowed or even stopped, and the intermediate reaction steps studied in detail. The results of just such controlled heating experiments are now described.

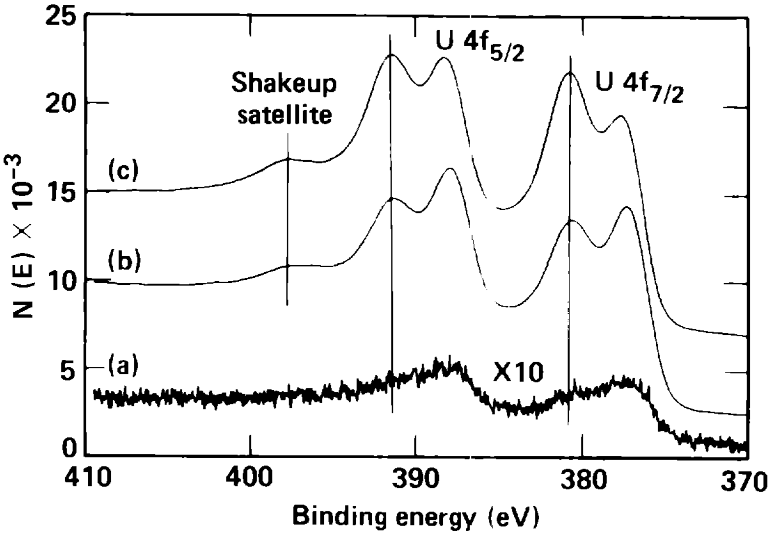

Fig. 5.2.9 U 4f spectra of clean uranium exposed to 40 L D_2O at a) 85 K, b) warmed to 197 K momentarily and cooled to 85 K, c) heated to 293 K in sequence.

The behavior of the U 4f core level peaks for water vapor exposures during controlled heating is depicted in Fig 5.2.9. The formation of an ice multilayer (see Fig. 5.2.11) attenuated the U 4f signal and shows that the region of the sample under analysis was completely covered by ice. Using the exponential attenuation expression discussed before, the ice layer is calculated to be ~5 nm thick at saturation coverages. Still, the presence of oxide formation even at 85 K is evident in the broadening of the metal lines toward higher energies. Upon heating to 197 K, just before the water desorption peak maximum (~200 K, see Fig. 5.3.1), and immediately cooling back to 85 K, the oxide peaks clearly emerged to make up about half of the total peak area. Further heating to 293 K completed the reaction as all the adsorbed water had left the surface and only a thin oxide layer remained. The persistence of the metal peaks clearly shows the incomplete oxidation of the near surface region, despite the total initial coverage by condensed water vapor. It is also interesting that the *metal* peaks shifted to higher binding energy by 0.3 eV upon heating while the oxide peaks remained substantially the same (see Table 5.1). This may be related to the binding energy shifts observed by Allen et al. [19] who attributed this behavior to changes in the work function induced by the presence of water vapor and initial island formation.

Changes in the O 1s spectra under similar treatment displayed even more interesting behavior as shown in Fig. 5.2.10. The spectrum at 85 K clearly shows an ice peak at 536.8 eV [76] and its associated X-ray satellite at 528 eV from the non-monochromatized source. Upon heating to 197 K and cooling back to 85 K two new peaks developed. The ice peak was diminished in intensity and shifted by 0.5 eV to higher binding energy. An oxide peak appeared at 531.5 eV, shifted higher by 0.2 eV from the room temperature value of 531.3 eV. There appeared an intermediate peak at 534.5 eV that is probably due to liquid water [57,58,74]. Heating past the water desorption peak maximum (~200 K) removed the ice layer and shifted both the liquid water and oxide peaks to lower binding energy. The intensity of the liquid water peak decreased as that of the oxide peak increased. In addition, a small

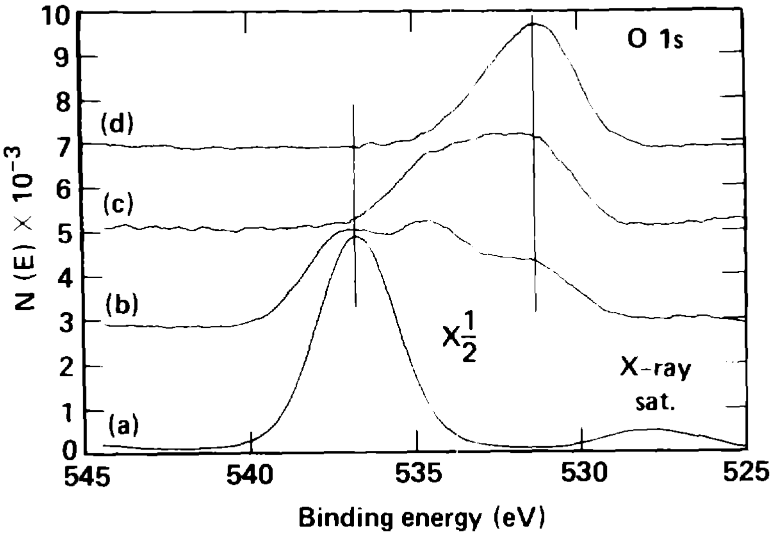

Fig. 5.2.10 The O 1s spectra for exposure of clean uranium to 40 L D_2O at a) 85 K, b) warmed to 197 K momentarily and recooled to 85 K, c) warmed to 205 K momentarily and recooled to 85 K, and d) warmed to 298 K in sequence.

peak at 533.0 eV appeared indicating the formation of surface hydroxide [61,62]. Finally, warming the sample to room temperature removed the liquid water peak and left a spectrum very similar to that observed after water vapor saturation at room temperature. Although the oxide

(531.2 eV) and hydroxide (533.3 eV) peaks maintained the same binding energy as those observed for room temperature water vapor saturation, the relative intensity of the hydroxide peak increased (see Table 5.1).

The changes in the O 1s spectra for water vapor adsorption at 85 K during heating are qualitatively the same as those observed by Nornes and Meisenheimer [27]. The reported persistence of a distinct intermediate peak at room temperature, ascribed to an OH-complex with the uranium surface, was observed here, although it was much less pronounced. The distinct peaks in the O 1s spectrum appeared only after partial desorption of the multilayer ice, which required heating to near 200 K. They observed an oxide peak at 532 eV even after adsorption of 54 L H_2O at 120 K contrary to the attenuating behavior of condensed water observed here and elsewhere [74]. This discrepancy might have resulted from an inaccurate calibration of the water vapor exposures used in their study. This would also explain why they observed such a small U $4f_{7/2}$ oxide peak after saturation with water vapor. They observed a +0.6 eV shift in binding energy for the O 1s photopeak, and a +1.2 eV shift in binding energy for the U $4f_{5/2}$ photopeak, in going from oxygen saturation to water saturation of clean uranium [27]. Although the trend to higher binding energies was also observed here, the magnitude of the shifts (~+0.3 eV) was far less.

The valence band region exhibited behavior similar to that of the O 1s spectra during controlled heating and is illustrated in Fig. 5.2.11. Only multilayer ice was present at the start of the experiment. The O 2s peak position (28.9 eV) and relative intensity is in good agreement with previously reported values for ice [76]. During heating, the dominant U 5f peak emerged, narrowed, and grew in intensity. Similarly, the U $6p_{3/2}$ peak narrowed and intensified during heating. There is some interesting behavior in the O 2p bonding band near 8 eV, two small peaks appeared in Fig.5.2.11c that persisted up to room temperature and may be due to hydroxide bonding directly with the

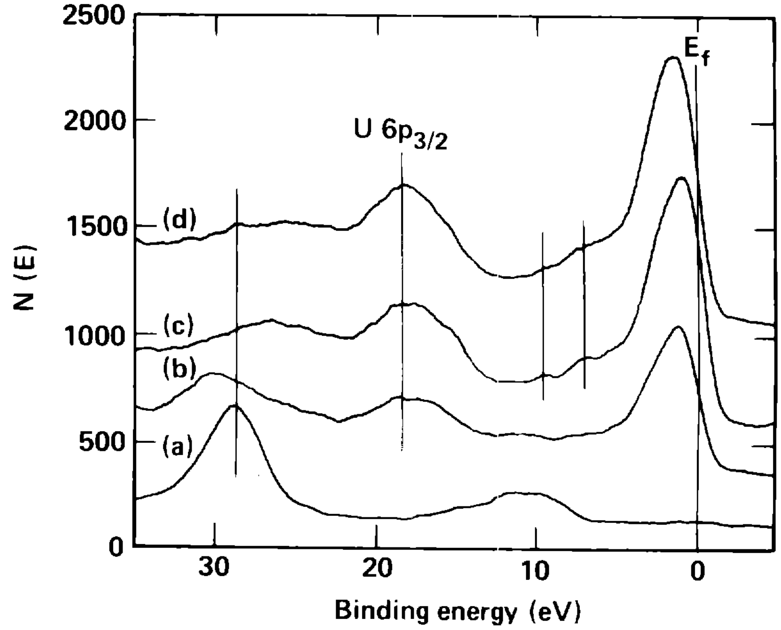

Fig. 5.2.11 Valence band region for exposure of clean uranium to 70L D_2O at a) 85 K, b) warmed to 197 K momentarily and recooled to 85 K, c) warmed to 220 K momentarily and recooled to 85 K, and d) warmed to 298 K in sequence.

uranium or to hydride formation [77]. This region of the valence spectrum showed significant differences compared to the spectrum observed after water vapor exposure at room temperature.

Ward et al. [77] have studied UO_2 and UD_3 with XPS. They observed a broad peak near 8 eV in the photoelectron spectrum of UD_3 that they attributed to hydrogen bonding levels. The observed valence level spectrum appeared very much like that of UO_2, except that the U 5f peak was shifted by ~1 eV to higher binding energy. The similarity of the photoelectron spectra of UO_2 and UD_3 is somewhat surprising, considering the very different chemical bonding taking place in each case, and may indicate possible contamination of the UD_3 by oxygen in the residual gas.

The broad U $6p_{3/2}$ peaks in Fig. 5.2.11 display the hint of an additional component. Because the U 4f core levels (see Fig. 5.2.9) contain substantial metal contributions, it is reasonable to expect that the broader U $6p_{3/2}$ peaks are composed of both a metal and an oxide contribution. The much narrower U $6p_{3/2}$ peak of the stoichiometric oxide (Fig. 5.2.8), where no metal contribution would be expected, supports this interpretation.

The O 1s spectra for water vapor exposure to oxygen-precovered uranium during controlled heating is shown in Fig. 5.2.12. The intensity of the ice peak in Fig 5.2.12a appears to be less than the corresponding peak in Fig. 5.2.10. However, the number of scans taken for the spectra in Fig. 5.2.10 was twice the number recorded for the spectra in Fig. 5.2.12, so that the intensity of the ice peak for water vapor (70 L) adsorption on the oxygen-precovered surface was actually greater than that for water vapor (40 L) adsorption on the initially clean surface, as would be expected.

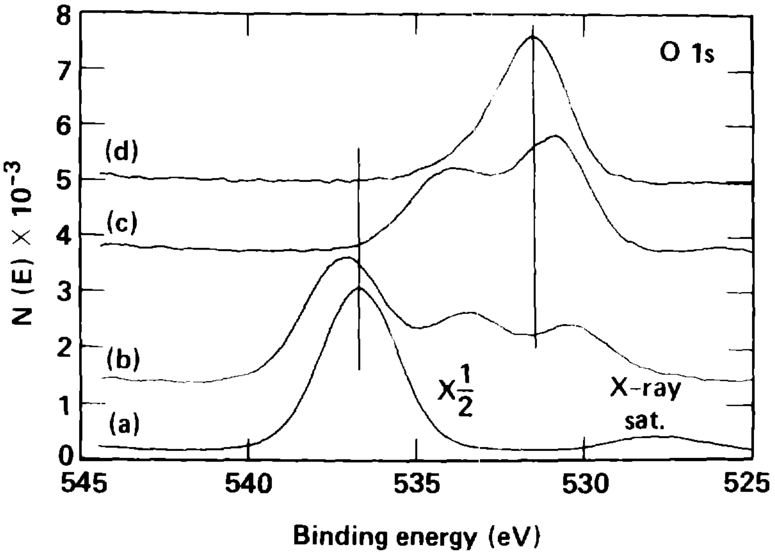

Fig. 5.2.12 O 1s spectra for exposure of clean uranium to 40 O_2 at 298 K followed by 70 D_2O at a) 85 K, b) warmed to 197 K momentarily and recooled to 85 K, c) warmed to 220 K momentarily and recooled to 85 K, and d) warmed to 298 K in sequence.

After heating to 197 K and recooling, two new peaks appeared as observed before for water vapor adsorption on clean uranium, although they were shifted toward lower binding energies (see Table 5.1). The shifted ice peak at 537.1 eV disappeared after heating to 220 K and the other two peaks moved to higher binding energies. The lowest-binding-energy peak is clearly due to the presence of an oxide layer and continued to grow during the heating as the condensed water overlayers were removed and oxide formation took place. The peak near

534 eV also grew during heating in direct proportion to the decrease in the ice peak, suggesting again that this peak is due to the presence of liquid water on the surface. Further heating to room temperature led to an O 1s spectrum similar to that for exposure of clean uranium to water vapor at room temperature, except that the peaks were shifted 0.2 eV to higher binding energies (see Table 5.1).

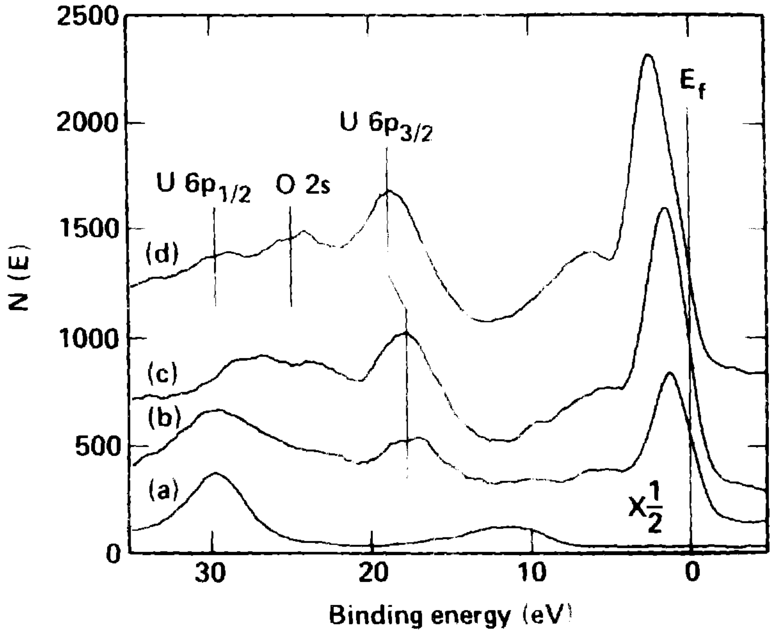

Fig. 5.2.13 Valence band region for clean uranium exposed to 40 L O_2 at 298 K followed by 70L D_2O at a) 85 K, b) warmed to 197 K momentarily and recooled to 85 K, c) warmed to 220 K momentarily and recooled to 85 K, and d) warmed to 298 K in sequence.

The valence band region for exposure of the oxygen-precovered uranium surface to water vapor during controlled heating, shown in Fig. 5.2.13, exhibited some differences in behavior compared to that for exposure of an initially clean surface to water vapor. Both the U 5f and U 6p peaks were narrower, and the final state spectrum had a better defined O 2p bonding peak similar to that for exposure of clean uranium to oxygen at room temperature.

It is perhaps surprising that the behavior of the photoelectron spectra for water vapor adsorption on clean and oxygen-covered uranium surface are so similar after the initial ice layer begins to desorb. Yet the rapid formation of an initial surface oxide layer after water vapor adsorption on the clean surface, beginning even at 85 K, shows that both systems are composed of condensed water-covered uranium oxide surfaces upon warming the surface. A similar conclusion was reached by Huber and Kirk [78] as a result of changes in the work function that were observed after water vapor adsorption on clean and oxygen-covered aluminum surfaces. Condensed water reacts rapidly with the exposed uranium metal surface, but the reaction is impeded by the underlying oxide layer. The large shifts to lower binding energy exhibited by the O 1s oxide peak after adsorption of water vapor on the oxygen-covered uranium surface during controlled heating (see Table 5.1) may be due to the complete arrest of the rapid corrosion of the metal by condensed water as a result of the protective oxygen coverage. OH^- ions could hydrogen-bond to the surface oxygen with multilayer water formation taking place on top of the initial bonded layer. The liquid water would form a dipole layer with a negative surface charge leading to a reduction in binding energy until the water is completely desorbed. The gradual increase of the O 1s oxide peak binding energy from its initial low value of 530.3 eV to its room temperature value of 531.5 eV (see Table 5.1) as the sample is warmed and the water desorbs, supports this hypothesis.

The reduction in the intensity of the hydroxide contribution to the O 1s spectrum for water vapor adsorption on oxygen-covered uranium compared to adsorption on clean uranium might be due to the blocking of adsorption sites available to the OH ions by the chemisorbed oxygen on the surface. The pronounced O 2s peak in the valence spectrum (Fig. 5.2.13) after water vapor adsorption in the presence of oxygen compared to the unresolved O 2s peak after adsorption of water vapor on the clean metal suggests that the water vapor-uranium reaction is inhibited in the presence of oxygen. Considering the very low coverages in these experiments, inhibition by a surface mechanism is most likely. This topic is further discussed in section 6.

5.3 Thermal Desorption Spectroscopy

Thermal desorption spectra were measured for clean and oxygen-covered uranium surfaces for a variety of water vapor exposures. The spectra shown in Fig. 5.3.1 are typical of the results obtained.

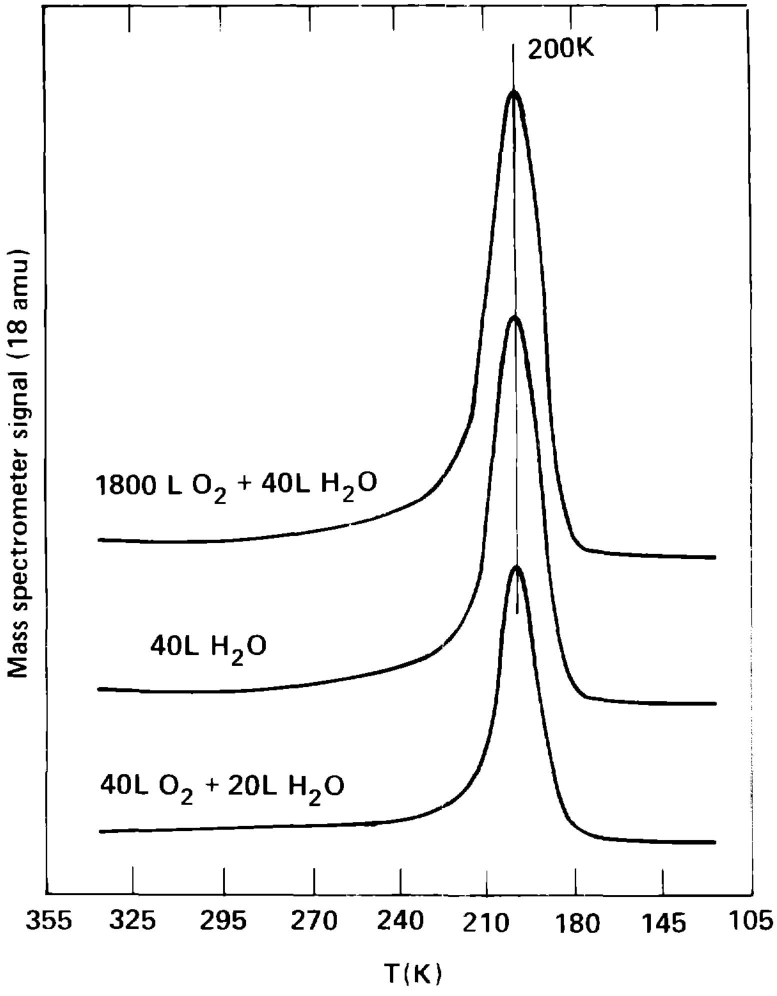

Fig. 5.3.1 Thermal desorption spectra for various exposures.

In each case, oxygen exposures were carried out at room temperature and water vapor exposures through the capillary doser were performed below 100 K. The heating rate used for each experiment was ~1 K/s.

A single desorption peak was observed in each experiment regardless of the amount of adsorbed water vapor or oxygen precoverage and is ascribed to multilayer ice. This is hardly a surprising result considering the high reactivity of the uranium metal and oxide. However, the observation of a single desorption peak on Cu(100) for all water vapor coverages was attributed to physisorbed water on the *inert* copper surface [79]. On uranium, initial oxide formation is rapid and hydroxyl groups or oxygen species can strongly chemisorb onto the oxide surface. The condensed water molecules can only weakly adsorb (through hydrogen bonding) onto the chemisorbed first layer, which behaves like an inert surface by preventing the water molecules from strongly interacting with the metal or the oxide. The broad tail toward higher temperatures might be due to the desorption of water molecules hydrogen-bonded directly to the oxide surface where the interaction might be stronger. The broadness of the desorption peak is indicative of the wide energy range of adsorption sites expected for a polycrystalline material.

The area under the top peak in Fig. 5.3.1 is greater by ~50% than that under the second peak for the same water vapor exposure. This indicates that the presence of a relatively thick stoichiometric oxide layer slowed the reaction of water vapor with the uranium metal. The initial adsorption on the less reactive oxide allowed more of the water vapor to subsequently desorb. This correlates well with the observation that the integrated peak intensity of the small O 1s companion peak (OH), 2 ev above the main peak, was 20% smaller after water vapor adsorption on the stoichiometric oxide than after adsorption on the metal at room temperature.

The absence of higher temperature desorption peaks implies that OH, or OD, is rapidly incorporated into the oxide once the initial multilayer has desorbed, and that any remaining surface hydroxyl ions must be strongly bound to the oxide layer. If this were not so, higher temperature peaks would be expected as the adsorbed OH^- ions recombine to form water vapor and leave adsorbed oxygen on the surface. Such disproportionation reactions have been observed on several single-crystal transition metal surfaces [39]. Bange et al. [80] have observed a single desorption peak after water vapor adsorption at 80 K on Ag(110) which was attributed to molecularly adsorbed water. However, in the presence of oxygen, several additional desorption peaks were observed due to just such disproportionation reactions.

As mentioned before, both Jupille et al. [38] and Stuve et al. [39] observed two desorption peaks for water adsorbed on clean single-crystal Re(0001) and Pd(100), respectively. The two states were ascribed to mulilayer ice and water molecules directly bound to the surface. On uranium surfaces, the formation of an oxide layer after water vapor adsorption on the clean metal is rapid even at 85 K (see Fig. 5.2.9). Only multilayer ice is available for desorption because the first layer is strongly chemisorbed on the metal to form the oxide.

Jupille et al. [38] found that oxygen preadsorption prevented the dissociation of water vapor on the Re(0001) surface. Similarly, Stuve et al. [39] found that preadsorbed oxygen actually blocked the initial adsorption of water molecules. Madey and Yates [81] also observed that adsorbed oxygen blocked the chemisorption of H_2O directly onto the Ru(001) surface, but did not affect the desorption of the condensed H_2O multilayer. The oxygen atoms interfere with the water vapor reaction by occupying adsorption sites on the metal surface normally available to the water molecules. These effects are dependent on the particular surface structures of the single-crystal metals involved and might not be operative on polycrystalline uranium metal surfaces. Also, the formation of an oxide layer does not occur on the transition metals at low exposures. An oxide layer forms readily on uranium metal so that desorption actually occurs from the oxide surface. Therefore, it is not surprising that the desorption spectra for water vapor adsorption on the clean metal and on the stoichiometric oxide are so similar. In each case, only condensed water from the oxide surface is being observed.

5.4 Electron-Induced Luminescence

Clean uranium surfaces exposed to saturation coverages of either CO, O_2, or H_2O and excited with a 5 keV, 150 μA electron beam displayed a faint blue luminescence which was the same at any location on the sample surface. The luminescence spectrum for clean uranium exposed to 120 L dry O_2 is shown in Fig. 5.4.1

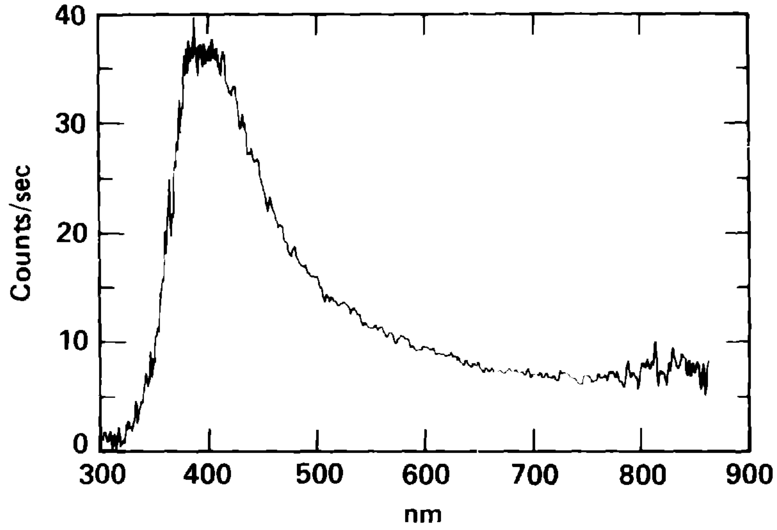

Fig. 5.4.1 Luminescence of clean uranium exposed to 120 dry O_2.

The luminescence did not change with time even though the Auger spectrum indicated that CO from the residual gas had been adsorbed on the surface after the exposures. There is a hint of a double peak with components at 395 and 405 nm that is more readily apparent upon smoothing the spectrum. The luminescence behavior observed for clean uranium exposed to each reactant gas is clearly related to the formation of an oxide layer. Bastasz et al. [46] have inferred the presence of a weakly adsorbed molecular oxygen species in addition to chemisorbed oxygen on Th surfaces during low pressure oxygen exposures from changes in the luminescence intensity as a function of pressure. However, no such increase in luminescence intensity was observed for uranium surfaces in low pressure oxygen environments. Because the intensity for low exposures is correlated with the amount of oxygen detected by AES, and the initial oxide formation is observed to be rapid, it must be concluded that the oxide layer is the source of the blue luminescence.

Breysse et al. [82] have studied the photoluminescence of thoria and have attributed the observed spectral peaks at 390 nm and 450 nm to excitation of F-centers in the oxide lattice. Substitutional cationic impurities of valence lower than 4+ were proposed to produce F-centers in the form of anionic vacancies. Vook et al. [47] have examined the cathodoluminescence of clean Th surfaces exposed to oxygen and carbon monoxide. They also attributed the major luminescence emission band at 468 nm to excitation of F-centers in the thoria lattice, and proposed that weaker bands in the spectrum arose from surface F^+- and F-centers.

It seems reasonable to propose that the uniform luminescence is due to the presence of F-centers formed from anionic vacancies in the oxide lattice. The dual peak structure of the luminescence spectra at

390 nm (3.23 eV) and 410 nm (3.07 eV) is probably due to the excitation of F^+- and F-centers respectively [83]. Surface F-centers are an alternate source for the second peak.

Coon [84] has observed a 0.2 eV shift in the broad photoluminescence emission spectrum of MgO compared to the bulk values. The shift was attributed to the possible creation of surface F-centers by electronic bombardment and their subsequent excitation. The peak shift observed for the luminescence of uranium oxide surfaces, 0.16 eV, is in excellent agreement with the shift observed by Coon for MgO. Further investigation is required to determine the precise nature of the F-centers responsible for the observed blue luminescence.

The strong asymmetry in the luminescence spectrum might be a result of clustering of point defects into defect complexes. Evidence for the presence of such complexes in hyperstoichiometric bulk uranium oxides has been obtained with X-ray diffraction [14], XPS [31], and thermogravimetric [17] techniques, but defect complex formation at very low exposures has not been investigated. It may be that these luminescence results provide the first such evidence for defect complex formation during the initial stages of uranium oxidation. Although this possibility, if correct, would have important implications for our understanding of uranium oxidation, the identification of defect complexes after very low exposures must remain speculative.

The asymmetry in the high wavelength side of the peak might also be indicative of contributions to the luminescence emission from centers other than anion vacancies. Optical emission spectra of U^{+4}, U^{+5}, and U^{+6} ions in crystal hosts exhibit a series of intense peaks between 500 and 600 nm [41-43]. Also, the strong green luminescence observed from many uranyl-containing compounds has been attributed to the uranyl group (UO_2^{+2}) itself [41]. It is not likely that U^{+5} and U^{+6} ions exist in the thin surface oxides produced in this study because either specific crystal symmetries, thicker oxide layers, or the action of hard radiation is required for their formation or stability [41,42]. However, one can envision the formation of uranyl groups on the surface for low coverages and this is a possible source for the asymmetry observed in the luminescence spectrum [44].

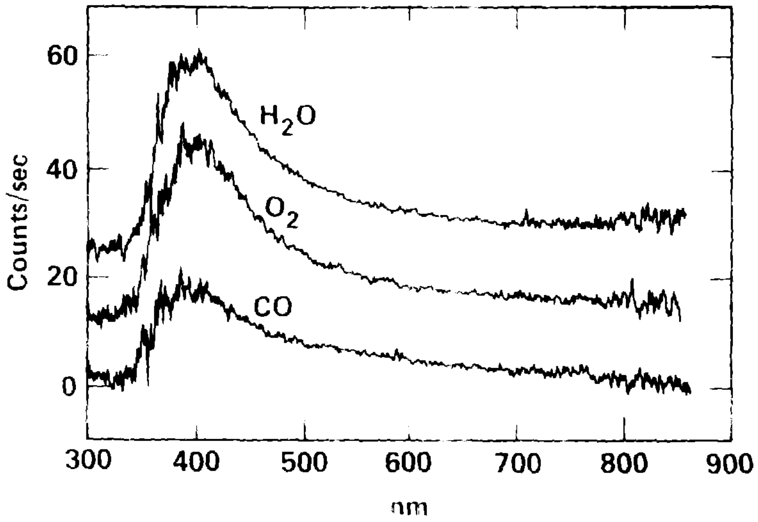

Fig. 5.4.2 Luminescence of clean uranium after saturation with pure water vapor, dry oxygen and dry carbon monoxide at room temperature.

Relative intensities of spectral peaks are difficult to compare owing to the number of variables such as beam voltage, current density or sample position that can vary from measurement to measurement. However, all of the luminescence spectra of the various oxides prepared by exposing clean uranium to either pure water vapor, dry oxygen or dry CO maintained the relative intensity relationship shown in Fig. 5.4.2 regardless of sample temperature (100 to 320 K) or variations in beam voltage or current density.

The intensity of the luminescence after water vapor exposure is about the same as that after oxygen exposure, but the intensity of the luminescence produced by exposing clean uranium to CO is about half that produced by either H_2O or O_2 exposure. This indicates that the uranium-carbon monoxide reaction produced only about half as much surface oxide as either O_2 or H_2O, a result consistent with AES data (see Fig. 5.1.2).

Previously published preliminary results for the luminescence produced from clean uranium exposed to increasing amounts of dry oxygen are shown in Fig. 5.4.3 [85]. The spectra were taken at room temperature and were not corrected for the response of the detection system. Fig. 5.4.3 shows that the intensity of the luminescence decreased as the oxygen exposure increased while the peak position remained constant at 470 nm (400 nm if corrected for detector response).

The change in the luminescence spectrum for increasing oxygen exposures displays the key role played by anion vacancies in the luminescence process. At low exposures, nominal UO_2 should form on the uranium surface which contains roughly equal numbers of oxygen vacancies and interstitials. The diffusion of surface oxygen to the bulk metal is rapid and a higher vacancy concentration would be

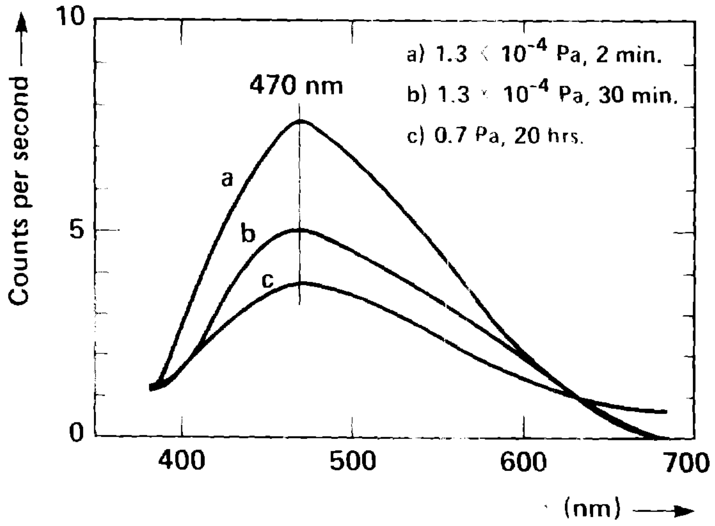

Fig. 5.4.3 Luminescence of clean uranium exposed to increasing amounts of dry oxygen.

expected at the surface after some time for low initial exposures. As the amount of oxygen at the surface increases to saturation and beyond, the number of vacancies in the oxide layer should decrease until the formation of UO_{2+x} is achieved, which is interstitial-rich [2]. The luminescence behavior shows just the sort of decrease in intensity for increasing oxygen exposure that would be expected if anionic vacancies were responsible for the luminescence [35].

The luminescence of clean uranium exposed to dry O_2, followed by H_2O produced markedly different behaviour as shown in Fig. 5.4.4. In addition to the previously described faint blue luminescence, there also appeared several localized spots on the surface that exhibited a bright red luminescence. The red luminescence was brightest when excited with a sharply focused beam and faded as the beam size was increased. This red luminescence has not been observed for any other combination of exposures including re-exposure of U + O_2 to O_2 or U + H_2O to H_2O.

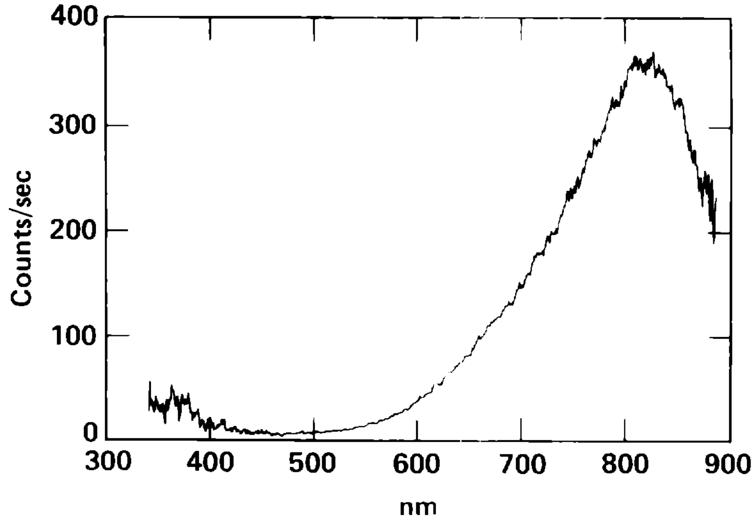

Fig. 5.4.4 Luminescence of clean uranium exposed to 2700 L dry O_2 followed by 240 L H_2O.

The bright intensity of the red luminescence made it possible to examine the spots with AES while simultaneously observing the luminescence. When the electron beam was moved to one of the localized spots, the oxygen peak-to-peak intensity increased by about 50% over the peak-to-peak intensity of the background surface oxide. No rare earth or other impurities were detected by AES that might have caused the luminescence so that it must be due to localized concentrations of oxide or specific oxygen species on the surface.

During the course of XPS measurements, the sample was repeatedly exposed to oxygen and water vapor, separately and in combination. After several such exposures, localized oxide spots were detected that could not be easily removed by sputtering. The precise nature of these spots is discussed in section 5.5, but it should be noted here that upon further exposure of the cleaned sample to water vapor, these spots exhibited the same type of bright red luminescence that had been seen in previous experiments.

Summers et al. [83] studied the photoluminescence of MgO single-crystals and showed that F^+- and F-center emissions at 394 nm (3.2 eV) and 548 nm (2.3 eV), respectively were strongly influenced by the presence of H^-. Both the lifetimes and the relative intensities of the luminescence emissions varied with hydrogen content. Breysse et al. [82,86] have proposed that photoluminescence emission from ThO_2 might be due to OH groups on the oxide surface. These groups were postulated to substitute for normal lattice oxygen atoms on the surface and luminesce via the broadened OH-band emission.

The presence of OH^- on the surface or in the oxide by itself is an unlikely cause of the observed red luminescence because it should be observed when clean uranium is exposed to water vapor alone. The XPS results show that OH^- is retained on the oxide surface after such exposures. Also the correlation of the localized luminescence spots with the surface pits suggests that the species responsible for this luminescence exist only in special surface environments.

Clement and Hodson [87] have observed a broad-band emission from γ-ray-irradiated MgO crystals at 700 nm that was explained on the basis of transitions involving substitutional metallic impurities, namely Fe^{2+} and Cr^{3+}. The red luminescence was attributed to excitation of the Cr^{3+} ion impurity giving rise to the characteristic doublet emission at 700 nm and 720 nm, and to emission from the Fe^{1+} to Fe^{2+} transition.

The uranium samples used in this study contain about 12 ppm Fe and 3 ppm Cr impurities (Table 4.2.1). The observation of Fe lines in the Auger spectrum from one of the initial oxide pits provides some evidence for emission from metallic impurities as the source of the red luminescence. However, Fe was only observed on one spot and was depleted after several hours of sputtering so that it may have been an isolated inclusion. But even the presence of impurities in amounts below the detection limit of AES could be responsible for the luminescence. However, intense emission from substitutional impurities can be dismissed as the cause of the observed red luminescence because it appeared only after specific surface preparation. Unless the chemisorption of oxygen on uranium oxide, followed by water vapor exposure somehow allowed the preferential excitation of impurity levels, another explanation must be sought.

It has long been known that molecular oxygen exhibits a strong red chemiluminescence [88]. The emission spectrum of electrically discharged oxygen is dominated by two intense peaks at 760 nm and 800 nm [88]. It is possible that the localized red luminescence observed here is due to excitation of adsorbed molecular oxygen that is stabilized by the presence of water vapor or hydroxide in the oxide layer. Alternatively, the molecular oxygen might form part of a complex with uranium and OH^- in the near surface. If the luminescence were due to molecular oxygen, the broadening of the peaks must be due to the interaction with the oxide lattice. It could be that the relatively thick oxide region in the pits after repeated water vapor and oxygen exposures creates the right environment for the existence of molecular oxygen.

The presence of strongly chemisorbed O_2^- or O^- after oxygen exposures has been inferred from the results of the AES and XPS measurements in sections 5.1 and 5.2. Upon water vapor adsorption, the chemisorbed oxygen may associate with chemisorbed hydroxyl ions or hydrogen-bonded water molecules to form large complexes on the surface [63]. These large complexes would still be bound to the surface, though perhaps not as strongly as the individual species, and could produce a broadened luminescence emission in the near infrared as a result of electron beam excitation. These complexes could be related to paramagnetic defect centers observed on hyperstoichiometric uranium oxide surfaces by EPR [64]. In fact, it would not be surprising to find that the centers responsible for the red luminescence observed here and those responsible for the complex EPR spectra obtained for UO_2 after exposure to water vapor and oxygen [64] were closely related.

Although several explanations are feasible, the precise determination of the nature of the centers responsible for the red luminescence must await further experimentation.

Any evaluation of EIL as a surface technique must consider both its advantages and disadvantages. EIL does not appear to be sensitive to surface adsorbates, as is XPS. There is no distinction between the luminescence of water vapor- and oxygen-saturated uranium, and therefore no distinction between chemisorbed oxygen and hydroxyl ions. This is because EIL is sensitive to the electronic defect structure of the *oxide*. Herein lays one of its major advantages. The intensity of the luminescence is sensitive to the concentration of point defects in the form of F-centers in the oxide. Thus it was possible to observe changes in the point defect concentration as a function of oxygen exposure, and to infer the presence of point defect clustering for low exposures, although only speculatively. One of the major disadvantages of EIL is its inability to provide quantitative information regarding the surface composition. But the use of an electron beam to excite the luminescence allowed this information to be obtained by the complementary technique of AES. Through the use of AES, the surface pits were shown to contain a high concentration of oxygen, but the chemical nature of the oxygen could not be determined with AES alone. The bright red luminescence observed in these pits indicates that the oxygen species responsible for this behavior were quite different than those existing on or in the uniform oxide layer. This is important information that would be difficult to obtain by other means. The precise nature of the centers responsible for the red luminescence would require the use of techniques sensitive to the chemical state of the luminescing species, such as small-spot XPS. It seems that EIL is a very useful technique for the study of metal oxides, and that it nicely complements the existing standard techniques of surface analysis.

5.5 Surface Morphology

The characterization of the morphology of surfaces is an important aspect of the study of the initial oxidation reaction.

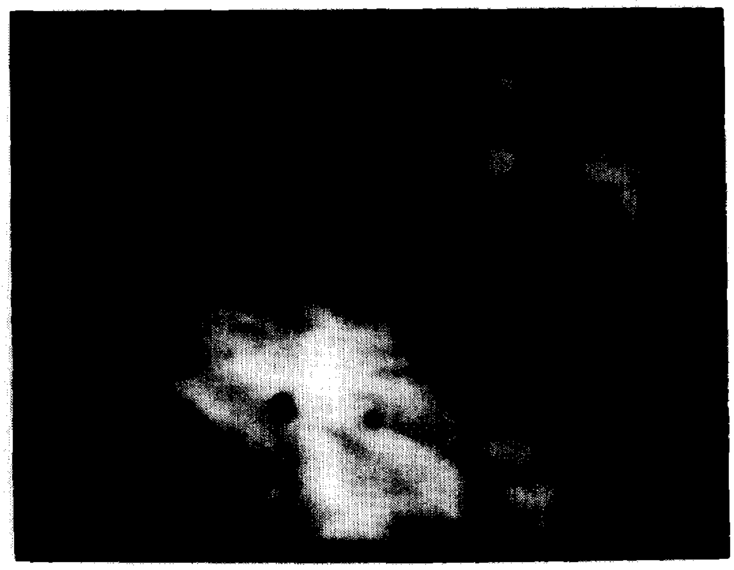

Fig. 5.5.1 Secondary electron image of the uranium surface after several exposures to oxygen and water vapor. The magnification of the image is 250x and the length scale is 1 cm = 40 μm.

XPS studies were performed in an analysis chamber equipped with a scanning Auger microprobe (SAM) capable of imaging the secondary electron distribution (SED) of surfaces. The secondary electron image of the surface was regularly observed during the initial sample cleaning phase and before and after each experiment. Although the surface was initially polished with 1 μm diamond paste and had a mirror finish, several days of constant argon ion sputtering and heating left the surface rough and uneven.

The sample was exposed to oxygen and water vapor at room temperature, separately and in combination, several times with no apparent change in the sample surface. After the initial controlled heating experiment, with 40 L D_2O adsorbed at 85 K and the surface warmed back up to room temperature, several dark spots appeared in the center of the sample as shown in Fig. 5.5.1.

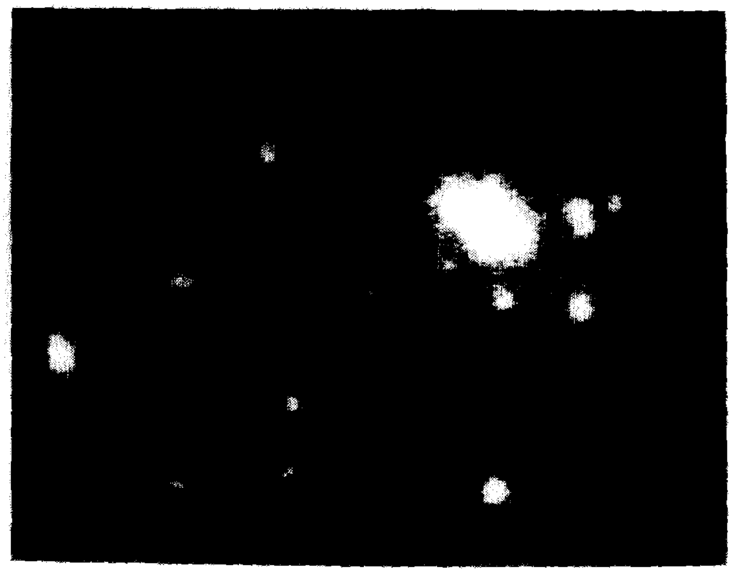

Fig. 5.5.2 Scanning Auger image of the contribution from the surface to the O (KLL) peak-to-peak intensity. The magnification is 250x and the length scale is 1 cm = 40 μm.

Examination of the surface with AES showed that the spots contained a high concentration of oxide which persisted even after several hours of sputtering. Iron was detected in one of the spots, but disappeared after several hours sputtering with a 6x6 mm^2 raster. Iron was not detected at any other location of the sample nor at any other time during the experiment. However the spots continued to multiply after each controlled heating experiment.

The spots were concentrated in the center of the sample in an area approximately 3 mm in diameter, where water vapor exposures using the capillary doser were carried out. The use of a single capillary doser for water vapor exposures provides a large pressure enhancement factor but suffers from a highly non-uniform distribution of vapor over the surface [54].

A scanning Auger micrograph of the same sample region shows that the dark spots are composed of localized concentrations of oxide on the surface about 20 μm across, probably in the form of pits several microns deep. Although the O (KLL) signal from these pits could be diminished ($O/U < 0.01$), it could not be completely eliminated. Similarly, the pits themselves could not be removed even after several days of constant sputtering of the surface. The oxygen content of the pits could not be detected by XPS and does not affect the conclusions based on XPS measurements.

For most of the exposures, the capillary doser was placed about a millimeter above the center of the sample. Because the flux decreases rapidly away from the center for a doser of this design, the water vapor should have been concentrated in an area roughly 3 mm in diameter in the center of the sample [54]. This correlates with the high concentration of these pits in the central region of the sample and indicates that water vapor was the principle cause of the localized attack of the surface. The fact that pit formation was not observed after the first few water vapor exposures performed at ambient temperatures, but only appeared after the first exposure at 85 K, could mean that there is a long incubation time for pit formation or that reduced temperatures delay the depletion of species responsible for pitting.

One possible explanation for pit formation is the selective hydriding (UH_3) of the surface as a result of the prolonged presence of hydrogen-containing species in the oxide layer during the slow warming of the sample from LN temperatures. The retention of OH^- ions and water vapor on the surface should be longer as the sample is slowly warmed to room temperature over the period of an hour or two. Also, the condensed water overlayers may provide the high overpressures required for hydriding. Hydriding of uranium metal and alloys has been shown to proceed by selective attack of the surface to form hydride islands that can pop off the surface to leave pits [89,90]. Bedere and Sans [91] proposed that hydrogen attack on $UV_{0.095}$ at 343 K took place under the oxide layer and spread until this layer ruptured.

Hydride formation as a result of the water vapor–uranium reaction has been postulated [60,92,93] and inferred from metallurgical studies [94]. Kondo et al. [94] studied the oxidation of uranium in moist environments with gas chromatography and optical micrography. They observed a thin layer (~270 nm) of material just underneath the metal–oxide interface that they attributed to uranium hydride formation. They concluded that the fracture of this layer above some critical thickness lead to the observed rapid oxidation of uranium near ambient temperatures. Baker et al. [60] studied the reaction of uranium with water vapor–oxygen mixtures and observed that for water condensation conditions, the reaction rate increased, hydrogen was evolved, and surface pitting occured. They interpreted this behavior to the partial exclusion of oxygen from the oxide surface by water, with the oxygen deficient sites being preferentially attacked. They did not observed surface pitting in the absence of oxygen and, with the observed dependence of the reaction rate on the water vapor pressure, concluded that the reaction did not proceed by an "electrochemical cell" mechanism [93]. They proposed that hydride and oxide formation occured simultaneously.

Surface pitting was not observed for the oxygen–uranium reaction so it must be concluded that hydrogen–containing species, perhaps in high concentrations and in the presence of surface impurities or grain boundaries, are responsible for the selective attack of the uranium surface during oxidation. It was mentioned that the clean polycrystalline surface of uranium is composed of high concentrations of microcrystallites randomly oriented and separated by grain boundaries. Grain boundary diffusion through the oxide surface layer may be responsible for the surface pit formation by bypassing the normal interstitial transport of OH^- ions through the oxide layer for a more direct route along grain boundaries.

The observation of liquid water on the surface during controlled heating by XPS (see section 5.2) suggests that the possibility of aqueous corrosion must be considered. Surface pitting was observed after adsorption of pure water vapor on clean uranium at 85 K followed by heating to ambient temperatures, contrary to the findings of Baker et al. [85]. Although liquid water was formed, an underlying layer of oxide was present that separated the liquid water from the bulk metal (see Figs. 5.2.9-10). This layer greatly reduces the solvation of uranium ions and impedes the attack by liquid water. Local imperfections in this oxide layer may cause breaks in the film and lead to rapid corrosion of the underlying metal which result in the formation of pits [95]. This is similar to the process proposed by Baker et al. [60] for pit formation in water vapor-oxygen mixtures. The presence of pre-adsorbed oxygen should delay this process by producing a protective oxide layer that decreases the chance of liquid water attack.

It is clear that more work in this area is necessary before a complete understanding of the selective oxidation of uranium by water vapor is achieved.

6. INITIAL REACTION MECHANISMS

The reaction of clean uranium with dry oxygen, pure water vapor and dry carbon monoxide is fast at room temperature. Surface contamination by the residual gas can be detected with AES after only three minutes at a base pressure of 1 x 10^{-8} Pa. One Langmuir exposure of either gas immediately produces a prominent oxygen peak in the Auger spectrum. At 10 L exposure, shifts in the valence Auger peaks are observed indicating the formation of an oxide layer.

Bulk oxidation mechanisms for the reaction of dry oxygen with clean uranium have been extensively studied and are relatively well understood [2]. Oxygen is molecularly chemisorbed onto the clean uranium surface and rapidly dissociates and combines with the surface uranium atoms to form an oxide layer. Heating the oxygen-saturated surface above ambient temperatures accelerates the transport of oxygen into the bulk; the O (KLL) AES peak nearly disappears upon heating to 1000 K. This rapid diffusion of surface oxygen into the bulk has implications for any claims of a stable UO surface phase [24] (see section 5.1).

Once the initial oxide layer is formed, molecular oxygen continues to adsorb on the oxide surface. Most of it dissociates and is transported into the oxide lattice in the form of O^{2-} where it diffuses to the metal-oxide interface. Some of the oxygen remains on the surface as chemisorbed O_2^- or O^-, or in the near-surface as interstitial O^-. The ability to create surfaces with O/U ratios in excess of the stoichiometric value of two (as measured by AES, see section 5.1) indicates that the oxide surface is capable of adsorbing additional oxygen. Such a "supersaturated" surface can hold chemisorbed oxygen in the form of O_2^- or O^-, and the near-surface becomes interstitial-rich. Similarly, the metal-oxide interface is not monolithic and probably consists of a sub-stoichiometric transition region betwen the bulk metal and the stoichiometric oxide. Thus for low exposures, one can envision the situation where UO_{2+x} predominates near the gas-oxide interface, UO_{2-x} predominates near the metal-oxide interface, and nominal UO_2 exists between the two thin non-stoichiometric regions. For longer exposure times or higher oxygen pressures, the UO_{2+x} region grows and moves toward the metal-oxide interface until the entire oxide layer becomes interstitial-rich UO_{2+x} [17].

The initial reaction of water vapor on clean and oxygen-covered uranium is not well understood [2]. Reaction of the clean surface involves the chemisorption of the water molecules onto the uranium surface through the metal-oxygen bond. The chemisorption breaks one of the O-H bonds in a dissociation reaction to leave a strongly chemisorbed OH^- and an H^+ weakly bound to the surface hydroxyl ion. The H^+ ions recombine to form molecular H_2 that escapes into the gas phase. Hydride formation is probably not important at this stage of the reaction. This process continues on the metal surface until an oxide layer is formed.

The presence of an oxide layer changes the adsorption mechanism of the water molecules. With no metal surface nearby to promote dissociation reactions, the water molecules probably hydrogen bond to the oxygen atoms in the oxide lattice. Multilayer formation can then take place on top of this hydrogen-bonded layer. The molecules hydrogen-bonded to the surface can react with the adsorbed lattice oxygens via a hydrolysis reaction to form lattice OH^- and surface OH^- as follows:

$$H_2O(s) + O^{2-}(l \text{ or } i) = OH^-(l \text{ or } i) + OH^-(s)$$

also

$$H_2O(s) + O^-(i) + e^- = OH^-(i) + OH^-(s),$$

where s, l, and i designate surface, lattice, and interstitial species, respectively.

The chemisorbed OH^- ions diffuse through the oxide lattice in much the same way as O^{2-} ions do in the case of dry oxygen exposure. Thermogravimetric studies of the water vapor-uranium reaction give pressure dependences consistent with transport of singly-ionized species, such as O^- or OH^-, probably by an interstitialcy mechanism (see Fig. 2.2.2). The transport of OH^- in the fluorite lattice has been shown to require less energy than transport of either O^- or O^{2-} due to the lower Coulomb energy opposing displacement of OH^- from the lattice site [2]. The interstitial OH^- ions combine with the uranium atoms at the metal-oxide interface releasing protons that combine to form molecular H_2. The H_2 molecules can then either rapidly diffuse to the surface and escape into the gas phase or combine with the uranium to form a hydride according to the following reaction:

$$2U + 3H_2 = 2UH_3.$$

This fairly simplified view of the oxidation of uranium in water vapor environments has been shown to be inadequate to explain some aspects of the reaction of water vapor with solid and liquid uranium [96].

The presence of both hydrogen-bonded and strongly chemisorbed surface OH^- ions is likely, but the latter is probably energetically more favorable and therefore dominant as evidenced by the ~0.3 eV increase in O 1s photoelectron binding energies observed in going from oxygen to water vapor saturation of the clean surface. The strongly bound oxygen of the OH^- would result in a positive surface dipole charge. This would lead to a decreasing work function and an increase in binding energy as is observed. Also there is no reason to think that the same affinity for strongly chemisorbed O_2^- shown by the oxide layer would not also operate for the oxygen atoms in the OH^- ions. The properties of the highly reactive oxide dominate the further initial oxidation of uranium in both dry oxygen and pure water vapor environments. In particular, the strong chemisorption on the active oxide surface promotes the formation of UO_{2+x} even at an early stage in the oxidation process. This is important because it has been suggested that a thin layer of UO_{2+x} is a prerequisite for further oxide growth [2,97].

The initial carbon monoxide-uranium reaction was briefly discussed in section 5.1. A detailed discussion of this reaction was given by McLean et al. [26] and need not be repeated here. However, there are some observations worth noting. As mentioned before, carbon competes with oxygen adsorption sites on the uranium metal and interferes with the growth of the surface oxide layer. The formation of a carbide beneath the surface might also impede the transport of oxygen into the bulk which would limit the oxide growth. Because this reaction was not studied with XPS or SIMS, the role of chemisorbed species, such as CO or O^-, in the further growth of the oxide is unknown, but strong chemisorption probably precedes incorporation into either the oxide or the carbide as in the case of oxidation by oxygen or water vapor.

That oxygen inhibits the water vapor-uranium reaction has been clearly established by thermogravimetric studies (see Fig. 2.2.7) [12]. Yet there are differing views of the mechanism for this behavior [2,12,19]. Colmenares et al. [12] have suggested that chemisorbed oxygen on uranium oxide can block adsorption sites normally available to water molecules to undergo hydrolysis, thus interfering with the formation of OH$^-$ in the oxide lattice. This blocking action would be confined to the oxide surface and would cease to operate with the depletion of the chemisorbed oxygen as it diffused into the bulk. Studies of the water vapor-uranium reaction in controlled volumes have shown that in the presence of oxygen, the evolution of hydrogen from the oxidation reaction is completely stopped, but is resumed when the oxygen concentration in the gas phase falls below a certain well defined value [60,98,99].

Studies of water vapor adsorption on clean and oxygen-predosed single-crystal transition metal surfaces have shown that oxygen can prevent the dissociation of water vapor at the surface [38] and even reduce the initial adsorption of water vapor [40], lending support to the mechanism proposed by Colmenares et al. This mechanism would require oxygen rather than water vapor to preferentially chemisorb on the vacant surface sites left by oxygen atoms diffusing to the metal-oxide interface [2,60]. Some evidence for this behavior was observed in the XPS results during controlled heating as discussed in section 5.2.

Colmenares [2] has pointed out that the amount of oxygen inhibition increases as the water vapor pressure increases, and this is readily apparent in Fig. 2.2.7. Yet the inhibited reaction rate seems to be independent of oxygen concentration. The sharp cutoff of the reaction rate is similar to a phase transition and may indicate the onset of a diffusion-controlled process.

Allen et al. [19] noted that the initial oxidation reaction appeared to be independent of oxygen concentration in water vapor-oxygen mixtures and therefore was controlled by a tunneling process. Their results suggested that the effect of oxygen is not apparent until a relatively thick (>3 nm) oxide layer is formed where oxygen might control the transport of OH^- through the oxide layer. They postulated that the presence of oxygen promotes the formation of defect complexes that would diffuse more slowly through the oxide layer. These complexes would present an additional barrier to OH^- diffusion making the rate of reaction depend on the oxygen concentration. However, they noted none of the satellite structure on the high binding energy side of the U 4f photoelectron peaks that is characteristic of such defect formation [19,30,31].

As mentioned previously, OH^- probably diffuses through the oxide layer to the bulk by an interstitial mechanism as does O^- and O^{2-}. Transport of OH^- is energetically more favorable than the oxygen ions and therefore faster under similar conditions. A simpler mechanism for the inhibition of the water vapor-uranium reaction than that proposed by Allen et al. [19] is that the presence of oxygen might cause a sort of traffic jam on the avenues of transport in the oxide layer. Because both OH^- and O^- or O^{2-} diffuse via an interstitial mechanism, at some concentration of oxygen, the OH^- ions may have to wait for the slower oxygen ions to migrate out of the way before proceeding on toward the metal. For low concentrations of oxygen, the transport of OH^- is virtually unaffected. As the oxygen concentration increases, more and more of the hydroxyls are temporarily blocked by the slow moving (relative to the OH^-) oxygen ions. At some critical concentration, the transport of oxygen dominates all interstitial transport in the layer.

This scheme does not require the formation of defect clusters as suggested by Allen et al. [19], which have only been observed for much thicker oxide layers [30,31]. A reduction in hydrogen production is explained by the reduction in the number of OH^- ions reaching the metal-oxide interface as in the previous mechanisms. The constant rate of inhibited reaction, moreover, is close to that for the reaction of dry oxygen with uranium, further supporting this impeded transport model of this inhibition.

Alternative proposals have been put forward to explain the oxygen inhibition of the water vapor-uranium reaction. Fuller et al. [100] have proposed that some of the hydrogen released at the metal-oxide interface during the water vapor-uranium reaction diffuses into the metal and aids in the further oxidation of the metal by a process related to hydrogen embrittlement. They concluded that the inhibiting effect ofoxygen on the water vapor-uranium reaction was actually a result of the dimunition of the hydrogen enhancement of the oxidation reaction which results from the scavenging of excess hydrogen by oxygen to form water vapor. However, this explanation is not consistent with the sharp drop in the reaction rate above a certain oxygen concentration as is observed (see Fig. 2.2.7) [2,99].

Despite many experimental investigations of the inhibiting effect of oxygen on the water vapor-uranium reaction in the bulk [2,60,99], and several studies of the water vapor-uranium surface reaction [19,27] including the present study, insufficient information exists to allow a choice between the various proposed mechanisms for this behavior.

7. SUMMARY AND SUGGESTIONS FOR FUTURE WORK

The initial oxidation reactions of clean, high-purity polycrystalline uranium metal surfaces with dry oxygen, pure water vapor, and dry carbon monoxide for temperatures between 85 and 298 K were studied with Auger electron spectroscopy (AES), X-ray photoelectron spectroscopy (XPS), thermal desorption spectroscopy (TDS), and electron-induced luminescence (EIL).

Saturation of the clean uranium surface at room temperature occured after 7.5, 40, and 36 Langmuirs exposure to CO, O_2, and H_2O, respectively. The oxygen concentration on the surface at saturation was found to be the same after O_2 and H_2O exposure, but was reduced by one-third after CO exposure. This low surface oxygen coverage was interpreted as arising from the competition between carbon and oxygen atoms for adsorption sites on the surface during the reaction. Sequential heating and oxygen saturation of the uranium surface produced a grossly sub-stoichiometric oxide layer as oxygen diffused into the bulk during heating: the formation of a stable UO phase was not observed.

Saturation of the clean uranium surface with oxygen or water vapor at room temperature produced a sub-stoichiometric oxide layer with contributions from the metal to the U 4f core level spectra of ~30% and

~43%, respectively, which was interpreted as non-uniform oxidation of the near-surface. The O 1s spectra for oxygen and water vapor exposures consisted of a main peak at 531.0 or 531.3 eV, respectively, and a small companion peak 2 eV higher in binding energy. The companion peaks were interpreted as arising from strongly chemisorbed O_2^- or O^- in the case of oxygen exposure, and strongly chemisorbed OD^- in the case of D_2O exposure. These assignments were confirmed by secondary-ion mass spectroscopy (SIMS) which showed negligible amounts of OH^- ($OH^-/O^- < 0.01$) on the surface after oxygen saturation, but a substantial amount of OD^- ($OD^-/O^- \sim 0.1$) after D_2O saturation.

XPS measurements during controlled heating of the water vapor-saturated surface from 85 K to 298 K showed that water chemisorbed on the surface at 85 K to form a strongly bound first layer covered by multilayer ice. Heating the surface produced liquid water which completely desorbed at room temperature to leave an oxide and strongly chemisorbed hydroxyl ions on the surface.

Preadorption of oxygen was shown to have a strong effect on the photoelectron spectra during controlled heating. Multilayer ice formation still took place at 85 K, but the O 1s oxide peak was observed at sharply lower binding energy upon warming the surface than that observed for adsorption of water vapor on the clean surface. After warming to 298 K, the peak positions returned to their previously observed values indicating that the resultant surface oxide was not affected by an oxygen precoverage of the surface. The lower binding energies observed after water vapor adsorption on the oxygen-precovered surface while warming were interpreted as arising from chemisorbed oxygen blocking the adsorption sites normally available to water molecules. Water molecules could then only be hydrogen-bonded to the surface oxygen atoms until adsorption sites were freed by oxygen diffusing into the bulk. Hydrogen-bonded water molecules produce a negative surface charge that would result in a decrease in the binding energy, as observed.

Thermal desorption measurements for water vapor adsorbed on clean and oxygen-covered uranium displayed a single desorption peak at 200 K attributed to multilayer ice. The lack of higher temperature desorption peaks was interpreted as a result of the strong chemisorption of OH^- on the oxide surface.

Examination of the surface with electron micrographic techniques showed that surface pitting took place after controlled heating experiments. The pits were ~20 μm in diameter and contained a high concentration of oxide. The pits were interpreted as arising from the electrochemical interaction of liquid water on the surface with possible local hydride formation taking place.

Luminescence measurements of the uranium surface saturated with O_2, CO or H_2O produced a faint blue emission peaked at 400 nm with a hint of a dual peak. This luminescence arose from the excitation of F-centers formed in the uniform oxide layer. Adsorption of water vapor on an oxygen-covered surface produced localized spots of bright red luminescence with a broad peak centered at 800 nm that was 100 times more intense than the uniform blue background emission. These luminescence spots were correlated with the pits observed by electron micrography. It was proposed that this intense luminescence arose from the excitation of molecular oxygen stabilized by the presence of hydroxyl ions on the surface, or to large surface complexes of O and OH.

Reaction mechanisms for the initial oxidation of uranium by O_2, CO, and H_2O were proposed and discussed. The inhibition of the uranium-water vapor reaction by oxygen was proposed to result from the preferential chemisorption of oxygen species on the surface that block the strong chemisorption of water molecules and hydroxyl ions.

Because this study is one of only a very few investigations of the initial oxidation reactions of uranium, its results should be considered preliminary and by no means conclusive. Much more work remains to be done before a complete understanding of the uranium oxidation reactions is achieved. In particular, the effect of CO on both the oxygen- and water vapor-uranium reactions is unknown. The strong interaction between carbon and uranium would be expected to significantly effect the adsorption of oxygen and water vapor on uranium and its subsequent oxidation. Systematic studies of water vapor and oxygen adsorption on clean and CO-covered uranium should be carried out with surface-sensitive techniques to explore this possibility. The nature of the red luminescence from uranium oxides also deserves further attention. Distinctly different behavior after specific surface preparation indicates that potentially very interesting new reactions are taking place. It is not clear whether this behavior is unique to uranium oxides. Attempts should be made to observe this luminescence on similar oxides such as ThO_2 or MgO. The correlation of the red luminescence with selective oxidation of the surface and subsequent pitting increases the importance of this mode of attack. The formation of surface pits should be carefully monitored with electron micrography and small-spot XPS to determine the nature of the reactants responsible for this behavior. The possibility of hydride formation during the water vapor-uranium reaction is still an important problem that has not been resolved. Further studies of uranium hydrides and deuterides with XPS would be very helpful in clarifying the role of hydriding in the water vapor-uranium reaction. The mechanism of the inhibition of the water vapor-uranium reaction is also still uncertain. Dynamic studies of the uranium surface reactions by XPS in flowing water vapor and oxygen gas may shed some light on this question.

8. LITERATURE CITED

[1] W.L. Meyer, Z. Phys. 85 (1933) 278, from L. Manes and J. Naegele, in *Plutonium 1975 and Other Actinides*, H. Blank and R. Lindner, eds., (North Holland, Amsterdam 1976).

[2] C.A. Colmenares, "Oxidation Mechanisms and Catalytic Properties of the Actinides," in *Progress in Solid State Chemistry*, Vol. 15, 257-364, G.M. Rosenblatt and W.L. Worrell,eds., (Pergamon Press, New York, 1985).

[3] *Actinides in Perspective Proceedings*, N. Edelstein, ed., (Pergamon Press, New York, 1982).

[4] *Nuclear Reactor Materials*, C.O. Smith, (Addison-Wesley, Reading, Mass., 1967).

[5] C.A. Colmenares, "The Oxidation of Thorium, Uranium and Plutonium", in *Progress in Solid State Chemistry*, Vol. 9, 139-239, J.O. McCaldin and G. Somorjai, eds., (Pergamon Press 1975).

[6] Hj. Matzke, Journal de Physique, C9 11-12 (1973) 317-325.

[7] A.B. Auskern and J. Belle, J. Nuclear Materials 3, No. 3, (1961) 267-276.

[8] C.R.A. Catlow, J. Nuclear Materials 79 (1979) 432-434.

[9] J. Naegele,L. Manes and U. Birkholz in *Plutonium 1975 and Other Actinides*, H. Blank and R. Lindner, eds., (North Holland, Amsterdam, 1976).

[10] C.R.A. Catlow, Proc. Royal Soc. Lond. A353 (1977) 533-561.

[11] L.E. Cox, J. Electron Spectroscopy 26 (1982) 167-171.

[12] C. Colmenares, R.H. Howell, R.K. MacCrone and S.R. Shatynski, *Application of Positron Annihilation, Electron Paramagnetic Resonance and Thermogravimetric Techniques to the Study of Uranium Oxidation*, Proceedings of the 9th Int. Cong. Met. Corr., Vol. 4, p. 44, Toronto, Canada, June 3-7, 1984. Published by the National Research Council of Canada.

[13] G.C. Allen and P.A. Tempest, J. Chem. Soc. Dalton Trans. (1982) 2169-2173.

[14] B.T.M. Willis, Acta Crystallogr. A34 (1978) 88-90.

[15] G.C. Allen, P.A. Tempest and J.W. Tyler, Nature (London) 295 (1982) 48-49.

[16] C.R.A. Catlow, Proc. Royal Soc. Lond 74 (1978) 1901-1907.

[17] R.H. Howell, C. Colmenares and T. McCreary, J. Less Common Metals 98 (1984) 267-278.

[18] R.K. MacCrone, S. Sankaran, S.R. Shatynski, and C.A. Colmenares, 1985 TMS-AIME, New York, Feb. 24-25, 1985, to appear in Met. Trans.

[19] G.C. Allen, P.M. Tucker and R.A. Lewis, J. Chem. Soc. Faraday Trans. 2, 80 (1984) 991-1000.

[20] M.P. Seah, Chapter 3, in *Surface Analysis of High Temperature Materials: Chemistry and Topography*, 101-130, edited by G. Kemeny, (Elsevier Publishers, New York 1984).

[21] R.J. Ackermann, R.J. Thorn and G.H. Winslow, J. Opt. Soc. Am., 49 (1959) 1107-1112.

[22] J.C. Riviere, The Analyst, Vol. 228 No. 1287 (1983) 649-684.

[23] T.E. Gallon, "Current problems in AES", in *Electron and Ion Spectroscopies*, 230–272, L. Fiermans, J. Vennik and W. Dekeyser eds., (Plenum Press, New York, 1978).

[24] W.P. Ellis, Surface Science 61 (1976) 37-59.

[25] G.C. Allen and P.M. Tucker, J. Chem Soc. Dalton (1973) 470–474.

[26] W. McLean, C.A. Colmenares, R.L. Smith and G.A. Somorjai, Phys. Rev 8–24. B 25 (1982) 8–24

[27] S.B. Nornes and R.G. Meisenheimer, Surface Science 88 (1979) 191–203.

[28] J.C. Riviere, Chapter 2, 93–100, in *Surface Analysis of High Temperature Materials: Chemistry and Topography*, ed. G. Kemeny, (Elsevier 1984).

[29] L.J. Brillson and G.P. Caesar, J. Appl. Phys. 47 (1976) 4195.

[30] G.C. Allen, P.M. Tucker and J.W. Tyler, J. Phys. Chem. 86 (1982) 224.

[31] Yu. A. Teterin, V.M. Kulakov, A.S. Baev, N.B. Nevzorov, I.V. Melnikov, V.A. Strelsov, L.G. Mashirov, D.N. Suglobov and A.G. Zelenkov, Phys. Chem. Minerals 7 (1981) 151.

[32] L. Apker, Ind. Eng. Chem. 40 (1948) 846.

[33] P.A. Redhead, Vacuum 12 (1962) 203-321.

[34] D.A. King, Surface Science 47 (1975) 384–402.

[35] D. Menzel, "Thermal Desorption", in *Chemistry and Physics of Solid Surfaces, IV*, edited by R. Vanselow and R. Howe, Springer Series in Chemical Physics, Vol. 20, 1982.

[36] J.T. Randal and M.H.. Wilkins, Proc. Roy. Soc. A184 (1945) 366.

[37] P.L. Land, J. Phys. Chem. Solids 30 (1969) 1681–1692 and J. Phys. Chem. Solids 30 (1969) 1693–1708.

[38] J. Jupille, J. Fusy. and P. Pareja. Surface Science 143 (1984) L433–L438.

[39] E.M. Stuve, S.W. Jorgensen and R.J. Madix, Surface Science 146 (1984) 179–198.

[40] *Luminescence in Crystals*, D. Curie, (Wiley, New York, 1963)

[41] G. Blasse, K.C. Bleijenberg and D.M. Krol, J. of Luminescence 18/19 (1979) 57–62.

[42] R. Parrot, C. Naud, C.J. Delbecq, and P.H. Yuster, Phys. Rev. B15 (1977) 137–145.

[43] A. Lupei and V. Lupei, J. Phys. C: Solid State Phys., Vol. 12 (1979) 1123–1130.

[44] D.L. Perry, L. Tsao and H.G. Brittain, Inorg. Chem. 213 (1984) 1232–1237.

[45] E.T. Rodine, Technical Report, Aerospace Research Laboratories no. 70–0138, Aug. 1970.

[46] R. Bastasz, C.A. Colmenares and G.A. Somorjai, Surface Science 71 (1978) 397–406.

[47] R.W. Vook, C.A. Colmenares, R.J. Smith and R.G. Gutmacher, J. of Luminescence 27 (1982) 115–126

[48] W.A. Coghlan and R.E. Clausing, Atomic Data 5 (1973) 317–469.

[49] L.E. Davis, N.C. MacDonald, P.W. Palmberg, G.E. Riach, and R.E. Weber, *Handbook of Auger Spectroscopy*, (Physical Electronics Industries, Eden Prairie, Minnesota 1976).

[50] R. Bastasz and T.E. Felter, Phys Rev. B 26 (1982) 3529-3533.

[51] J.G. Dillard, H. Moers, H. Klewe-Nebenius, G. Kirch, G. Pfennig, and H.J. Ache, Surface Science 145 (1984) 62-86.

[52] G.R. Sparrow, presented at the 25th Annual Conf. on Mass Spectroscopy and Allied Topics, Washington D.C., 1977.

[53] W.P. Ellis, Surface Science 109 (1981) 1567-1570.

[54] C.T. Campbell and S.M. Valone, J. Vac. Sci. Technol. A 3(2) Mar/Apr (1985) 408-411.

[55] A. Proctor and P.M.A. Sherwood, Analytical Chemistry, Vol. 54, No. 1, January 1982, 13-19.

[56] J.T. Yates and N.E. Erickson, Surface Science 44 (1974) 489-514.

[57] L.M. Moroney, R.St C. Smart, and M.W. Roberts, J. Chem. Soc. Faraday Trans. 1, 79 (1983) 1769-1778.

[58] C. Au, S. Singh-Boparai, M.W. Roberts, and R. Joyner, J. Chem. Soc. Faraday Trans. 1 79 (1983) 1779-1791.

[59] M. Breysse, B. Claudel, M. Prettre, and J. Veron, J. Catal. 24 (1972) 106.

[60] M.McD. Baker, L.N. Less, and S. Orman, Trans. Faraday Soc. 62 (1966) 2525.

[61] B.E. Koel, G. Praline, H.I. Lee, J.M. White, and R.L. Hance, J. Electron Spec. Rel. Phenom. 21 (1980) 31-46.

[62] M.W. Roberts and P.R. Wood, J. Electron Spec. Rel. Phenom. 11 (1977) 431-437.

[63] A.F. Carley, S. Rassias, and M.W. Roberts, Surface Science 135 (1983) 35-51.

[64] H. Hopster and C. R. Brundle, J. Vac. Sci. Technol. 16(2) (1979) 548-551.

[65] F. Freund, Contrib. Mineral Petrol. 76 (1981) 474-482.

[66] J.C. Fuggle, A.F. Burr, L.M. Watson, and W. Lang, J. Phys. F: Metal Phys. Vol. 4 (1974) 335-342

[67] N. Beatham, A.F. Orchard, and G. Thornton. Journal of Electron Spec. and Rel. Phen. 19 (1980) 205-211.

[68] G.C. Allen and P.M. Tucker, Chem. Phys. Lett. 43 (1976) 254.

[69] W. Schneider and C. Laubschat, Phys. Rev. Lett. 46 (1981) 1023.

[70] J. Naegele, J. Ghijsen, and L. Manes, "Actinides and Their Compounds", in *Structure and Bonding*, L. Manes ed., Vol. 59/60 Ch. E, (Springer-Verlag 1985).

[71] M.P. Seah, "Quantification of AES and XPS", in *Practical Surface Analysis by Auger and X-ray Photoelectron Spectroscopy*, D. Briggs and M.P. Seah, eds., Ch. 5 p. 211, (John Wiley and Sons, New York, 1983).

[72] K. Kretzschmar, J.K. Sass, and A.M. Bradshaw, Surface Science 115 (1982) 183-194.

[73] E.Kh. Enikeev, A.I. Loskutov, I.L. Rozenfel'd, and V.N. Alekseev, Izvestiya Akademii Nauk SSSR, Seriya Khimicheskaya, No. 11 (1979) 2595-2598.

[74] C. Benndorf, C. Nobl, and F. Thieme, Surface Science 121 (1982) 249-259.

[75] G. Blyholder and R.W. Sheets, J. Catalysis 39 (1975) 152.

[76] K. Siegbahn, C. Nordling, G. Johansson, J. Hedman, P.F. Heden, K. Hamrin, U. Gelius, T. Bergmark, L.O. Weine, R. Manne and Y. Baer, *Esca Applied to Free Molecules*, (North Holland, Amsterdam, 1971).

[77] J.W. Ward, L.E. Cox, J.L. Smith, G.R. Stewart, and J.H. Wood, Journal de Physique, C4 (1979) C4-15.

[78] E.E. Huber, Jr., and C.T. Kirk, Jr., Surface Science 5 (1966) 447-465.

[79] A. Spitzer, A. Ritz, and H. Luth, Surface Science, 152/153 (1985) 543-549.

[80] K. Bange, T.E. Madey, and J.K. Sass, Surface Science 152/153 (1985) 550-558.

[81] T.E. Madey and J.T. Yates, Jr., Chemical Phys. Lett. 51 (1977) 77-83.

[82] M. Breysse, B. Claudel, L. Faure, and M. Guenin, Proc. 7th Intern. Vac. Congr. and 3rd Intern. Conf. Solid Surfaces (Vienna 1977).

[83] G.P. Summers, T.M. Wilson, B.T. Jefferies, H.T. Tohrer, Y. Chen, and M.M. Abraham, Phys. Rev. B 27 (1983) 1283-1291.

[84] V.T. Coon, Surface Science 88 (1979) 42.

[85] K. Winer, C. Colmenares, and F. Wooten, J. of Luminescence, 31 and 32 (1984) 357-359.

[86] M. Breysse, B. Claudel, L. Faure and M. Guenin, J. Luminescence, 18/19 (1979) 402-406.

[87] S. Clement and E.R. Hodgson, Phys. Rev. B 30 (1984) 4684-4688.

[88] A.U. Khan, "Singlet Molecular Oxygen Spectroscopy: Chemical and Photosensitized", in *Singlet* O_2, Vol. 1 (1985), A.A. Frimer, ed., (CRC Press, Boca Raton, Florida).

[89] J. Fontaine and M. Fiot, Commisariat A'Energie Atomique, unpublished research (1985).

[90] R. Musket, G. Robinson-Weis, and R.G. Patterson, Mat. Res. Soc. Symp. Proc. Vol. 27 (1984), Elsevier Pub. Co., Inc.

[91] D.B. Bedere and P. Sans, J. of the Less-Common Metals, 91 (1983) 33-48.

[92] J.B. Condon, J. of the Less-Common Metals, 73 (1980) 105-112.

[93] M. McD. Baker, L. N. Less ,and S. Orman, Trans. Faraday Soc. Vol. 62(4) (1966) 2513-2524

[94] T. Kondo, F.H. Beck, and M.G. Fontana, Corrosion (Houston) 30 (1974) 330-339.

[95] A.G. Guy, *Introduction to Materials Science*, Chapter 11, pp. 54, McGraw-Hill Book Company, New York, 1971.

[96] M. Balooch, D.R. Olander, and W.J. Siekhaus, 12th DOE Surface Science Conf., Oak Ridge, Tenn., June 1984.

[97] S. Sunder, D.W. Shoesmith, M.G. Bailey, F.W. Stanchell, and N.S. McIntyre, J. Electroanal. Chem. 130 (1981) 163-179.

[98] C.A. Colmenares, private communication (1985).

[99] L.J. Weirick, *The Oxidation of Uranium in Low Partial Pressures of Oxygen and Water Vapor at 100 C*, Sandia Report 83-0618, Sandia National Laboratories, Albuquerque, New Mexico 87185, June 1984.

[100] E.L. Fuller, Jr., N.R. Smyrl, J.B. Condon, and M.H. Eager, Journal of Nuclear Materials 120 (1984) 174-194.